NASA Contractor Report 4750

# Handbook of Analytical Methods for Textile Composites

*Brian N. Cox*
*Rockwell Science Center • Thousand Oaks, California*

*Gerry Flanagan*
*Materials Sciences Corporation • Philadelphia, Pennsylvania*

National Aeronautics and Space Administration
Langley Research Center • Hampton, Virginia 23681-0001

Prepared for Langley Research Center
under Contract NAS1-19243

March 1997

**1. INTRODUCTION** . . . . . 1-1

**1.1 Scope** . . . . . 1-1
**1.2 Layout of the Handbook** . . . . . 1-2
**1.3 Historical Origins** . . . . . 1-3
**1.4 Internet Access** . . . . . 1-3

**2. OVERVIEW OF TEXTILES** . . . . . 2-1

**2.1 Textile Processes** . . . . . 2-3
***2.1.1 Categorizations*** . . . . . 2-3
*2.1.1.1 Dimensionality* . . . . . 2-3
*2.1.1.2 Quasi-Laminar and Nonlaminar Textiles* . . . . . 2-4
***2.1.2 Preforms*** . . . . . 2-5
*2.1.2.1 Weaving* . . . . . 2-5
*2.1.2.2 Flat Braiding from Cylindrical Mandrels* . . . . . 2-5
*2.1.2.3 3D Braiding* . . . . . 2-6
*2.1.2.4 Uniweaves* . . . . . 2-7
*2.1.2.5 Warp Knits* . . . . . 2-8
*2.1.2.6 Stitching* . . . . . 2-9
***2.1.3 Molding*** . . . . . 2-10
**2.2 Materials** . . . . . 2-12
**2.3 The Geometry of Textile Reinforcement** . . . . . 2-15
***2.3.1 Ideal geometry***. . . . . 2-15
*2.3.1.1 Unit Cells* . . . . . 2-15
*2.3.1.2 2D Weaves* . . . . . 2-15
*2.3.1.3 2D Braids* . . . . . 2-16
*2.3.1.6 3D Interlock Weaves* . . . . . 2-20
*2.3.1.7 3D Braids* . . . . . 2-21
*2.3.1.8 Orthogonal Nonwoven Composites* . . . . . 2-21
***2.3.2 The relation of volume fraction and fabric geometry to process parameters***. . . . . 2-22
*2.3.2.1 2D Weaves* . . . . . 2-22
*2.3.2.2 2D Braids* . . . . . 2-24
*2.3.2.3 3D Weaves* . . . . . 2-24
*2.3.2.4 3D Braids* . . . . . 2-26
***2.3.3 Irregularity*** . . . . . 2-28
**2.4 Integral Structures made by Textile Processes** . . . . . 2-31

**References** . . . . . 2-33

**3. THE CHOICE BETWEEN TEXTILES AND TAPE LAMINATES** . . . 3-1

**3.1 Handling and Fabricability** . . . . . 3-1
**3.2 Consistency of Fiber Content** . . . . . 3-2
**3.3 Stiffness** . . . . . 3-3
**3.4 In-Plane Strength** . . . . . 3-5
*3.4.1 2D Weaves* . . . . . 3-6
*3.4.2 2D Braids* . . . . . 3-8
*3.4.3 Stitched Laminates* . . . . . 3-10
*3.4.4 3D Interlock Weaves* . . . . . 3-11
**3.5 Out-of-Plane Strength; Delamination and Impact Resistance** . . . . . 3-12
**3.6 Work of Fracture and Notch Sensitivity** . . . . . 3-12
**References**. . . . . 3-13

**4. FAILURE MECHANISMS** . . . . . 4-1

**4.1 Shear** . . . . . 4-1

**4.2 Monotonic Compression** . . . . . 4-3
***4.2.1 2D Weaves and Braids*** . . . . . 4-6
***4.2.2 Stitched and Stitched-Knitted Laminates*** . . . . . 4-8
***4.2.3 3D Weaves*** . . . . . 4-8
***4.2.4 3D Braids*** . . . . . 4-9
**4.3 Monotonic Tension** . . . . . 4-9
***4.3.1 2D Weaves and Braids*** . . . . . 4-11
***4.3.2 Stitched, Stitched-Woven, and Stitched-Knitted Laminates*** . . . . 4-12
***4.3.3 3D Weaves*** . . . . . 4-12
**4.4 Delamination under Through-Thickness Tension (Curved Structures)**. . . . . 4-13
**4.5 Shear Delamination in Bending** . . . . . 4-16
**4.6 Notch Sensitivity** . . . . . 4-16
***4.6.1 Cohesive Zones*** . . . . . 4-16
***4.6.2 Splitting at a Notch*** . . . . . 4-18
**4.7 Fatigue** . . . . . 4-19
***4.7.1 2D Weaves and Braids*** . . . . . 4-19
***4.7.2 3D Interlock Weaves*** . . . . . 4-20
**References** . . . . . 4-20

**5. PREDICTION OF ELASTIC CONSTANTS AND THERMAL EXPANSION** . . . . . 5-1

**5.1 Concepts** . . . . . 5-1

***5.1.1 Isostrain and Isostress*** . . . . . 5-1

***5.1.2 Tow Properties*** . . . . . 5-2

***5.1.3 Fiber Packing and Resin Pockets*** . . . . . 5-5

***5.1.4 Unit Cells and Periodic Boundary Conditions*** . . . . . 5-6

***5.1.5 Macroscopic Length Scales*** . . . . . 5-8

***5.1.6 Fundamentals of Heterogeneous Elastica*** . . . . . 5-11

***5.1.7 Orientation Averaging*** . . . . . 5-14

***5.1.8 Bending or Axial Shear?*** . . . . . 5-16

***5.1.9 Geometrical Irregularity*** . . . . . 5-18

**5.2 Summary of Available Codes for Analyzing Stiffness** . . . . . 5-19

***5.2.1 Quasi-laminar and Nonlaminar Textiles*** . . . . . 5-20

***5.2.2 Geometry*** . . . . . 5-21

***5.2.3 Modeling Thermo-Elastic Properties*** . . . . . 5-25

**5.3 Comparison of Code Predictions for Plain Woven Textile Composite** . . . . . 5-30

**5.4 Code Calibration** . . . . . 5-33

***5.4.1 Fiber Dominated Elastic constants*** . . . . . 5-33

***5.4.2 Matrix Dominated Elasstic Constants*** . . . . . 5-34

***5.4.3 Calibrating the Fiber Volume Fraction*** . . . . . 5-34

***5.4.4 Calibrating Fiber Waviness*** . . . . . 5-35

**References** . . . . . 5-35

**6. NONLINEAR STRESS-STRAIN BEHAVIOUR AND STRENGTH** . . . . 6-1

**6.1 Nonlinearity Beyond the Proportional Limit** . . . . . 6-1

***6.1.1 Tensile (Transverse) Matrix Cracking*** . . . . . 6-2

***6.1.2 Shear Deformation*** . . . . . 6-2

***6.1.3 Plastic Tow Straightening*** . . . . . 6-2

**6.2 Tessellation Models** . . . . . 6-3

**6.3 Ultimate Strength** . . . . . 6-4

***6.3.1 Ultimate Tensile Strength*** . . . . . 6-4

***6.3.2 Compressive Strength*** . . . . . 6-5

***6.3.3 Shear Strength*** . . . . . 6-7

***6.3.4 Multi-Axial Loads*** . . . . . 6-7

**6.4 Codes for Predicting Nonlinear Stress-Strain Behaviour and Ultimate Strength** . . . . . 6-8

***6.4.1 Nonlinearity*** . . . . . 6-8

***6.4.2 Ultimate strength*** . . . . . 6-9

**6.5 Notched Strength** . . . . . 6-10

**References** . . . . . 6-11

**7. FATIGUE LIFE** . . . . . 7-1

**7.1 Kink Formation in Compression-Compression Fatigue** . . . . . 7-1

**7.2 Tension-Tension Fatigue and Load Ratio Effects** . . . . . 7-3

**7.3 Delamination Crack Growth in Quasilaminar Textile Composites** . . . 7-3

**References** . . . . . 7-4

**8. SUMMARY OF AVAILABLE CODES** . . . . . 8-1

**8.1 μTex-10** . . . . . 8-2

**8.2 μTex-20** . . . . . 8-5

**8.3 TEXCAD** . . . . . 8-7

**8.4 PW, SAT5, SAT8** . . . . . 8-10

**8.5 SAWC (Stress Analysis of Woven Composites)** . . . . . 8-12

**8.6 CCM-TEX** . . . . . 8-15

**8.7 WEAVE** . . . . . 8-17

**8.8 BINMOD** . . . . . 8-19

**9. SELECTIVE ANNOTATED BIBLIOGRAPHY** . . . . . 9-1

## Tables


Table 2.1 Fiber Properties . . . . . 2-13

Table 2.2 Typical Yarn Weights and Dimensions . . . . . 2-14

Table 3.1 Braid and Equivalent Tape Laminate Specifications for Fig. 3-1 . . . . . 3-5

Table 3.2 Comparison of Unnotched Tensile Strengths for Various AS4/1895 Triaxial Braids . . . . . 3-10

Table 4.1 Compression Data for Gr/Ep Triaxial Braids (from [4.16]) . . . . . 4-7

Table 5.1 Some models of unidirectional fiber composites . . . . . 5-4

Table 5.2 Estimated mechanical properties of tows . . . . . 5-4

Table 5.3 Summary of code capabilities . . . . . 5-20

Table 5.4 Constituent property input used in code comparisons . . . . . 5-24

Table 5.5 How codes model quasi-laminar plates . . . . . 5-29

Table 5.6 Constituent property input used in code comparisons . . . . . 5-31

Table 5.7 Geometric parameters assumed for code comparisons . . . . . 5-31

Table 5.8 Comparison of homogenized, 3D elastic constants for a plain weave fabric, using various codes . . . . . 5-32

Table 5.9 Comparison of homogenized, 3D thermal expansion coefficients for a plain weave fabric, using various codes. . . . . 5-32

Table 5.10 Comparison of plate stiffnesses for a plain woven composite, using vaarious codes. . . . . 5-32

Table 6.1. Predicted and measured ultimate strengths of some triaxial glass/urethane braids and 3D carbon/epoxy interlock weaves . . . . 6-5

Table 6.2. Code capabilities for predicting nonlinear behaviour and strength . . . . . 6-10

## Figures


Figure 2-1. Steps in the production of a textile composite structure . . . . . 2-2

Figure 2-2. Some of the textile forms available for high performance composite structures . . . . . 2-3

Figure 2-3. Maypole braider for production of 2D bias braid . . . . . 2-6

Figure 2-4. Two-step braiding process . . . . . 2-7

Figure 2-5. Four-step braiding process . . . . . 2-8

Figure 2-6. Multi-axial warp knit . . . . . 2-9

Figure 2-7. Types of stitching used for through-thickness reinforcement . . . . . 2-11

Figure 2-8. Resin infusion techniques . . . . . 2-12

Figure 2-9. Techniques for using thermoplastics in textiles . . . . . 2-13

Figure 2.10. Commonly used 2D weave patterns . . . . . 2-17

Figure 2-11. Angles of the diagonal patterns formed by exchange locations . . . . . 2-18

Figure 2-12. Triaxial weave . . . . . 2-18

Figure 2-13. Some common 2D braid patterns . . . . . 2-19

Figure 2-14. Three-dimensional weave patterns . . . . . 2-21

Figure 2-15. 3D orthogonal composite . . . . . 2-22

Figure 2-16. A unit cell for a plain weave . . . . . 2-25

Figure 2-17. 3D unit cell for 1x1, 4-step braid . . . . . 2-27

Figure 2-18. Inner yarn angle of inclination versus cycle length for 1x1, 4-step braid . . . . . 2-28

Figure 2-19. (a) Yarn volume fraction versus (a) inner yarn angle of inclination and (b) normalized cycle length for 1x1, 4-step braid . . . . . 2-29

Figure 2-20. Ratio of outer (surface) yarns to inner yarns . . . . . 2-29

Figure 2-21. Waviness in nominally straight axial tows in a triaxial braid . . . . . 2-30

Figure 2-22. Waviness induced in warp weavers in a 3D interlock weave by compression during processing . . . . . 2-31

Figure 2-23. Tracings of yarn cross-sections in a 3D braided composite . . . . . 2-31

Figure 2-24. Use of 3D weaving to create a branched structure . . . . . 2-32

Figure 2-25. An integrally woven skin/stiffener preform . . . . . 2-32

Figure 2-26. A stitched skin/stiffener assembly . . . . . 2-33

Figure 3-1. The Moduli of 2D Braids and Equivalent Tape Laminates . . . . . 3-5

Figure 3-2. Comparison of (a) unnotched and (b) notched strengths of 5-harness satin weave laminate and equivalent tape laminate . . . . . 3-7

Figure 3-3. Comparison of shear strengths of various T300/934 weaves, showing effect of crimp . . . . . 3-8

Figure 3-4. Comparison of unnotched and open hole tensile strengths for two triaxial braids and equivalent tape laminates. . . . . 3-9

Figure 3-5. Tensile strengths of stitched and unstitched IM7/3501-6 laminates. Stitching with 0.125 in. (3.1 mm) pitch (between penetrations within a row) and 0.20 in. (5.0 mm) spacing between the stitching rows . . . . . 3-11

Figure 3-6. Compression strengths and CAI data for stitched and unstitched laminates. . . . . 3-11

Figure 4-1. Arrays of ogive microcracks in (a) an AS4/1895 tape laminate (from [4.1]) and (b) a glass/urethane triaxial braid (from [4.2]). The fiber direction is parallel to the bands of microcracks . . . . . 4-2

Figure 4-2. Typical stress-strain response of a polymer composite when the deviatoricstress in plies is pure shear. (a) AS4/1895 tape laminate (b) AS4/3501-6 plain weave. . . . . 4-2

Figure 4-3. Micrograph of a typical kink band in an aligned tow in an AS4/1895 3D interlock weave . . . . . 4-4

Figure 4-4. Schematic of buckling under in-plane compression following delamination due to impact . . . . . 4-6

Figure 4-5. Schematic of delamination and shear failure events in a typical 2D weave. . . . . 4-7

Figure 4-6. Stress-strain curves for plain woven carbon/eopxy laminate. (a) Unnotched. (b) Notched ($d$ = 4 mm) . . . . . 4-11

Figure 4-7. Stress-strain data for a 3D interlock weave tested in uniaxial tension aligned with the stuffers . . . . . 4-13

Figure 4-8. Stitching bridging a delamination crack in a curved part . . . . . 4-14

Figure 4-9. Map of failure modes for a curved panel. . . . . 4-15

Figure 4-10. Schematic of a nonlinear damage band growing from a stress concentrator in a textile composite . . . . . 4-18

Figure 4-11. A kink band formed in fatigue in a misaligned segment of a stuffer in an AS4/1895 layer-to-layer interlock weave . . . . . 4-20

Figure 5-1. Translationally invariant 2D laminate . . . . . 5-2

Figure 5-2. Comparison of the elastic constants predicted for tows in an AS4/1895 composite using various models from the literature . . . . . 5-3

Figure 5-3. Alternative unit cells (short and long dash lines at upper left) in a plane woven laminate. The smaller, solid-lined rectangle (lower right) shows a reduced cell that takes advantage of reflection symmetry about a vertical plane . . . . . 5-7

Figure 5-4. Nonperiodic strains in a periodic structure under nonuniform external loads. Schematic of two unit cells in a larger array . . . . . 5-8

Figure 5-5. Schematic of a 3D interlock weave. The numbers at the right show the sequence of occurrence of warp weaver tows encountered on progressing into the plane of the figure . . . . . 5-9

Figure 5-6. Coefficient of variation of Young's modulus measurements as a function of the size of the gauge used relative to the unit cell dimension in that direction. Gauge sizes shown in inches in inset; 1 in. ≈ 25.4 mm. . . . . 5-10

Figure 5-7. Coordinates for transformation of tow properties . . . . . 5-15

Figure 5-8. Three orthogonal symmetry planes (two marked by dashed lines and the third being the plane of the figure) in a stack of woven plies, implying orthotropy over gauge lengths that are larger than the ply thickness and the period of the weave . . . . . 5-16

Figure 5-9. A simple paradigm for estimating the contributions of shear and bending to the deflection of a tow . . . . . 5-17

Figure 5-10. Schematics of buckling of an aligned tow under compression. (a) When relatively soft through-thickness reinforcement acts as a soft elastic foundation, allowing deflections over relatively long wavelengths. (b) When stiff through-thickness reinforcement restricts lateral deflections to the intervals between successive through-thickness tows . . . . . 5-19

Figure 5-11. Choices of unit cell in quasi-laminar textile composites. (a) Two approaches to modeling laminate properties. (b) Variant of whole thickness cell in (a) for analyzing stacking effects . . . . . 5-22

Figure 6-1. Measured compressive strengths of 3D interlock weaves compared with predictions based on measurements of misalignment angles and the critical shear flow stress . . . . . 6-6

Figure 6-2. Failure loci for individual tows or plies in terms of the local stress state. (a) Combined aligned and axial shear loads. (b) Combined transverse and axial shear loads. The *x*-axis is aligned with local fiber direction. The axes are not to scale . . . . . 6-9

## Acknowledgments

The authors acknowledge with pleasure the assistance of Dr. George Sherrick, Ms. Maria Lee, and Mr. Ron Martin of Rockwell, North American Aircraft Division, Tulsa, in collecting and checking source codes and preparing a scanned compendium of user's guides; and Ms. Barbara Burg of Rockwell Science Center, who worked for many hours with unflagging good humour in editing the final version.

They are especially indebted to Dr. Charles E. Harris and Mr. C.C. (Buddy) Poe of NASA Langley, whose vision in assembling the Textiles Working Group within the Advanced Composites Technology program provided the background out of which the handbook grew.

Drs. Tsu-Wei Chou, Ramesh Marrey, Rajiv Naik, Chris Pastore, Kishore Pochiraju, I. S. Raju, Bhavani Sankar, and John Whitcomb cooperated very graciously in supplying their codes and documentation.

# 1.0 INTRODUCTION

## 1.1 Scope

The purpose of this handbook is to introduce models and computer codes for predicting the properties of textile composites. The composites of primary interest are those best suited to applications in aircraft structures. This is first to say those ranked high in stiffness and strength; and many models are therefore discussed which detail the elastic regime and predict the proportional limit. But textile composites are also favoured for their superior damage tolerance. The handbook therefore includes several models for predicting the stress-strain response all the way to ultimate failure; methods for assessing work of fracture and notch sensitivity; and design rules for avoiding certain critical mechanisms of failure, such as delamination, by proper textile design.

The textile classes receiving at least some treatment are:

(i) 2D woven laminates
(ii) 2D braided laminates
(iii) laminates of knitted plies
(iv) stitched laminates
(v) 3D interlock weaves
(vi) 3D braids
(vii) 3D nonwoven composites.

The fiber and matrix materials need not be specified until the models are applied to a particular material. However, many models are based on assumptions that may be invalid if the degree of anisotropy is not as high as it is for stiff fibers such as carbon or glass in a polymeric matrix. Models assuming high anisotropy would not be appropriate for ceramic or metal matrix composites. Readers working with ceramics or metals should exercise caution accordingly.

The handbook deals mainly with models for textile composites manufactured as flat panels, with limited attention to curved panels. Yet one of the longer term attractions of textiles is that they promise a method of manufacturing net shape, integral structures, eliminating many machining and joining steps in manufacture, cutting material waste, preventing the possibility of debonding failures in service, and saving the attendant

necessity of continual inspection. Some textile technologies, especially stitching and braiding, are already on the verge of producing cost effective integral structures. Unfortunately, there are almost no models available at the time of writing for general part shapes, even though the technological advantage of integral textile structures is a strong motivation for their development. It is to be hoped they will be included in future editions of the handbook.

## 1.2 Layout of the Handbook

The intended audience for this handbook is the practicing design engineer, who might be assumed to be very familiar with the mechanics of composites. However, textile composites are sufficiently new and their mechanisms of failure so unlike those of tape laminates in so many ways, that it would be very imprudent for a designer to take any model of a textile composite at face value and proceed to use it. Whether a model will work, whether it is the best available, how it should be used, and what limits exist on its accuracy and domain of applicability are questions whose correct answer requires sound understanding of concepts that are peculiar to textiles and very recent in their development.

Therefore the handbook offers tutorial chapters on the technology and mechanics of textile composites before the models are presented. Section 2 surveys the rich diversity of textile processes and products. Section 3 highlights some of the distinctions between textiles and tape laminates that designers more familiar with the latter should remember. Section 4 details the known mechanisms of failure of textile composites, many of which have no parallel in traditional laminates, and offers a few failure maps in cases where the controlling microstructural and material parameters are known. Sections 5 through 7 present the models themselves, each section being prefaced by a summary of essential geometrical and modeling concepts, which must be mastered before any judgment can be exercised over the choice of code for a particular application. With the guidance of these concepts and available experimental data, a critical appraisal is offered of the relative merits of models that claim to calculate the same quantities. The reader is strongly advised to work through all these sections to acquire at least a rudimentary understanding of the special challenges in modeling textile composites.

Details of the codes, sample input and output decks, and user's guides written by the original authors are supplied in Section 8 and the appendices. Source codes for all the

models presented are available over the internet. All codes have been compiled on a Unix platform and verified to perform as claimed in at least a few representative cases.

Throughout the handbook, the names of codes are printed in **UPPER CASE BOLD TYPE**.

## 1.3 Historical Origins

Many of the models presented were developed by the Textiles Working Group within the Advanced Composites Technology (ACT) Program sponsored by NASA Langley Research Center. This research was conducted over a period of five years ending in 1994 by about a dozen groups in universities and industry.

Other key models and computer codes have also been included to ensure that the handbook's scope is representative of the growing population of models in the modern literature.

At least some of the models have had the advantage of being conceived in the midst of vigorous experimental programs, in which stiffness, strength, and damage mechanisms have been studied extensively, by which it might be hoped that they are more realistic than models formulated on entirely theoretical grounds.

The ACT program has also funded the writing of this first edition of the handbook.

## 1.4 Internet Access

This report is also available in electronic format from the Langley Technical Report Server (LTRS) using the Uniform Resource Locator (URL):

http://techreports.larc.nasa.gov/ltrs.

Instructions for accessing source codes and user's guides for programs described in this handbook is available at:

http://coins.larc.nasa.gov

Refer to NASA Contractor Report No. CR-4750.

# 2. OVERVIEW OF TEXTILES

Textile composites for engineering structures draw on many traditional textile forms and processes. In this section, the processes and architectures that can yield composites with the high performance required for aerospace structures will be summarized. These textiles are generally those that most effectively translate stiff, strong yarns into stiff, strong composites.

A textile composite has internal structure on several scales. At the molecular scale, both the polymer matrix and the fibers exhibit structural details that profoundly affect strength and stiffness. Matrix properties are determined by chain morphology and cross-linking, among other things. Carbon fibers, which are often the preferred choice in aerospace materials, owe their axial stiffness and strength to the arrangement of carbon atoms in oriented graphitic sheets. On a coarser scale, typically ~1 mm., lots of $10^3$ - $10^4$ fibers are bundled into yarns or tows. Within the finished composite, each tow behaves as a highly anisotropic solid entity, with far greater stiffness and strength along its axis than in transverse directions. Because tows are rarely packed in straight, parallel arrays, stresses and strains often possess strong variations from tow to tow. Thus composite mechanical properties such as elasticity can only be considered approximately uniform on scales that are even larger still, say ~ 10 mm or higher, where the effects of the heterogeneous structure at the tow level are averaged out. Finally, the textile forms part of an engineering structure, perhaps the stiffened skin of a wing or fuselage. Since the engineering structure itself usually has some dimensions as small as ~ 10 mm, the fabrication of the composite material and the fabrication of the engineering structure may no longer be considered distinct operations. To fabricate the textile composite *is* to fabricate the structure.

Figure 2-1 illustrates scales in one textile process. The part shown is an integrally formed skin/stiffener assembly. The first processing step is the formation of yarns from fibers. In the second step, the yarns are woven into plain woven cloth. The cloths are then laid up in the shape of the skin and stiffener and stitched together to create an integral preform. Finally, the composite part is consolidated by the infiltration of resin and curing in a mold.

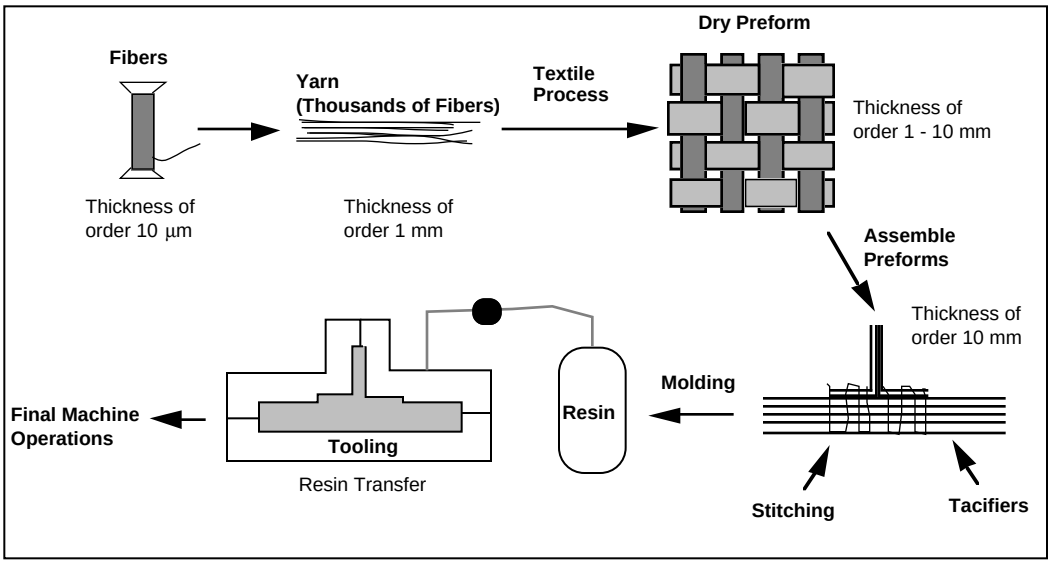


Figure 2-1. Steps in the production of a textile composite structure.

The fabrication method of Figure 2-1 also illustrates fairly high utilization of the axial stiffness and strength of the fibers. The fibers in the skin are arranged approximately in-plane and straight and with reasonably high volume fraction. High in-plane composite stiffness and strength can therefore be expected. Certain other traditional textiles do not achieve this. For example, many knitted fabrics loop yarns in highly curved paths, rather than aligning them; and, because of the openness of the fabric, can achieve only moderate fiber volume fractions. Composite stiffness and strength are consequently inadequate for airframes. For similar reasons, fiber mats and discontinuous reinforcements are usually unattractive to airframe designers. These materials will be excluded from further consideration in the handbook.

Figure 2-1 also exemplifies reinforcement that is heterogeneous on the scale of the structure. The length of the stitches varies with the thickness of the flange of the rib and their spacing is not far below the thickness of either the rib itself or the flanges. Just as the material and the structure are fabricated simultaneously, so in this case they must be analyzed simultaneously. Dealing adequately with the fiber architecture in determining stress distributions requires analyzing the external geometry of the part itself. However, computer programs to perform such a task are still being developed. Therefore, this handbook in its first edition focuses on solutions for skins, sheets, or slabs without complicating external shapes, for which developed and tested programs are already available.

## 2.1 Textile Processes

### *2.1.1 Categorizations*

Figure 2-2 introduces the most important groups of textile forms that are candidates for airframes, many of which were investigated during NASA's ACT Program. The left column (weaving, braiding, etc.) categorizes textiles according to the machines and processes used in creating them. High-performance composite structures have been created using all the processes listed, conventional textile machinery having been modified in many cases to handle the high modulus fibers needed in airframes and to reduce costs through automation.

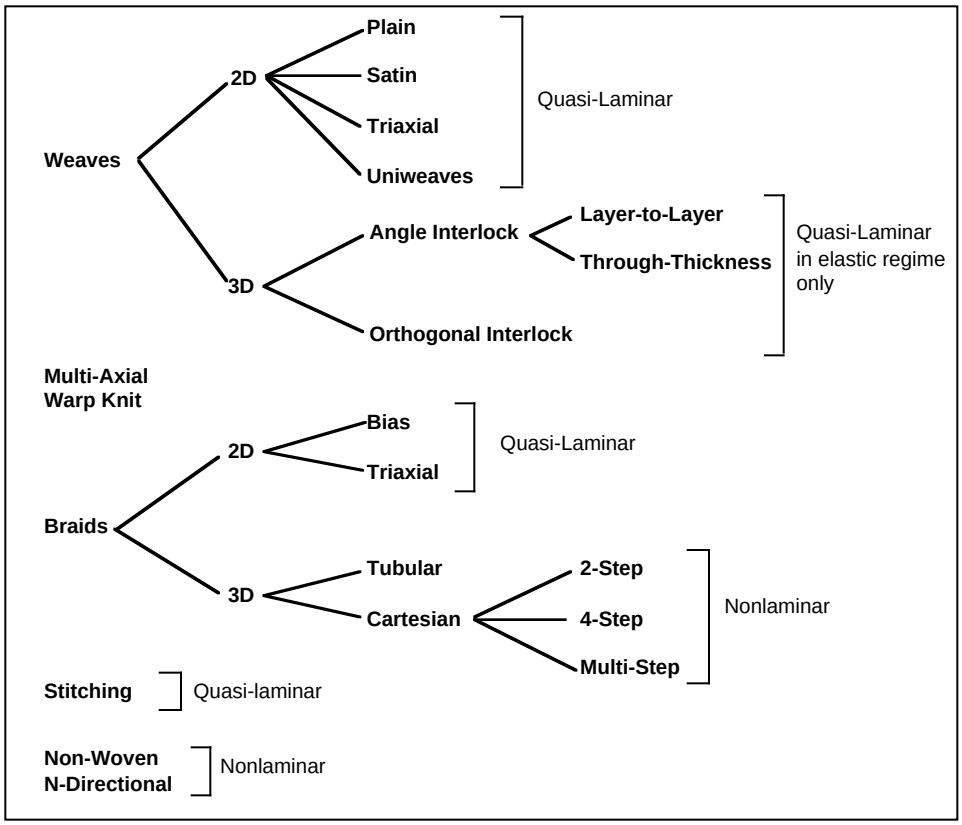


Figure 2-2. Some of the textile forms available for high performance composite structures.

#### *2.1.1.1 Dimensionality*

The division into 2D and 3D composites is determined by whether the fiber preform alone (in the absence of the matrix) can transport loads continuously in three or only two linearly

independent directions.[1] Thus a 2D composite has distinct layers, which may be separated without breaking fibers. Of course, yarns in textile composites that are defined to be 2D may still follow path segments with components in the through-thickness direction, as in a laminated plain weave; but surfaces may be defined through which no tows pass and which separate the composite into layers. This cannot be done for a 3D composite.

#### *2.1.1.2 Quasi-Laminar and Nonlaminar Textiles*

In modeling their macroscopic properties, all 2D and many 3D textile composites can be considered to function as laminates, with relatively minor allowance for their textile nature, even though the routes to their manufacture are very different from conventional tape lay-up. Most textile composites designed for skin or sheet applications fall into this category. When high in-plane stiffness and strength are demanded, the majority of fibers must lie in-plane; relatively few can be dedicated to through-thickness reinforcement without unacceptable loss of in-plane properties. And indeed for most sheet applications, damage tolerance and delamination resistance require modest volume fractions of through-thickness fibers (Sect. 4; [2.1,2.2]). Textile composites that behave in most ways like laminates will be called "quasi-laminar."

In structures where substantial triaxial stresses exist, the optimal reinforcement will no longer be a laminate with moderate through-thickness reinforcement. Instead, fibers will be arranged by some textile process with roughly equal load bearing capacity along all three axes of a Cartesian system. Such textile composites will be called "nonlaminar."

Nonlaminar textiles are often manufactured to respond to complex part geometry and triaxial loads, for example the union of a skin and stiffening element or a short beam with approximately equiaxed cross-section. But even a curved plate designed as a laminate with through thickness reinforcement must be considered nonlaminar if its curvature is sufficiently high. As the curvature increases, greater through-thickness tension is generated by applied bending moments, and so much through-thickness reinforcement is needed to suppress delamination that the part loses its laminar character (Sect. 4, [2.3]).

Figure 2-2 shows how the main classes of textiles may be categorized as quasi-laminar or nonlaminar. Occasionally, experience with damage modes obliges categorization

---

[1]Direction vectors are linearly independent if none of them can be expressed as a simple combination of the others. Thus three in-plane directions cannot be linearly independent.

of a textile as nonlaminar in describing its passage to ultimate failure, even though in the elastic regime it is clearly quasi-laminar.

Whether a textile is quasi-laminar or nonlaminar is a crucial question in choosing an appropriate approach to modeling its properties. Quasi-laminar composites can generally be modeled accurately by some modification of standard laminate theory. Nonlaminar textiles require a model that computes the distribution of stresses in all tows, which is a much more difficult problem.

### *2.1.2 Preforms*

#### *2.1.2.1 Weaving*

Weaves have been used in composites for many years. They offer a low cost method of fabricating large areas of material, with only a small sacrifice in the properties that would have been obtained with laminates of unidirectional tape. Weaves are made by interlacing two or more orthogonal sets of yarns (warp and weft) on a loom. Most weaves contain similar numbers of fibers and use the same material in both warp and weft. However, hybrid weaves [2.4] and weaves dominated by warp yarns (Sect. 2.2.2.4) have important roles in textile composites .

Woven broadgoods may be purchased either as a dry preform or pre-impregnated with a B-staged epoxy matrix. In most applications, multiple layers of 2D weaves are laminated together. As with tape laminates, the layers are oriented to tailor strength and stiffness.

3D woven fabrics are created on a multiwarp loom. As in a conventional loom, harnesses alternately lift and lower the warp yarns to form the interlacing pattern. In the multiwarp loom, separate harnesses lift different groups of warp yarns to different heights, so that some are formed into layers while others weave the layers together.

#### *2.1.2.2 Flat Braiding from Cylindrical Mandrels*

Traditional braiding involves a series of yarn carriers that follow intersecting circular paths so that the yarns interlace to form a tubular fabric (Fig. 2-3). A mandrel that passes through the braider may be used to control the final fabric configuration. The rotational speed of the yarn carriers relative to the transverse speed of the mandrel controls

the orientation of the yarns. The mandrel can vary in cross-section, with the braided fabric conforming to the mandrel shape (as long as the perimeter is not re-entrant).

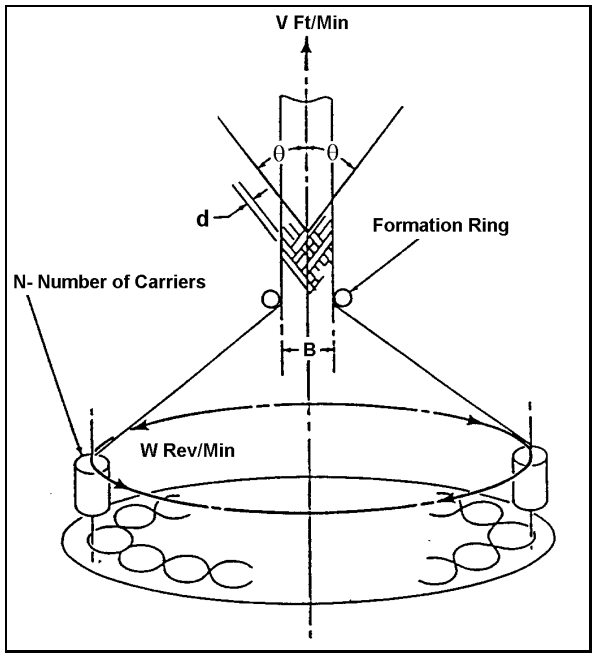


Figure 2-3. Maypole braider for production of 2D bias braid.

Fixed, straight axial yarns can also be introduced at the center of orbit of the braider yarn carriers. The braider yarns lock the axial yarns into the fabric, forming a triaxial braid, i.e. a braid reinforced in three in-plane directions.

A flat braided sheet can be formed by cutting the cylindrical sheet from the mandrel and stretching it out flat.

*2.1.2.3 3D Braiding*

3D braiding can produce thick, net section preforms, in which tows are so intertwined that there may be no distinct layers. In one process, the yarn carriers (bobbins) are arranged in a two-dimensional grid, often in rectangular or annular patterns, sometimes in the cross-sectional shape of the final component. Multiple rectangles can be concatenated to form more complex cross-sections. Braiding proceeds by alternately exchanging rows and columns of yarn carriers. While the tracks that move yarn carriers return to their original positions after a small number of steps, the carriers themselves can follow complex paths by passing from one track to another.

Three-dimensional braids can be characterized as two-step, four-step, and multi-step processes. The number of steps refers to the number of movements required for the yarn carrriers to return to their original positions. The two-step process is illustrated in Fig. 2-4. The braider yarns move in opposite directions along alternating diagonals formed by the axial yarns.

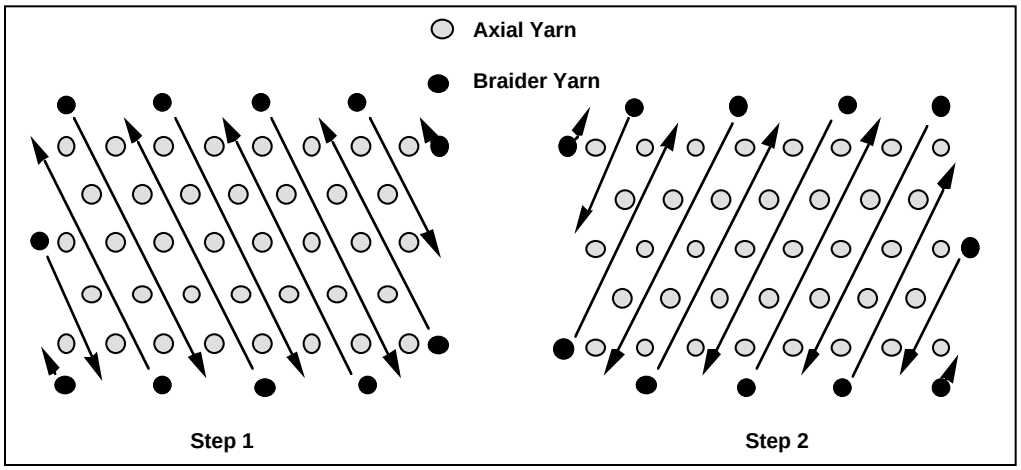


Figure 2-4. Two-step braiding process.

The four-step process is shown in Fig. 2-5. In the first step, alternate columns are shifted a prescribed relative distance. The next step involves shifting alternate rows. The third and fourth steps permute the columns and rows to return the device to its original configuration (although an individual bobbin does not return to its original position in one cycle). The 4-step process is a general term for processes that include Omniweave, Magnaweave, SCOUDID, and Cartesian braiding. Multistep braiding is a generalization of the four-step procedure which involves individual control over columns and rows.

The relative shifting distance of the rows and columns also controls the braid pattern. In a 1x1 braid, the shifting distances of the rows and columns are equal. More complex braid patterns are possible.

3D braiding machines use a beater to control compaction as the yarns interlace. The degree of compaction is a process variable which affects the resulting fabric geometry.

### *2.1.2.4 Uniweaves*

The uniweave concept combines the mechanical property potential of unidirectional tape with the handling advantages and low-cost fabrication of a fabric. Uniweave consists of primary yarns of strong, stiff fibers woven together with fine yarns of glass or polyester

thread. The glass or polyester threads, which contribute around 2% of the total weight, serve mainly to hold the primary yarns together during subsequent handling. The fibers in the primary yarns remain close to unidirectional. Multiple layers of uniweave are often stitched together to form a sheet of any desired thickness.

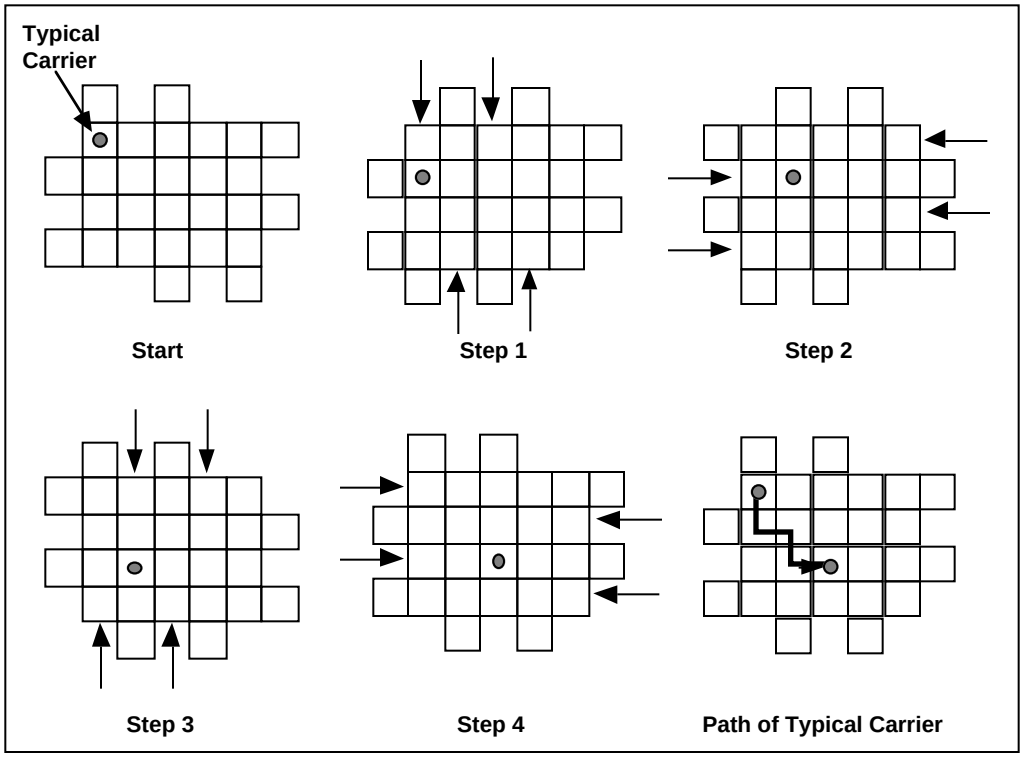


Figure 2-5. Four-step braiding process.

### *2.1.2.5 Warp Knits*

The multi-axial warp knit process ties yarns of primary fibers together in layers with 0°, ±45°, and 90° orientations. The knitting is done with fine polyester threads, which amount to a small percentage of the total weight. During knitting, the polyester threads are passed around the primary yarns and one another in interpenetrating loops (Fig. 2-6). The mechanical properties of the stack of layers can be controlled by selecting the yarn weight in each of the four orientations. The knitted stacks form building blocks which can be laminated to form the thickness desired for some structure. The knitted stacks can also be stitched together in a secondary operation. The major advantage of the knitting process is its low cost compared to conventional tape lay-up.

Stacks most commonly contain four oriented layers. However, a symmetric, seven layer stack may be preferred to control twist and bending in the final laminate.

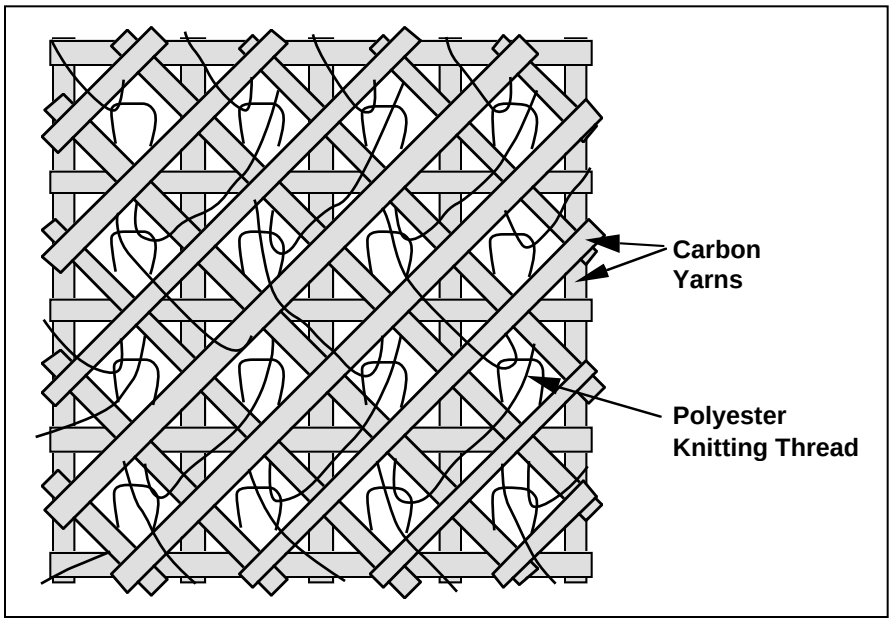


Figure 2-6. Multi-axial warp knit.

### *2.1.2.6 Stitching*

Stitching has been used for more than 20 years to provide through-thickness reinforcement in composite structures. It significantly enhances damage tolerance. The major manufacturing advance in recent years has been the introduction of resin transfer processes which allow one to stitch dry preforms, rather than prepreg material. This enhances speed, allows stitching through thicker material, and greatly reduces damage to the in-plane fibers.

As well as enhancing damage tolerance, stitching also aids fabrication. Many textile processes generate preforms that cannot serve as the complete structure. For example, bias plies usually must be attached to 0/90° weaves; or stiffeners to a skin. Stitching provides a mechanical connection between the preform elements before the resin is introduced, allowing the completed preform to be handled without shifting or damage. In addition, stitching compacts the fiber preform closer to the final desired thickness. Less mechanical compression need then be applied to the preform in the tool.

In many applications, strength and damage tolerance requirements would be satisfied by less than one volume percent of stitching fibers. However, the minimum volume of stitching is set by the fabrication process. While there is considerable latitude in stitch density, the lower bound in current technology sometimes exceeds the amount needed, thus unnecessarily sacrificing in-plane properties.

Two forms of stitching are of interest for structural applications; the modified lock stitch and the chain stitch (Fig. 2-7). The chain stitch uses only one stitching thread, whereas the lock stitch requires separate bobbin and needle threads. In the modified lock stitch, the thread tension is adjusted so that the knot forms on the outer surface of the laminate, rather than internally. This minimizes distortion of the laminate. The stitching parameters that may be controlled include the pitch between penetrations, the spacing between parallel rows of stitching, the stitching material, and the weight of the stitching yarn. Various stitching materials have been successfully demonstrated, including carbon, glass, and Kevlar, with Kevlar being the most popular. Yarn weights for Kevlar of between 800 and 2000 denier have been used. Stitching that contributes around 2% of the total areal weight of the completed fabric has usually been found to impart satisfactory damage tolerance (compression strength after impact).

### *2.1.3 Molding*

A key technology for making textiles practicable in composite structures is the ability to infuse a dry preform with a matrix. Numerous methods are available for this step. This handbook will focus on materials and processes suitable for polymer matrix composites. Other technologies such as vapor deposition have been developed for carbon-carbon, metal matrix, and ceramic matrix composites.

One approach to matrix infusion is called resin transfer molding or RTM (Fig. 2-8a). In this process, the preform is placed in a mold with the shape of the final part. A low viscosity resin is pumped in via a series of injection ports. Vent ports, connected to a vacuum pump, evacuate trapped gases and excess resin. The part is then cured at elevated temperature while still in the mold. In a successful RTM process, the preform is fully wetted with resin, but achieving full wetting can be challenging in a complex part. Resin flow is controlled by the permeability of the fiber preform and the viscosity of the resin. Permeability is higher for low fiber volume fractions, but of course high fiber volume is usually demanded to maximize structural performance. Despite this conflict, high quality parts have been made with fiber volume fractions exceeding 60%. Success often depends on having good process models to identify the optimum location of injection and venting ports.

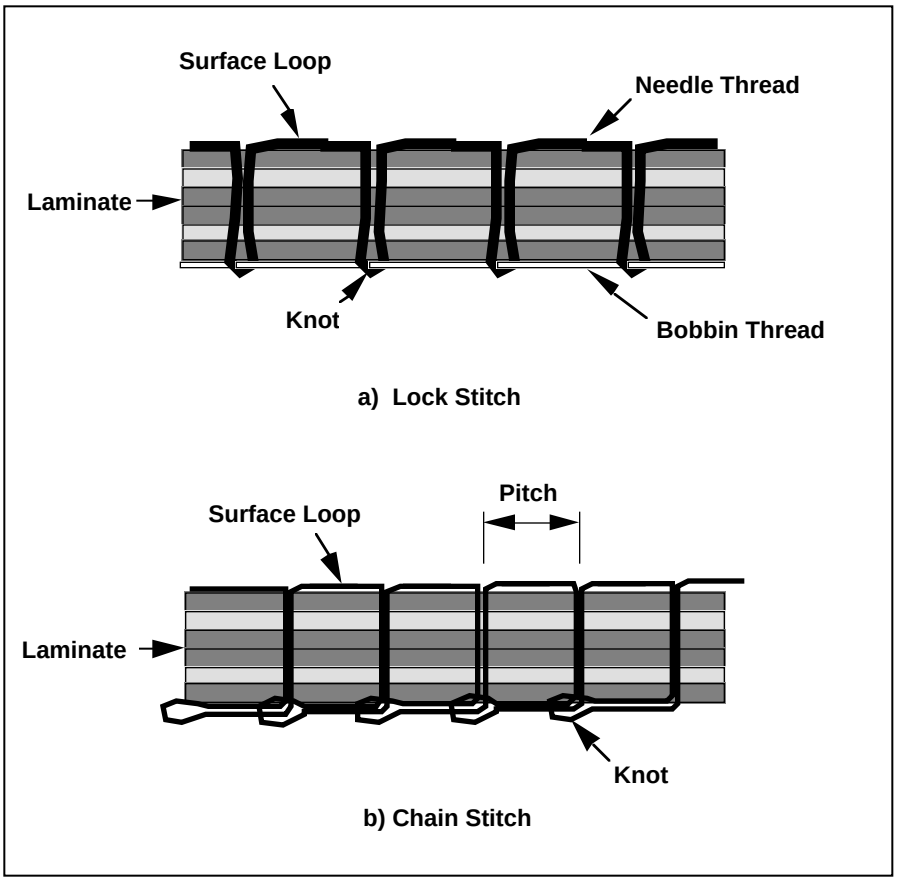


Figure 2-7. Types of stitching used for through-thickness reinforcement.

Another process is called resin film infusion (RFI) (Fig. 2-8b). In this process, solid sheets of resin material are placed next to the fiber preform. At cure temperatures, the viscosity of the resin drops dramatically and the resin flows through the thickness of the preform, wetting the fibers. Since the resin starts inside the tool, RFI allows the use of tooling methods developed for prepreg materials (single-sided tooling and vacuum bagging). The amount of resin is controlled by the number of sheets of resin used in a given area. The distance the resin needs to flow is usually less than in an RTM tool, which simplifies the problem of obtaining full wetting.

The RTM and RFI processes are both suitable for thermoset resin. Additional techniques are being developed for thermoplastic materials (Fig. 2-9, [2.5]). Thermoplastic materials can be spun into fibers. This offers the possibility of commingling the thermoplastic and reinforcing fibers to produce a hybrid yarn. The hybrid yarn is woven into a preform and placed into a tool. When heated, the thermoplastic fibers melt and form the matrix. Alternatively, the thermoplastic thread can be spun over the outside of the

reinforcing fiber bundle. In another process, the reinforcing yarns are coated with thermoplastic powder.

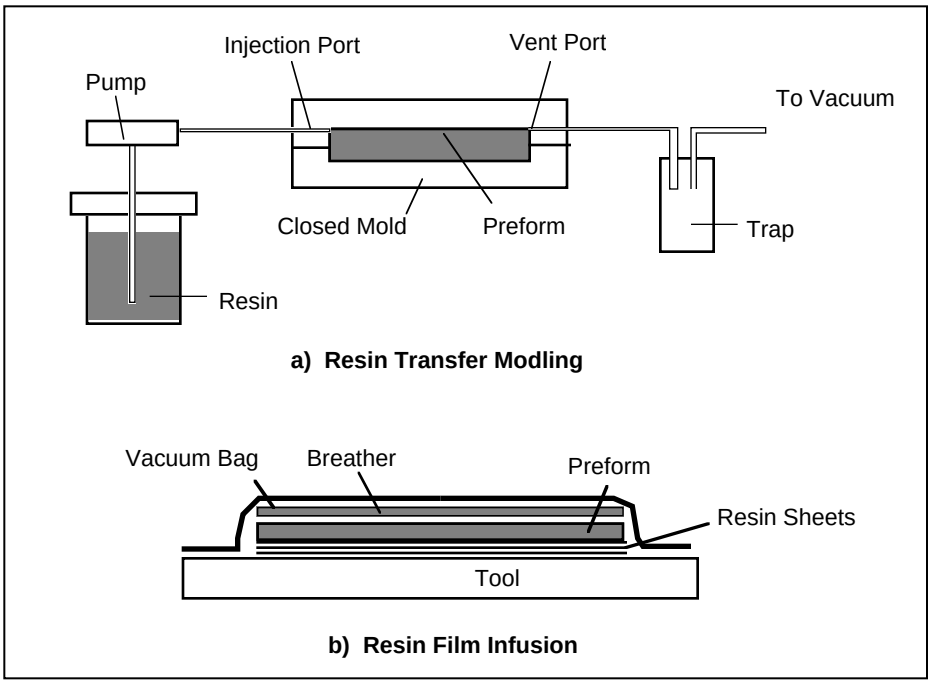


Figure 2-8. Resin infusion techniques

## 2.2 Materials

Textile processes have been adapted to handle most of the fibers commonly used in structural composites, including glass, aramid, and carbon. The only limitation to fiber selection is that most textile processes subject yarns to bending and abrasion. Machines have been modified to minimize fiber damage, but, in many processes exceptionally brittle or stiff fibers cannot be used.

Important properties of some popular fibers are shown in Table 2.1, with the usual assumption that they are transversely isotropic. Axial properties were obtained from manufacturers' data sheets. The transverse properties have been estimated indirectly by various techniques, since they cannot be measured by conventional mechanical tests. For example, there is a relationship between the axial and transverse moduli of a carbon fiber, which arises from the degree of alignment of the graphite crystals that make up the fiber. Nonaxial properties can also be inferred by fitting micromechanical relations to the measured transverse properties of composites.

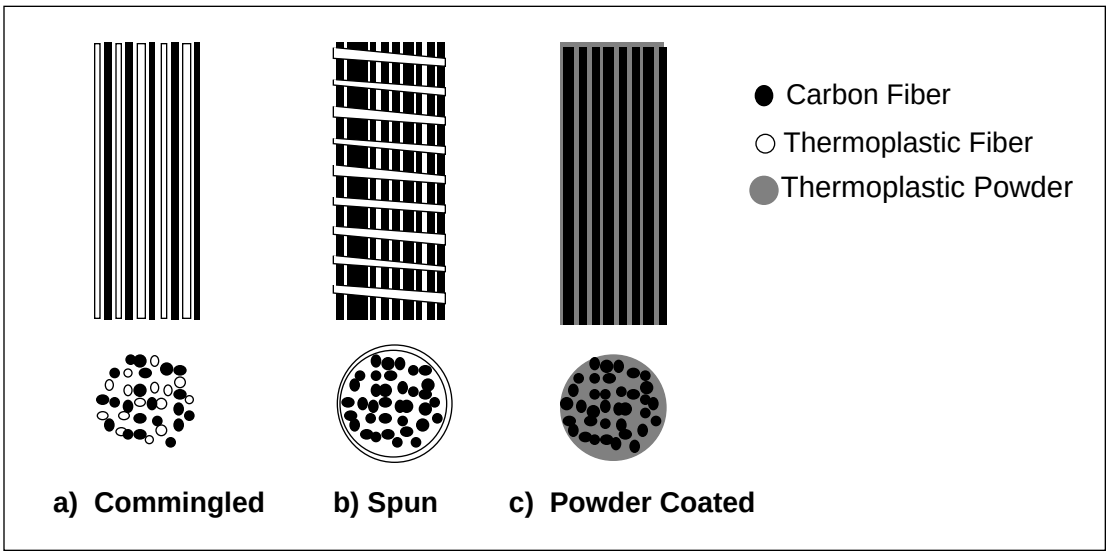


Figure 2-9. Techniques for using thermoplastics in textiles.

**Table 2.1 Fiber Properties**

| Name | Type | $E_A$ GPa | $E_T$ GPa | $G_A$ GPa | $\alpha_A$ $\mu$m/m-K | $k_A$ W/m-K | $\sigma^A_{Ten}$ MPa | $\sigma^A_{Comp}$ MPa | $\rho$ kg/m$^3$ |
|---|---|---|---|---|---|---|---|---|---|
| P100 | Pitch | 772 | 7 | 22 | -0.44 | 520. | 2440 | 700 | 2150 |
| T300 | PAN | 231 | 14 | 22 | -0.17 | 8.5 | 2970 | 2690 | 1770 |
| AS4 | PAN | 248 | 13 | 21 | -0.17 | 9.0 | 3490 | 2700 | 1800 |
| IM6 | PAN | 276 | 12 | 19 | -0.17 | 10.0 | 4500 | 2700 | 1770 |
| IM7 | PAN | 276 | 12 | 19 | -0.17 | 10.0 | 3940 | 2700 | 1740 |
| S-2 | Glass | 90 | 90 | 36 | 0.50 | 9.0 | 2990 | 1570 | 2490 |
| Kevlar-49 | Aramid | 112 | 7 | 3 | -1.50 | 0.04 | 3040 | 1050 | 1440 |

A - Axial, T - Transverse, $\sigma_A$ - Axial strength, $k_A$ - Axial thermal conductivity

The size of the yarn into which fibers are bundled is a very important parameter in a textile composite. Yarn size is expressed as a filament count (the number of fibers, usually in thousands or K); or as a linear density, either the denier (the number of grams in 9000 m of yarn) or the yield (length per unit mass). Table 2.2 shows the relation between these parameters for two carbon fibers and an aramid fiber. The nominal diameter of a circular yarn is based by convention on an assumed packing fraction (area of fibers over area of the circle) of 0.75. (This aasumption should not be carried into models of composite properties. Fiber volume fractions should always be measured. See Sect. 5.)

In the traditional textile industry, yarns are twisted to provide structural integrity and the ability to hold shape. In forming structural composites, in contrast, softer yarns are desirable, since this allows compaction to maximize the total volume fraction or flattening (especially in braids) to maximize coverage. Furthermore, twist would reduce the axial stiffness of yarns, which is paramount in airframe applications. Therefore, yarns with minimal or nominally zero twist (tows) are preferred.

Epoxy resins have been the predominant matrix in textile composites manufactured by RTM or RFI for commercial aircraft structures. Epoxies meet the requirement of having a low-viscosity state (100-500 cps), which is crucial for flow through a low permeability preform with complete wetting of the fibers. Some epoxies that have been used in prepregs, e.g. Hercules 3501-6 and 3502, have also been used for the RTM process (see Section 2.1.3). The extensive data available from their use in prepregs has made them attractive choices. There are now also a number of resins that have been especially formulated for RTM, including 3M PR-500, BP Chemical E-905L, and Shell RSL-1895.

PEEK is a typical thermoplastic for manufacture via commingling or spinning a matrix onto yarns, as described in Section 2.1.3.

**Table 2.2 Typical Yarn Weights and Dimensions**

| Fiber | Filament count | Area of Fibers ($mm^2$) | Diam. of Circular Yarn with $p_d$ = 0.75 (mm) | Denier (g/9000m) |
|---|---|---|---|---|
| Hercules AS4 | 3K | 0.12 | 0.45 | 1990 |
| Dia = 7.1 µm | 6K | 0.24 | 0.64 | 3980 |
| Density = 1850 $kg/m^3$ | 12K | 0.48 | 0.90 | 7960 |
| | 30K | 1.19 | 1.42 | 19900 |
| | 75K | 2.98 | 2.25 | 49800 |
| Hercules IM6 | 3K | 0.07 | 0.35 | 1190 |
| Dia = 5.6 µm | 6K | 0.15 | 0.50 | 2380 |
| Density = 1800 $kg/m^3$ | 12K | 0.29 | 0.71 | 4770 |
| | 30K | 0.74 | 1.12 | 11900 |
| | 75K | 1.84 | 1.77 | 29800 |
| Du Pont Kevlar 49 | 1K | 0.11 | 0.44 | 1450 |
| Dia=11.9 µm | 2K | 0.22 | 0.62 | 2900 |
| Density = 1440 $kg/m^3$ | 3K | 0.34 | 0.75 | 4350 |
| | 4K | 0.45 | 0.87 | 5800 |

## 2.3 The Geometry of Textile Reinforcement

### *2.3.1 Ideal geometry*

#### *2.3.1.1 Unit Cells*

The geometry of a periodic textile is conveniently described in terms of unit cells, following the example of crystallography ([2.6]; see also section 5.1.5). The unit cell is defined by the requirement that the entire textile can be constructed from spatially translated copies of it, without the use of rotations or reflections. The unit cell is not unique. Nevertheless, as in crystallography, symmetry in the textile usually suggests a preference.

#### *2.3.1.2 2D Weaves*

Weaves may be classified by the pattern of interlacing. The simplest pattern is the plain weave shown in Fig. 2-10(a). A disadvantage of the plain weave is the frequent exchanges of position from top to bottom made by each yarn. This waviness or yarn crimp reduces the strength and stiffness of the composite. Other weave patterns reduce the number of exchanges and increase the lengths of straight segments of yarn (known as the “float”). Of particular interest are the satin weaves shown in Fig. 2-10(b), (c), and (d). The satin weave pattern is defined by the number of yarn widths between exchanges. For example, the five harness satin weave shown in Fig. 2-10(c) has a 4-over, 1-under pattern. In addition, the exchanges are arranged so as not to connect; or in the case of the crow's-foot pattern (Fig. 2-10(b)), so as not to lie on continuous diagonals.

Individual layers of satin weave fabric are asymmetric. One side of the fabric is predominantly warp yarns; the other fill. Exchange sites also break symmetry because they bend yarns in an asymmetric way. Bending and stretching in a satin weave ply are consequently coupled. There is also coupling between stretching and in-plane shear, because exchange locations are not symmetric about either in-plane axis (Fig. 2-11). Coupling between bending and stretching will tend to cause warping during cure because of thermal strains. Warping can be minimized in a multilayer laminate by considering which side of each ply should face the tool.

The selection of a weave involves manufacturing considerations as well as final mechanical properties. The type of weave affects dimensional stability and the conformability (or drape) of the fabric over complex surfaces. Satin weaves, for example, exhibit good conformability. Unfortunately, good conformability and resistance to shear

are mutually exclusive. Thus, while woven fabrics are frequently the material of choice for complex geometries, the designer must be aware that specified material directions may be impossible to maintain on a doubly curved surface; and initially orthogonal yarns may not remain orthogonal in the fabricated product.

Most 2D weaves involve two orthogonal directions of yarn, implying weak in-plane shear resistance within a single ply. However, triaxial weaves, in which the yarns form 60° angles to each other, have also been fabricated (Fig. 2-12, [2.5]). A single ply of triaxial material would have approximately isotropic in-plane elasticity.

*2.3.1.3 2D Braids*

Figure 2-13(a) shows the interlacing pattern for a ±θ bias braid. Structurally, a 1x1 braid with yarns oriented at ±45° is indistinguishable from a plain weave rotated by 45°. (In a 2D braid, the designation "nxn" refers to the number of bias yarns between crossover points.)

Longitudinal or axial yarns can be introduced into the braiding process to create a triaxial braid. The axial yarns are trapped within the crossovers of the bias yarns. In principle, the axial yarns can remain straight, and therefore retain much of their unidirectional properties. By controlling the relative size of the axial yarns and the angle of the bias yarns, a wide range of final properties can be obtained. As with woven fabrics, the pattern of crossovers can be controlled. Figures 2-13(b), (c), and (d) show three possible patterns for triaxial brads. These figures show the braid patterns with gaps between the yarns for clarity; the actual braid would normally have complete coverage.

Applications for braids can be limited by the size of the braiding machines available. A large braider has 144 yarn carriers and a bed diameter of 2.25 m. Often, full coverage of the mandrel by the bias yarns alone is required on each pass to minimize gaps and resin pockets in the structure. Full coverage is obtained when [2.7]

$$w_b/\cos\theta = P/2N \tag{2.1}$$

where $w_b$ is the width of a bias yarn as it lies on the mandrel, $P$ is the perimeter of the mandrel, $N$ is the number of bias yarn carriers in operation, and $\theta$ is the angle between the bias yarns and the longitudinal axis of the structure. A less severe constraint is for full coverage on a pass including the area covered by the axial yarns. In that case, full coverage is obtained when

$$w_L + w_b / \cos\theta = P / 2N \tag{2.2}$$

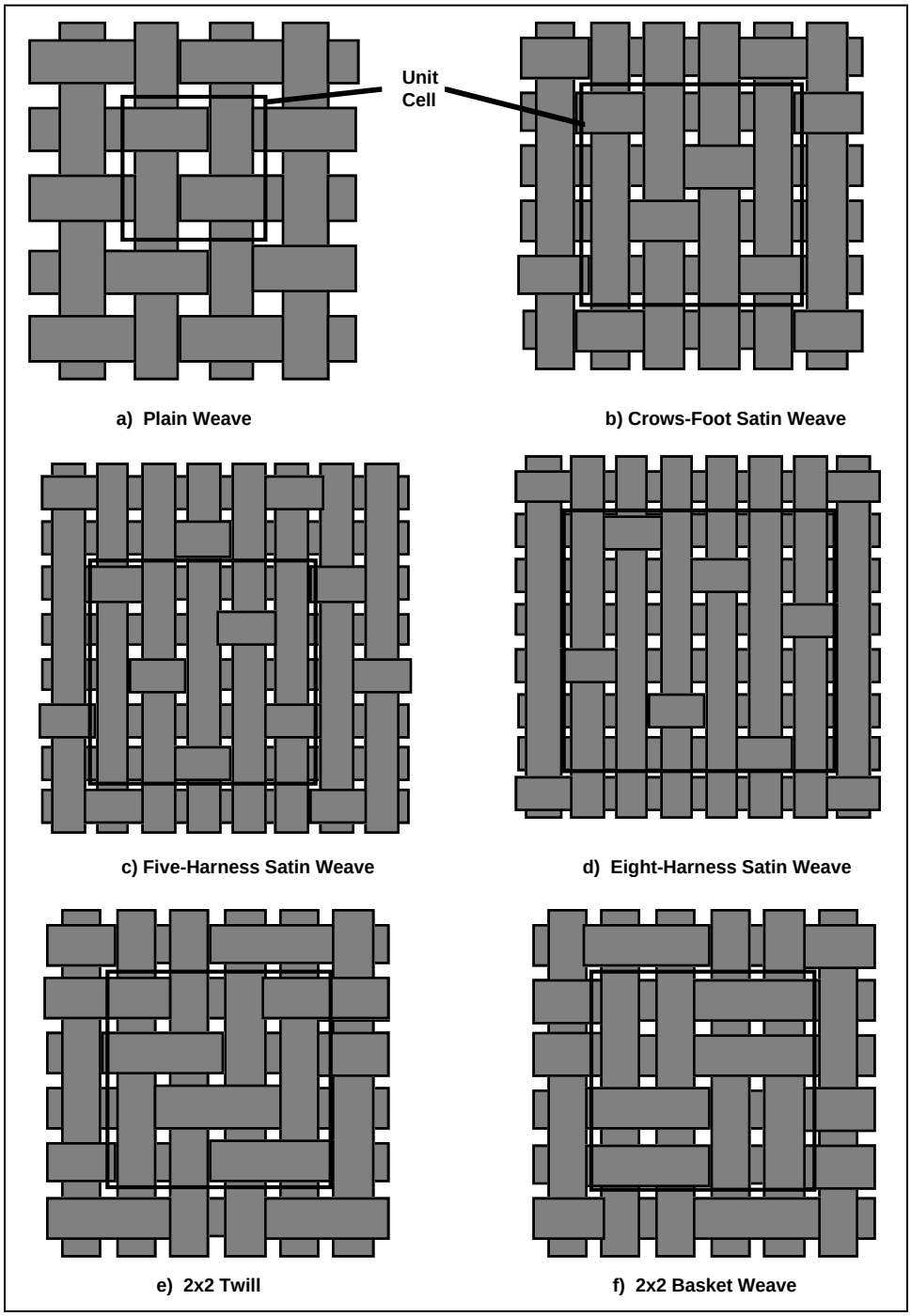


Figure 2.10. Commonly used 2D weave patterns.

where $w_L$ is the width of an axial yarn. The maximum width of the yarns is controlled by several parameters, including the linear density of the yarn, the degree of twist (twisting a

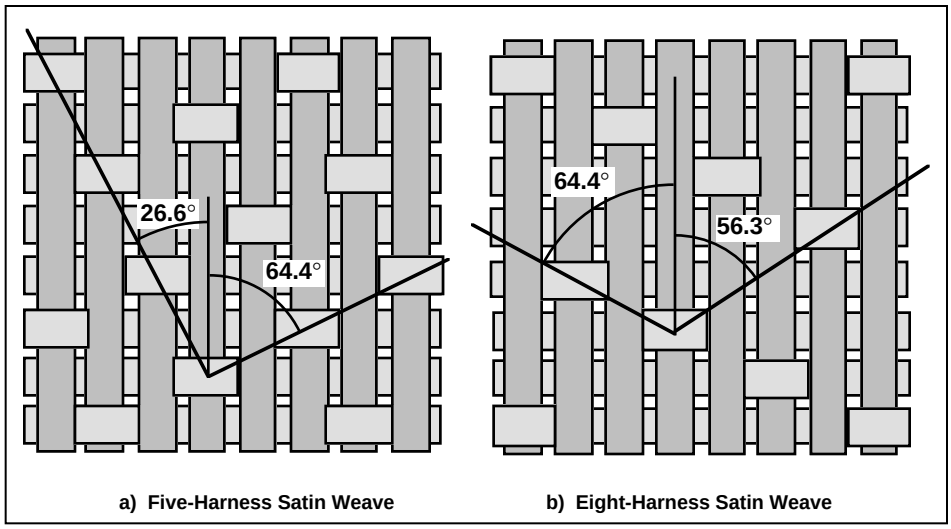


Figure 2-11. Angles of the diagonal patterns formed by exchange locations.

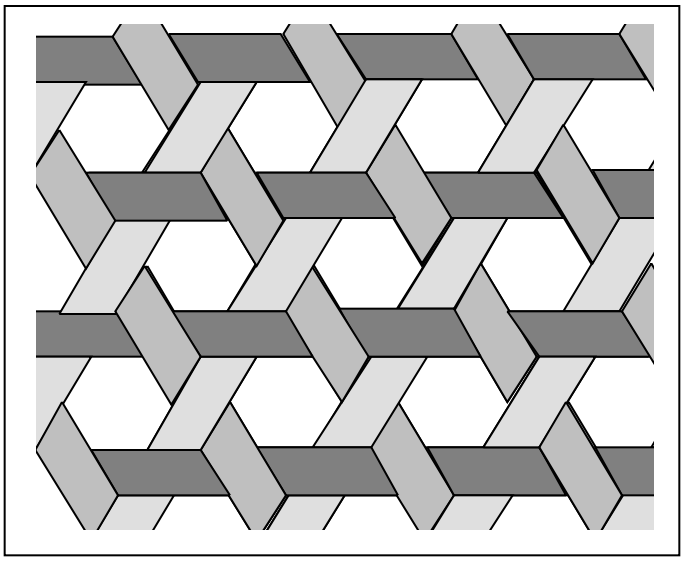

Figure 2-12. Triaxial weave.

yarn tends to prevent flattening), and the size of the carrier guides. The last factor imposes an upper limit to the width of approximately 5 mm [2.7]. Reference [2.5] reports a maximum width for a 6K carbon yarn of 1.9 mm; and 3.0 mm. for a 12K yarn.

The minimum and maximum braid angles are limited by the phenomenon of jamming, which is related to the maximum shear distortion that can be put on a fabric. Jamming also limits the ratio of the minimum and maximum radii of the mandrel.

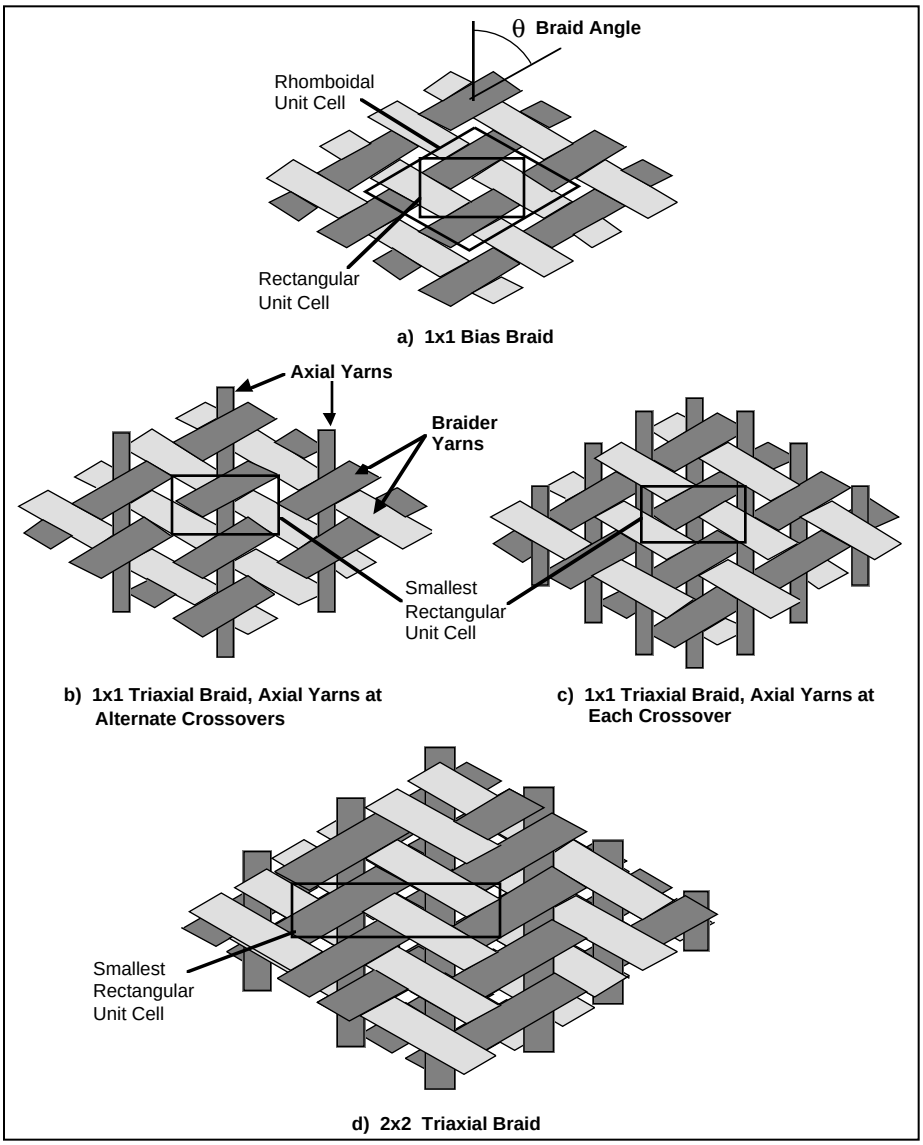


Figure 2-13. Some common 2D braid patterns.

The total thickness of a braided part may be controlled by overbraiding, in which multiple passes of the mandrel are made through the braiding machine. This lays down a series of nearly identical layers, similar to a lamination. For 2D braiding, there is no mechanical connection between the layers.

A convenient notation for triaxial braids is

$$[0_{nK} / \pm\theta_{mK}]\ Y\%\ \text{Axial}$$

where *n* is the size of the axial yarns in thousands of fibers (K), *m* is the size of the bias (or braider) yarns, and *Y* is the percentage of axial yarns in the preform. For example,

$$[0_{30K} / \pm 70_{6K}]\ 46\%\ \text{Axial}$$

indicates a braid with 30K axial yarns and 6K bias yarns, with 46% of the total fiber volume in the axial yarns, and a braid angle of 70°. While this notation does not convey many details of the fabric geometry, it suffices for estimates of properties based on modified 2D laminate theory.

*2.3.1.6 3D Interlock Weaves*

A 3D weave contains multiple planes of nominally straight warp and weft yarns that are connected together by warp weavers to form an integral structure. The most common classes are shown in Fig. 2-14. Within each class, there are several parameters that can be varied.

Angle interlock weaves can be categorized by the number of layers that the warp weavers penetrate. Figure 2-14(a) shows a through-the-thickness interlock fabric, in which the warp weavers pass though the entire thickness. Figures 2-14(b) and (c) show layer-to-layer interlock patterns, where a given weaver connects only two planes of weft yarns, but the weavers collectively bind the entire thickness. Various intermediate combinations can be fabricated, with the weavers penetrating a specified number of layers.

In orthogonal interlock weaves, the warp weavers pass through the thickness orthogonal to both in-plane directions, as shown in Fig. 2-14(d).

Interlock weaves are sometimes manufactured without straight warp yarns (stuffers) to produce a composite reinforced predominantly in one direction. They may also be fabricated with weft rather than warp yarns used for interlock.

A major limitation of 3D weaves is the difficulty of introducing bias direction yarns to achieve in-plane isotropy. One solution is to stitch additional 2D fabric plies oriented at ±45° onto the woven preform.

### *2.3.1.7 3D Braids*

An extension of braiding technology is the 3D braid, in which the braiding yarns interlock through a volume of material. There are no distinct layers in a 3D braid. A 3D

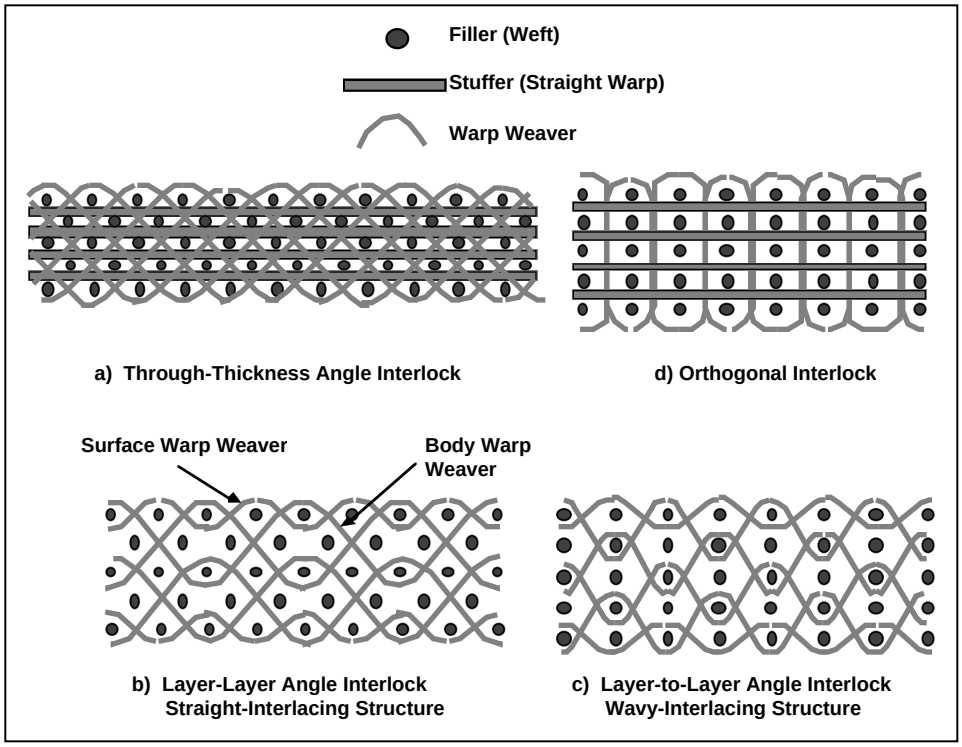


Figure 2-14. Three-dimensional weave patterns.

braid is also generally nonlaminar, although, as with a 2D braid, nominally straight axial yarns may be introduced to improve the stiffness and strength in one direction.

A 3D braiding machine can be set up to produce near net-shape matching to the cross-section of the final part. Typical stiffener cross-sections, such as "I" and "T" shapes can be produced.

### *2.3.1.8 Orthogonal Nonwoven Composites*

There is a long history of 3D, non-woven reinforcements, primarily in carbon-carbon composites. Orthogonal 3D materials are fabricated by fixing a series of yarns in one direction (or rods which will later be withdrawn and replaced by yarns), and then inserting planar yarns in the two orthogonal directions around the fixed yarns. Figure 2-15 shows a typical arrangement of fiber bundles that might be obtained in this process. Unlike other textile forms, the reinforcement remains relatively straight throughout the preform in

all directions. This pattern of reinforcement requires volumes of pure matrix material to fill the substantial interstitial areas created by the fiber bundles. The problem of shaping and arranging straight elements in several directions while maximizing the volume they occupy is an interesting one [2.8].

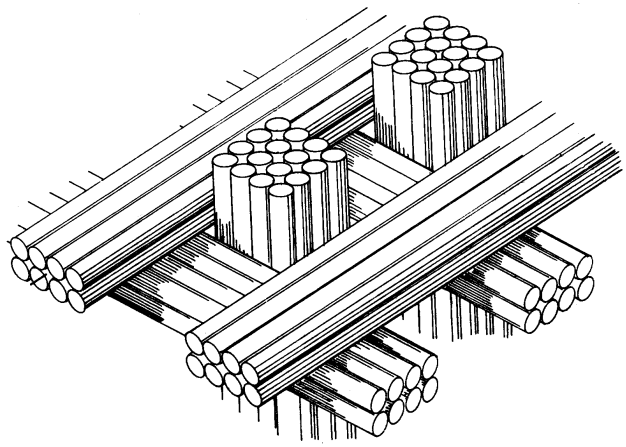

Figure 2-15. 3D orthogonal composite.

The concept of multiple direction linear reinforcement can be extended to a larger number of non-orthogonal fiber bundle orientations. These are termed nD materials (in a somewhat loose use of the term dimension!) For example, a 4D material could be created with fiber directions that connect the diagonal corners of a cube. There can be significant strength advantages to using a 4D or 5D material when shear and multidirectional loading are considered [2.9].

### *2.3.2 The relation of volume fraction and fabric geometry to process parameters*

The properties of textile composites depend most of all on the total volume fraction of all fibers and the proportions of the fibers that point in various directions. These characteristics can be predicted with useful accuracy by fairly simple models of the fabric geometry.

#### *2.3.2.1 2D Weaves*

Crucial properties of a 2D weave include yarn paths, cross-sectional shapes, and the pattern and geometry of exchange points. Calculations of these characteristics from

simple geometric models have been presented in Refs. [2.10] through [2.13]. The following illustrative formulae for a plain weave are reproduced from Ref. [2.10].

Consider a 2D plain weave composite. Assume that the fabric has full coverage, i.e., there are no gaps between the yarns; and that the yarn spacing and fiber counts are equal in the fill and warp directions. The yarn cross-sectional area, $A$, can be determined from

$$A = \frac{\pi d_f^2 n}{4 p_d} \tag{2.3}$$

where $d_f$ is the filament diameter, $n$ is the yarn filament count, and $p_d$ is the yarn packing density. The yarn packing density can be measured using photomicrographs of sections. Typical values are in the range 0.7 - 0.8.

Alternatively, if one knows the linear density of the dry yarn, $D_y$, then

$$A = \frac{D_y}{\left(9\times10^5 \rho_f p_d\right)} \tag{2.4}$$

where $D_y$ is in denier (g/9000 m), and $\rho_f$ is the fiber density (g/cm$^3$).

The overall fiber volume fraction for the unit cell shown in Fig. 2-16 is

$$V_f = \frac{2 p_d A}{H a} \tag{2.5}$$

where $a$ is the yarn spacing, controlled during fabrication by fixing the number of yarn carriers over the fabric width; and $H$ is the cell height, usually equated to the cured layer thickness specified by the manufacturer. Often, the areal weight of the dry fabric, $w_a$, is specified in g/m$^2$, and in this case

$$w_a = \frac{2D_y}{9000a} \quad . \tag{2.6}$$

The yarn thickness, $t$, is related to $H$ by $t = H/2$. For full coverage, the yarn width, $w$, must equal the yarn spacing.

The path taken by each of the four yarns in the unit cell consists of two straight portions and three curved portions (Fig. 2-16). The curves are commonly assumed to be sinusoidal, with the $z$-coordinate of the yarn centerline expressed as

$$z_c = \pm \frac{t}{2} \mathrm{Sin}\left( \frac{\pi x_c}{L_u} \right). \tag{2.7}$$

where $x_c$ is measured from the cross-over. The yarn cross-section shown in Fig. 2-16 consists of a straight central portion, with sinusoidal, lenticular ends. If the area of this shape is known (from eqs. 2.3 or 2.4) then the shape parameter $L_u$ (defined in Fig. 2-16) can be determined by

$$L_u = \frac{A - wt}{\left( \frac{2}{\pi} - 1 \right) \frac{t}{2}} \tag{2.8}$$

Textile composites are often characterized by the "crimp angle", $\theta_c$. This is the maximum angle the yarn makes with respect to the $x$-$y$ plane (Fig. 2-16). From the simple geometric description just given, the crimp angle must be given by

$$\theta_c = \mathrm{Tan}^{-1}\left( \frac{t\pi}{2L_u} \right) \tag{2.9}$$

The constraint $w \geq L_u$ imposes a minimum value for $\theta_c$.

The yarn cross-sections and crossover points are similar for satin weave fabrics. The distinguishing characteristic is the longer straight segments of yarn.

*2.3.2.2 2D Braids*

A simplified description of the unit cell geometry for a bias and a triaxial braid is given in Ref. [2.10]. The formulation is similar to that given for the plain weave in the previous section. However, because the yarns interlace at nonorthogonal angles, the equations are more complex. They are not reproduced here.

More advanced process models attempt to predict the yarn cross section from the mechanical interactions between yarns as the textile is formed. One such model includes the twisting that must occur when yarns cross at non-orthogonal angles [2.14]. However, even advanced models assume relatively simple forms for cross sections.

*2.3.2.3 3D Weaves*

Even though unit cells can be quite large because of the complex patterns preferred for the phases of warp weavers, geometric idealizations for 3D interlock weaves are quite

simple. The idealizations are relatively simple because most warp and weft yarns are nominally straight.

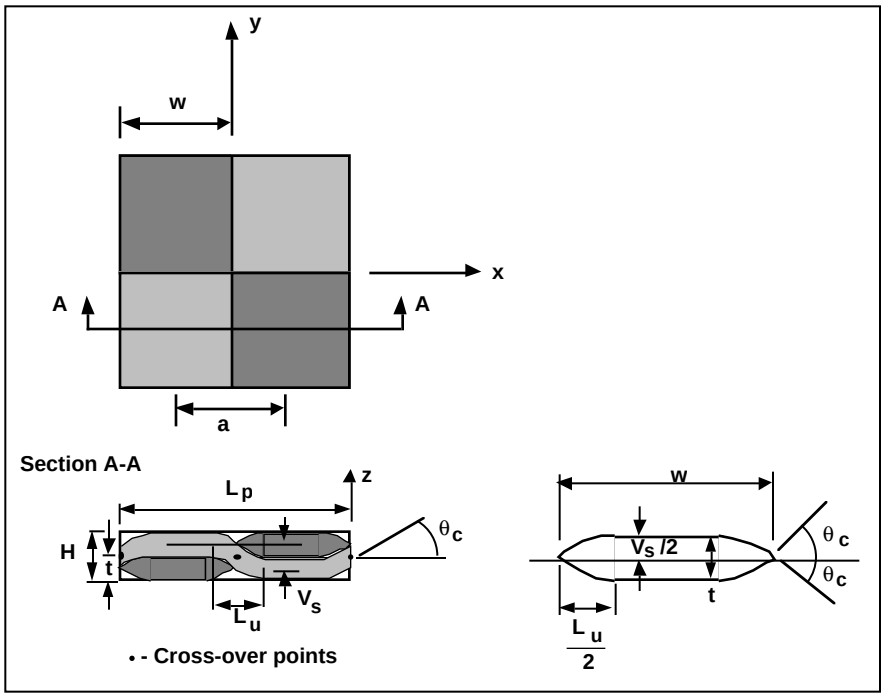


Figure 2-16. A unit cell for a plain weave.

In a composite of thickness $t$ with $n_s$ layers of stuffers alternating with $n_f$ layers of fillers, the volume fractions of fibers in stuffers and fillers are simply

$$V_s = e\, n_s /[y_s\, \rho_f\, t] \tag{2.10a}$$

and

$$V_f = p\, n_f /[y_f\, \rho_f t] \tag{2.10b}$$

where $e$ is the number of ends (stuffers) per unit length in the weft direction and $p$ is the number of picks (fillers) per unit length in the warp direction; $y_s$ and $y_f$ are the yields of the stuffers and fillers; and $\rho_f$ is the fiber density. The volume fraction of the warp weavers can be written

$$V_w = e\, n_w\, c_w/[y_w\, \rho_f\, t] \tag{2.10c}$$

where $n_w$ is the number of warp weavers between successive columns of stuffers, $y_w$ is the yield of warp weavers, and $c_w$ is a crimp or take-up factor. In principle, $c_w$ is computed simply as the ratio of the integrated path length of a warp weaver to its projected length in

the warp direction. In practice, $c_w$ is difficult to predict a priori, because the paths of warp weavers in the finished product vary greatly with process parameters. Experimentally determined values are typically between 1.1 and 1.3 for layer-to-layer angle interlock weaves, near 1.5 for through-the-thickness angle interlock weaves, and between 2 and 5 for orthogonal interlock weaves [2.15].

#### *2.3.2.4 3D Braids*

Various process models have been derived to describe the complex unit cells of 3D braids (see [2.16-2.20]). The following simple expressions were given in [2.18] for the 4-step, 1x1 braid (without inlaid axial yarns).

The 4-step, 1x1 braiding pattern produces the 3D unit cell shown in Fig. 2-17. The yarns in the unit cell are inclined in 4 directions; 2 parallel to surface ABDC, and 2 parallel to surface CDEF, as shown in the accompanying diagram. These surfaces are cut at 45° angles to the surface of the fabric.

Consider a rectangular array of yarn carriers, with $m$ columns and $n$ rows in the array. The total number of required yarns, $N$, is

$$N = (m+1)(n+1)-1 \tag{2.11}$$

The number of machine cycles required for all the yarn carriers to return to the original positions is given by $N/G$, where

$$G = m\,n/R_{mn} \tag{2.12}$$

with $R_{mn}$ the least common multiple of $m$ and $n$. The normalized cycle length, $h_d$, is defined as the fabric length produced in one cycle, divided by the diameter of the yarn, which is assumed to remain circular. The cycle length cannot be easily predicted, because it is a function of the beat-up.

The angle formed by internal yarns, $\gamma$, is given by

$$\gamma = \arctan(4/h_d) \quad . \tag{2.13}$$

Equation (2.12) is valid up to an angle of 55° ($h_d$ = 2.8), beyond which jamming is predicted. A plot of the fiber inclination angle versus $h_d$ is shown in Fig. 2-18.

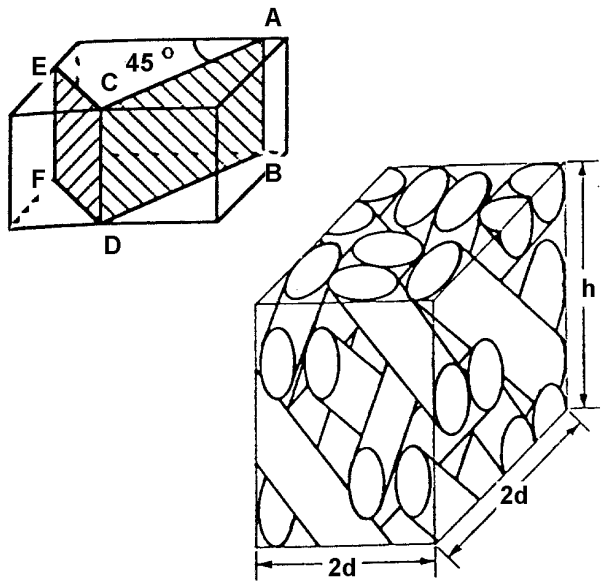


Figure 2-17. 3D unit cell for 1x1, 4-step braid.

Because yarn carriers on the surface of the rectangle travel less distance in a given cycle, the surface yarns incline at different angles. Furthermore, the apparent angle seen on the surface of a braid is actually the projection of the angle of inclination onto the plane of the surface. The relations between the surface yarn angle of inclination, $\beta$, the projected surface angle, $\alpha$, and the internal yarn angle of inclination, $\gamma$, are

$$\tan \alpha = \tan \gamma / \sqrt{8} = \tan\beta / \sqrt{5} \tag{2.14}$$

The yarn volume fraction is

$$V_y = \pi \sec(\gamma)/8 \tag{2.15a}$$

or

$$V_y = \pi\sqrt{h_d^2 + 16} / (8h_d) \tag{2.15b}$$

These relations are shown in Fig. 2-19.

The ratio of surface yarns to internal yarns is a function of the aspect ratio of the rectangle, $m/n$, and the total number of carriers, $N$. Figure 2-20 shows this relationship for a series of aspect ratios.

Given the circular yarn assumption, the width of the preform depends only on the number of yarns arranged on a side, *k*, and the diameter of the yarns, *d*. It is given by

$$w_k = (2^{1/2}\, k + 1)\, d \quad . \tag{2.16}$$

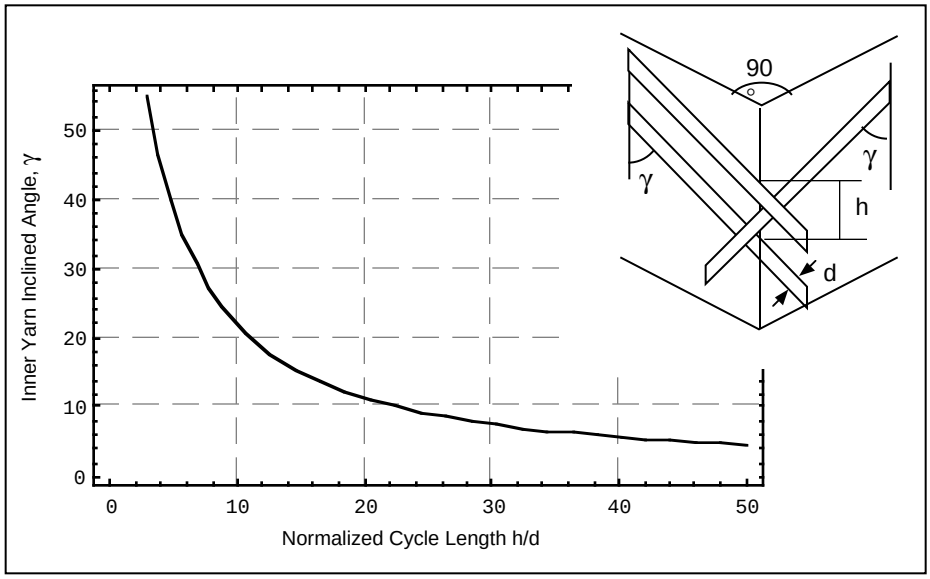


Figure 2-18. Inner yarn angle of inclination versus cycle length for 1x1, 4-step braid.

### *2.3.3 Irregularity*

The ideal geometry popularized in schematics of textiles, viz. a collection of straight tow segments and smoothly curved arcs of tows, with regular tow spacings and well-formed periodicity, is never realized in practice. The rigors and complexity of textile manufacture and the distortions caused by handling preforms and forcing them to conform to molds always introduce significant geometrical irregularity. Irregularity usually has a measurable effect on elastic properties [2.15,2.21,2.22]; and a dominant effect on strength, fatigue life, and all properties related to damage mechanisms and work of fracture [2.22-2.26].

Geometrical irregularity is manifested in many ways. The following list is indicative but not exhaustive.

1. Tow spacing. Inconsistency in tow tensioning during the textile process and handling of preforms after fabrication often results in uneven spreading or compacting of tows. Uneven spreading is indeed geometrically necessary when a flat preform is draped over a

surface that possesses curvature about more than one axis (requiring a nondevelopable transformation of shape).

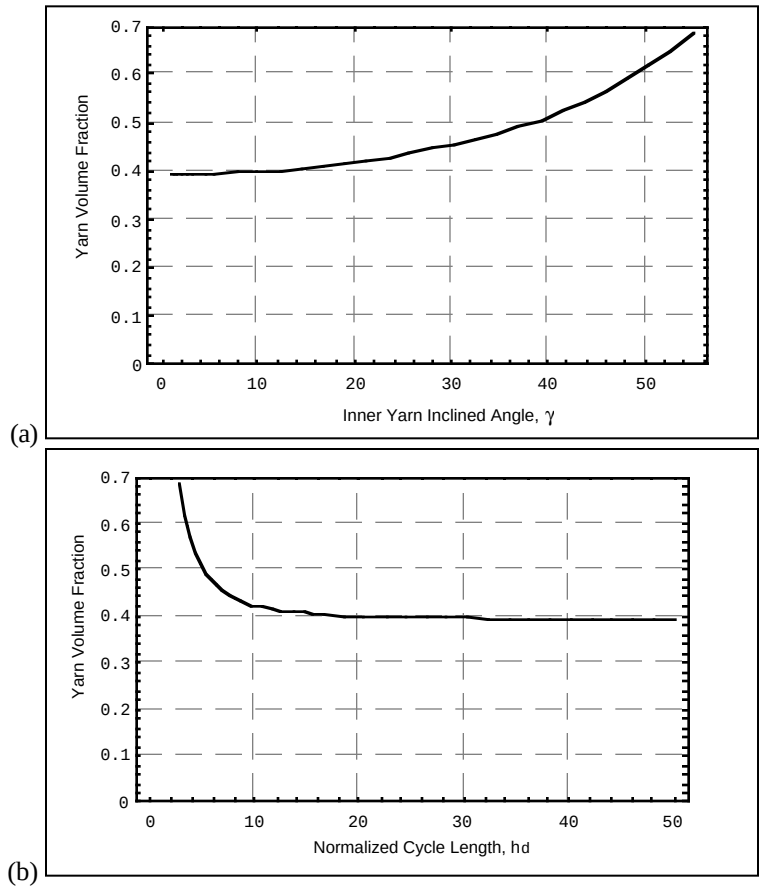


Figure 2-19. (a) Yarn volume fraction versus (a) inner yarn angle of inclination and (b) normalized cycle length for 1x1, 4-step braid.

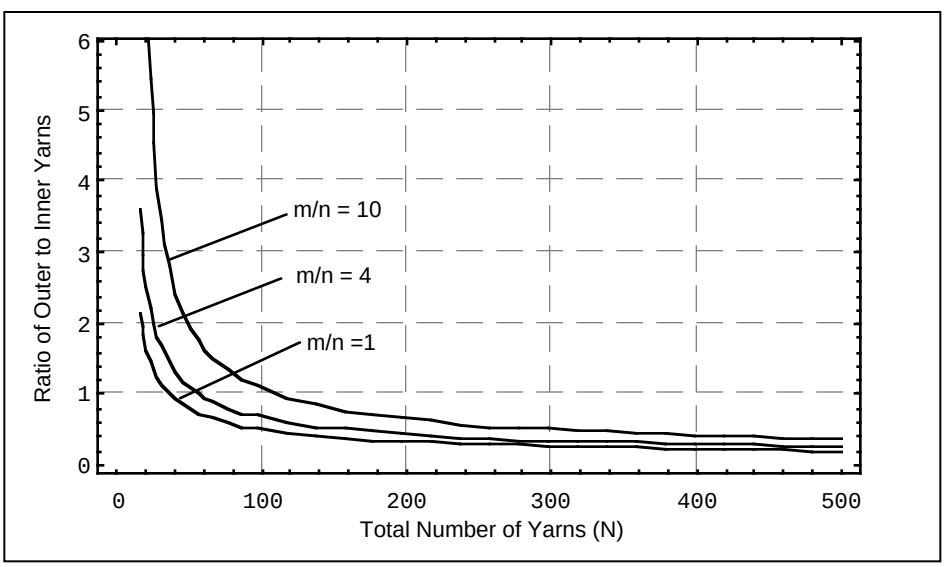


Figure 2-20. Ratio of outer (surface) yarns to inner yarns.

2. Tow waviness. Nominally straight tows, which are highly desirable in stiffness critical applications, always exhibit some degree of waviness. Fig. 2-21 shows waviness in the through-thickness direction typical of triaxial braids, in which the axial tows are nominally straight, and interlock weaves, which contain nominally straight stuffers. The misalignments even in quasi-laminar textiles are usually considerably greater than in tape laminates. Tow waviness tends to be commensurate with the spacing of tows that traverse the subject tow, but waviness deflections are not periodic. Tow misalignment has been described by normal distributions [2.15, 2.21] and power spectra [2.27,2.28]. In flat panel specimens of quasi-laminar textiles, out-of-plane tow waviness is often the larger component and is directly correlated with failure mechanisms ([2.21, 2.23, 2.24, 2.25] and Section 4), but in-plane waviness can also be significant.

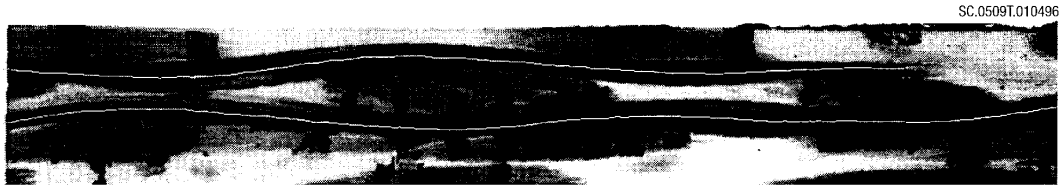


Fig. 2-21. Waviness in nominally straight axial tows in a triaxial braid. The fine white curves mark the centers of mass of nominally straight axial tows determined by digital image analysis.

Tow waviness can be especially pronounced in through-thickness tows in quasi-laminar textiles, e.g., stitching tows or warp weavers in an interlock weave. Through-thickness tows are very vulnerable to the through-thickness pressure that is favoured in consolidating plate-like parts to enhance the in-plane fiber volume fraction (Fig. 2-22). Waviness in through-thickness tows can only be controlled by forming the textile preform as nearly as possible to its desired final thickness before the consolidation process.

3. Tow pinching. In all textiles, the cross-sectional aspect ratios of tows are not uniform along their axes. Each tow is subjected to irregular pressures imposed by neighboring tows during both manufacture of the textile preform and the consolidation process. Each tow is pinched in different directions at different points. The resulting cross-sectional variations are especially pronounced in textiles with predominantly curved tows. Fig. 2-23 shows tow outlines sketched from a photomicrograph of a 3D braid. Cross-sectional variations are also a major form of irregularity in textiles formed predominantly of nominally straight tows.

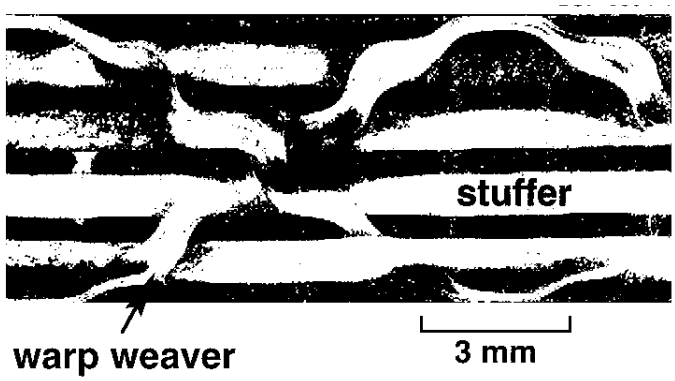


Fig. 2-22. Waviness induced in warp weavers in a 3D interlock weave by compression during processing.

Measuring geometrical irregularity in textile composites is very difficult; predicting it from process models probably impossible. Therefore, detailed knowledge of types and degrees of irregularity are not likely to become part of any practicable scheme for predicting strength and life. More reasonably, the degree of regularity should be correlated experimentally with process parameters, so that a maximum degree of irregularity can be guaranteed given sufficient quality control in composite fabrication. While irregularity is difficult to quantify, it dominates strength and fatigue life and therefore must be able to be bounded for textile composites to be regarded as reliable. Neither should any model of a textile be accepted as giving accurate predictions without an assessment of how irregularity would affect the outcome.

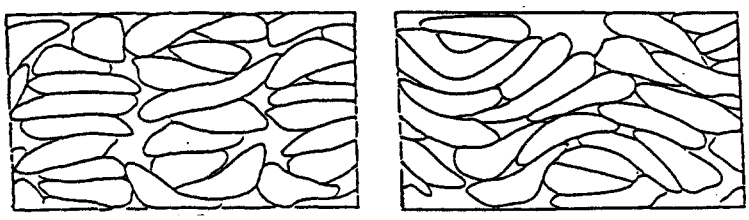

Fig. 2-23. Tracings of yarn cross-sections in a 3D braided composite (from [2.29]).

## 2.4 Integral Structures made by Textile Processes

The performance and manufacturing advantages of eliminating joints make integral structures a particularly exciting prospect in textile composite technology. Unfortunately, models for integral structures are not yet developed and they therefore receive little attention in the remainder of this handbook. A few examples are offered here in anticipation of future developments.

A weaving pattern does not need to be constant over the entire breadth or length of a fabric. By programming the loom, it is possible to have segments of a fabric that are not locked through the thickness along a specified plane. After weaving, the flat fabric may be unfolded to create a branched structure (Fig 2-24). This approach can be used to fabricate crossing stiffeners with continuous reinforcements passing through the intersection. The final yarn paths in the intersection are difficult to predict.

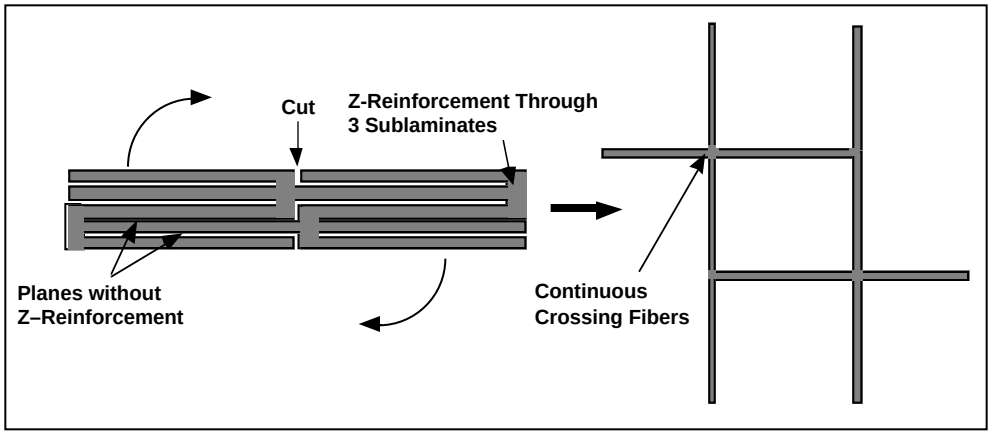


Figure 2-24. Use of 3D weaving to create a branched structure.

Figure 2-25 illustrates the use of weaving technology to produce an integral skin and stiffener assembly. The skin contains orthogonal warp and weft, as well as ±45° bias

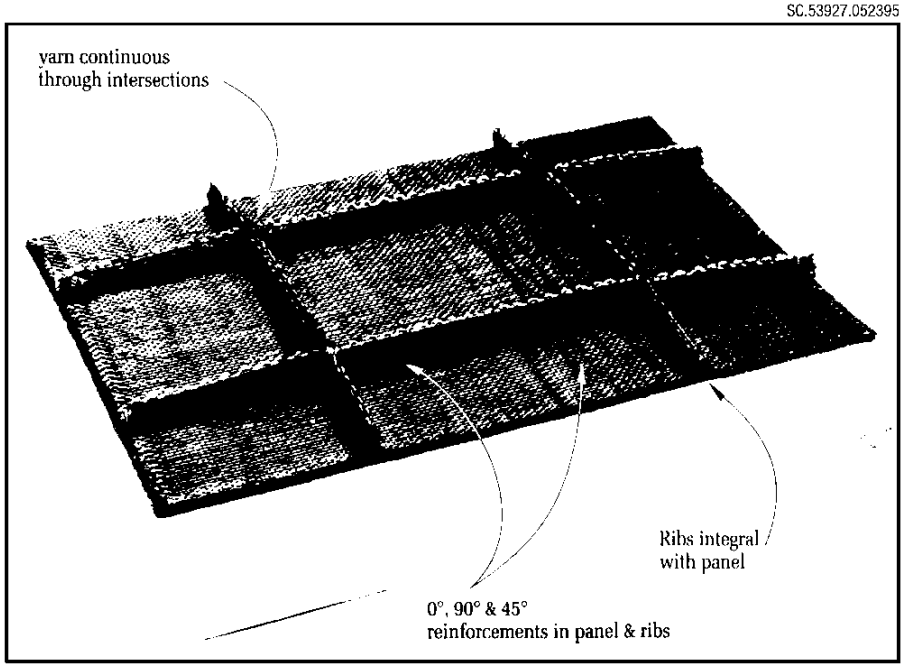


Figure 2-25. An integrally woven skin/stiffener preform. (Courtesy of Techniweave Inc.)

tows. These are all embraced by through-thickness reinforcement in an interlock architecture. The stiffeners are formed by the bias tows, which pass continuously from the skin up and over each stiffener in turn and back into the skin again. Thus the stiffeners and skin are formed in the same weaving process in an entirely integral manner. The part is finished to net shape by placing the preform in a mold, introducing matrix, for example by resin transfer molding, and curing.

Figure 2-26 shows a schematic of a skin and stiffener formed integrally by stitching. Once again, finishing can be accomplished by resin transfer molding and curing in a net shape tool. Alternatively, resin can be introduced by resin film infusion, which is the preferred process in the new McDonnell-Douglas stitched wing program.

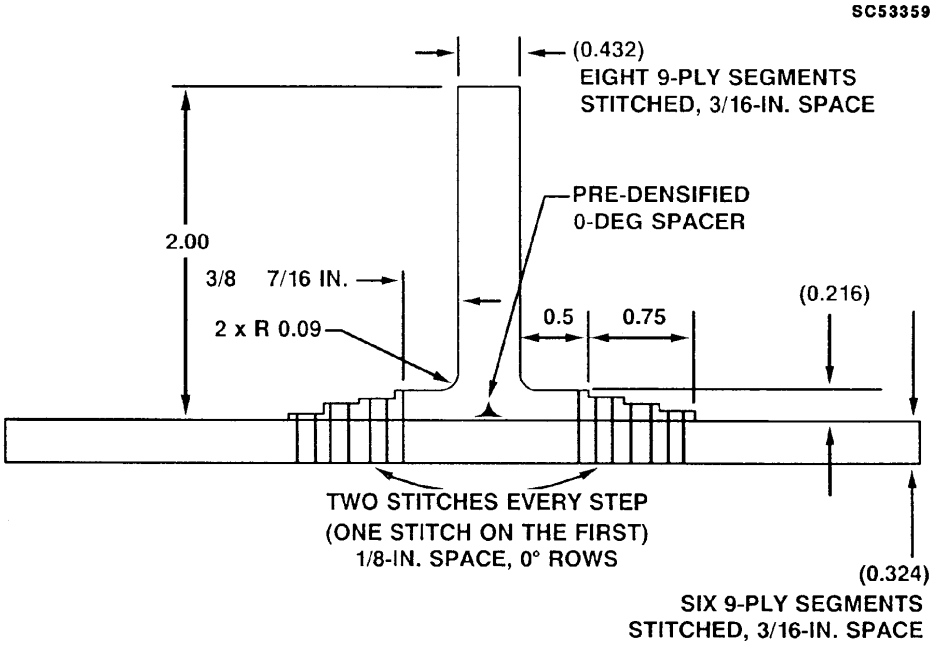


Figure 2-26. A stitched skin/stiffener assembly. (From Ref. [2.30])

## References

2.1 B. N. Cox, “Fundamental Concepts in the Suppression of Delamination Buckling by Stitching,” in *Proc. 9th DoD/NASA/FAA Conf. on Fibrous Composites in Structural Design*, Lake Tahoe, Nevada, November 1991, ed. J. R. Soderquist, L. M. Neri, and H. L. Bohon (U.S. Dept. Transportation, 1992) pp. 1105-1110.

2.2 B. N. Cox, "Delamination and Buckling in 3D Composites," *J. Comp. Mater.*, **28** (1994) 1114-26.

2.3 B. N. Cox, R. Massabó, and K. Kedward, "The Suppression of Delamination in Curved Structures by Stitching," *Composites*, in press.

2.4 T. Ishikawa, and T.W. Chou, “Elastic Behavior of Woven Hybrid Composites,” *J. Composite Materials* **16**, 2-19 (1982).

2.5 S.A. Hasselbrack, C.L. Pederson, and J.C. Seferis “Evaluation of Carbon-Fiber Reinforced Thermoplastic Matrices in a Flat Braid Process,” *Polymer Composites* **13**[1], 38-46 (1992).

2.6 C. Kittel, "Introduction to Solid State Physics," John Wiley and Sons, New York, 1967.

2.7 J.M. Yang, T.W. Chou, “Thermo-Elastic Analysis of Triaxially Woven Fabric Composites,” in Textile Structural Composites, edited by Tsu-Wei Chou and Frank K. Ko, Elsevier, New York, 1989, pp. 265-277.

2.8 M. Maistre, "Three-Dimensional Multi-Directional Structure," U. S. Patent No. 4,219,597, August, 1980.

2.9 R.N. Naik, “Analysis of Woven and Braided Fabric Reinforced Composites,” NASA CR-194930, June 1994.

2.10 N.K. Naik, P.S. Shembekar, “Elastic Behavior of Woven Fabric Composites: I - Lamina Analysis,” *J. of Composite Materials* **26**[15], 2196-2225 (1992).

2.11 I..S. Raju, and J.T. Wang, “Classical Laminate Theory Models for Woven Fabric Composites,” *J. of Composites Technology and Research* **16**[4], 289-303 (1994).

2.12 N.F. Dow, and V. Ramnath, “Analysis of Woven Fabrics for Reinforced Composite Materials,” NASA Contract Report 178275, Apr. 1987.

2.13 J. Skelton, “Triaxially Braided Materials for Composites,” in Textile Structural Composites, edited by Tsu-Wei Chou and Frank K. Ko, Elsevier, New York, 1989, pp. 117-128.

2.14 J. E. Masters, R.L. Foye, M.Pastore, and Y.A. Gowayed, “Mechanical Properties of Triaxially Braided Composites: Experimental and Analytical Results”, *J. of Composites Technology & Research* **15**[2], 112-122 (1993).

2.15 B.N. Cox and M.S. Dadkhah, "The Macroscopic Elasticity of 3D Woven Composites," *J. Comp. Mater.* **29**, 795-819 (1995).

2.16 F.K. Ko, and C.M. Pastore, “Structure and Properties of an Integrated 3-D Fabric for Structural Composites,” *Recent Advances in the United States and Japan, ASTM STP 864*, J.R. Vinson and M. Taya, Eds., American Society for Testing and Materials, Philadelphia, 1985, pp. 428-439.

2.17 J.H. Byun, T.J. Whitney, G.W. Du, and T.W. Chou, “Analytical Characterization of Two-Step Braided Composites,” *J. of Composite Materials* **25**, 1599-1618 (1991).

2.18 T.D. Kostar, and T.W. Chou, “Microstructural Design of Advanced Multi-Step Three-Dimensional Braided Preforms,” *J. of Composite Materials* **28**[13], 1180-1201 (1994).

2.19 E.T. Camponeschi, Jr., and R.M. Crane, “A Model for the Fiber Geometry and Stiffness of Multidirectionally Braided Composites,” in *3-D Composite Materials*, NASA Conference Publication 2420, 1985, pp. 75-89.

2.20 W. Li, T.J. Kang, and A. El Shiekh, “Structural Mechanics of 3-D Braided Preforms for Composites,” in *Fiber-Tex 1987*, NASA Conference Publication 3001, 1987, pp115-133.

2.21 J. Xu, B.N. Cox, M.A. McGlockton, and W.C. Carter, "A Binary Model of Textile Composites - II. The Elastic Regime," *Acta Metall. Mater.* **43**[9], 3511-24 (1995).

2.22 M.S. Dadkhah, J.G. Flintoff, T. Kniveton, and B.N. Cox, "Simple Models for Triaxially Braided Composites," *Composites* **26**, 91-102 (1995).

2.23 B.N. Cox, M.S. Dadkhah, R.V. Inman, and W.L. Morris, "Mechanisms of Compressive Failure in 3D Composites," *Acta Metall. Mater*. **40**, 3285-98 (1992).

2.24 B.N. Cox, M.S. Dadkhah, W.L. Morris and J.G. Flintoff, "Failure Mechanisms of 3D Woven Composites in Tension, Compression, and Bending," *Acta Metall. Mater.* **42**, 3967-84 (1994).

2.25 A. K. Roy, "In Situ Damage Observation and Failure in Model Laminates Containing Planar Yarn Crimping of Woven Composites," *Mechanics of Composite Materials and Structures*, in press..

2.26 M. S. Dadkhah, B. N. Cox, and W. L. Morris, "Compression-Compression Fatigue of 3D Woven Composites," *Acta Metall. Mater.* **43**[12], 4235-45 (1995).

2.27 D.E. Newland, "An Introduction to Random Vibrations and Spectral Analysis," 2nd Ed., John Wiley and Sons, New York (1984).

2.28 W.S. Slaughter and N.A. Fleck, "Microbuckling of Fiber Composites with Random Initial Fiber Waviness," *J. Mech. Phys. Solids*, in press.

2.29 S.K. Sharma, and B.V. Sankar, "Visualization of a Unit Cell of 3-D Braided Composite Plate," Quarterly Progress Report for the period January - March, 1993, NASA Mechanics of Textiles Working Group, pp 93-95.

2.30 V. Chen, McDonnell-Douglas Aircraft Co., Long Beach, California, 1990.

# 3. THE CHOICE BETWEEN TEXTILES AND TAPE LAMINATES

The main factors to weigh in deciding whether to use a textile composite or a conventional tape laminate are mechanical properties and the ease and cost of manufacture. Generally speaking, textiles are somewhat inferior in stiffness and strength for sheet applications; superior in any application, including sheet applications, requiring high strain to failure, high work of fracture, or damage or impact tolerance; and superior when triaxial loads must be carried. Their relative cost depends very much on the state to which applicable textile technologies have been developed for the particular application. If parts can be manufactured automatically to net shape, or the number of joints reduced by forming integral structures, or robotic manufacture substituted for manual set-up and handling, then textiles become increasingly cost competitive. In short, whether textiles are the better choice depends strongly on the application and the class of textile chosen.

In the following, quasi-laminar textiles will frequently be compared with so-called "equivalent tape laminates."These are laminates configured to have the same volume fraction of in-plane fibers in all orientations and plies of thickness roughly equal to the thickness of tows in the textile in the through-thickness direction.

In other instances, data are unavailable for equivalent tape laminates. Estimates of the penalty in stiffness or strength associated with using a textile will then be inferred from comparisons of measurements for textiles with data for unidirectional tape laminates, with due allowance for reduction of aligned fiber volume fraction in the former.

All the following remarks reflect the current status of textiles and their manufacturing technology. The reader should be prepared to update the relative merits of textiles as research and development progress. This is an active and dynamic field.

## 3.1 Handling and Fabricability

The main handling advantage of textiles is that they are manufactured as dry fiber preforms that hold together when they leave the textile machinery without any polymer or other matrix. The textile preform can be shipped, stored, draped (within limits that depend on the kind of fabric), and pressed into shaped molds. As described in Section 2, the finished product can be formed in the mold by resin transfer molding (RTM), reaction injection molding, resin film infusion (RFI), or the melting of commingled thermoplastic fibers, which are all cost competitive processes. Separate preforms can easily be joined by

co-curing if joints of moderate strength suffice; or by stitching if joints must be very strong. The handling advantages of textiles are so considerable that even when the finished product is intended to be a 2D laminated structure, for example a laminate of uniweave plies, with no special demand for the excellent delamination resistance of textiles, there is still a case for preferring textile fabrics over tape laminates.

But textiles allow designers to step beyond conventional laminate concepts. For example, with conventional tape layup, a laminar skin is stiffened against buckling by nonintegral ribs, which must be attached in a separate process. The use of textile preforms and processes such as RTM allows the manufacture of integral parts to net shape. Thus the skin and stiffeners can be manufactured as one piece. Some other examples of integral structures were recalled in Sect. 2. Net shape manufacture of integral structures provides considerable potential cost savings over tape layup, because forming complex shapes via layup is difficult and integral structures eliminate joining steps. Integral structures are superior in performance too, because failure by debonding of attached parts should be eliminated as a mechanism of failure, given correct design.

## 3.2 Consistency of Fiber Content

Since the stiffness and strength of polymeric composites are dominated by the reinforcing fibers, maintaining accurate positioning of fibers tows during all steps of manufacture is paramount. Poorly made textile preforms can have considerable variance in tow spacing, which translates directly into total fiber volume fraction and thence mechanical properties (e.g. [3.1]). In contrast, well made preforms, especially those manufactured by well established textile processes, such as 2D braiding and weaving, regularly achieve a high degree of consistency. However, even in the best cases, poor handling and processing after textile manufacture can destroy this uniformity. Uncontrolled material handling, laying material over curved tools, debulking, and tool closure can spread or distort tows. Manufactured prove-out parts should be examined to establish that minimum fiber volume fractions have been met throughout, with particular attention paid to geometric details such as joints.

The problem of maintaining the designed fiber content is most challenging when fabrics are draped. Fabrics are therefore often chosen for complex geometries because of their handling characteristics. The draping characteristics of a fabric over a singly curved (e.g., cylindrical) surface are directly related to its shear flexibility. Satin weaves have fewer cross-over points than a plain weave; and therefore have lower shear rigidity and are

found to be more easily draped over a cylinder. Draping characterictics over a doubly curved surface (i.e., a surface that requires nondevelopable transformation strains for snug coverage) also depend on in-plane extensibility and compressibility. This is difficult for fabrics containing high volume fractions of more or less straight in-plane fibers, as required for most airframe applications. For these textiles, only mild double curvature can be created by draping without significant loss of fiber regularity. However, double curvature can be achieved via net shape textile processes, such as braiding onto a mandrel (Section 2), thus avoiding the problems of draping.

### 3.3 Stiffness

Compared to tape laminates, quasi-laminar textile composites with equal volume fractions of in-plane fibers will usually have slightly lower in-plane stiffness because of tow waviness. In a 2D textile, such as a plain weave or triaxial braid, waviness is topologically inevitable: tows must be wavy to pass under and over one another. The waviness can be reduced by selecting a satin weave rather than a plain weave, or using tows with flat cross-sections; but not eliminated. In a 3D textile, such as an interlock weave, in-plane tows are nominally straight. But even still, waviness is always greater in practice than in an equivalent tape laminate, because of the disruptive effects of through-thickness reinforcing tows.

Various more or less complicated models will be described in Sections 4 and 5 for calculating the knockdown in composite stiffness due to tow waviness. Here a simple rule is presented, which illuminates the essential trends and gives a fair estimate.

Suppose the waviness takes the form of sinusoidal oscillations in the path of an in-plane tow, with wavelength $\lambda$ and amplitude $d$. If either the stress or the strain remains uniform along the length of the tow, then under an aligned load its stiffness is knocked down by the factor [3.2]

$$\eta = \left\{ 1 + 2\left(\frac{\pi d}{\lambda}\right)^2 \left[ \frac{E_x}{G_{xy}} - 2(1+\nu_{xy}) \right] \right\}^{-1} \tag{3.1}$$

where $E_x$ and $G_{xy}$ are the axial and shear moduli of the tow and $\nu_{xy}$ is its axial Poisson's ratio. For carbon/epoxy composites, the anisotropy factor in square brackets in Eq. (3.1) takes a value near 40. The fractional loss of modulus, $1-\eta$, rises approximately as $(d/\lambda)^2$.

Equation (3.1) also holds if the waviness takes the form of a continuously varying, normally distributed random misalignment angle, $\xi$, with variance $\sigma_\xi = \sqrt{2}\pi d/\lambda$ [3.2].

For measured degrees of tow waviness, Eq. (3.1) yields knockdown factors of just a few percent for nominally straight stuffers in well made 3D weaves [3.2]; and 2-10 % for nominally straight axial tows in 2D triaxial braids [3.1]. For nominally straight fillers in 3D weaves, the knockdowns are usually 10 - 30%. The knockdown is higher because fillers are untensioned during weaving and therefore significantly less regular than stuffers [3.2]. For bias tows in triaxially braided glass-fiber composites, knockdowns are between 30% and 50%, which are high values because the braid architecture demands that bias tows follow wavy paths. Knockdowns for plain weaves would be similarly high for the same reason. For a satin weave, knockdowns can be estimated by applying Eq. (3.1) just to the exchange region, assuming no knockdown over the much straighter float, and taking a weighted average. For typical satin weave, knockdowns of ~ 10% result.

Experimental measurements of elastic constants generally confirm the order of magnitude predicted by Eq. (3.1). While stiffness measurements have not been reported for equivalent tape laminates, stiffness knockdowns can be estimated by comparing measurements for textiles with rule-of-mixtures estimates based on fiber and resin data or data for unidirectional laminates. Knockdowns ≈ 5% are found in the warp direction for 3D interlock weaves with reasonably straight stuffers [3.2,3.3] and for the axial direction in triaxial braids [3.1,3.3]; and 10-40% in the weft direction of many 3D interlock weaves (the fillers frequently being much more distorted by the through-thickness warp weavers) or the bias direction of a triaxial braid [3.1-3.3]. Equation (3.1) is concluded to be a reasonable guide to the stiffness of quasilaminar textile composites relative to equivalent tape laminates, assuming that the latter have negligible stiffness knockdown due to waviness.

Experimentally measured moduli for various 2D braids and equivalent tape laminates are compared in Fig. 3-1. The braid and laminate specifications are given in Table 3.1. Fiber volume fractions were measured for all the panels used in these experiments and the results normalized to 60% fiber volume fraction, assuming a proportional variation. The longitudinal (0° direction) modulus for tension and compression agree closely. There is a larger reduction in transverse tensile modulus, as would be expected from the greater waviness of the braiding yarns. It is surprising that the transverse compressive stiffness of all the braids is higher than their transverse tensile stiffness, even though the tape equivalent modulus decreases in compression. This trend is not reported elsewhere.

**Table 3.1 Braid and Equivalent Tape Laminate Specifications for Fig. 3-1**

| Braid | Braid Designation | Equivalent Laminate |
|---|---|---|
| 1 | $[0_{36K},\pm45_{15K}]$ 46% Axial | $[(45/0/-45/0)_2/45/0/-45]_S$ |
| 2 | $[0_{30K},\pm70_{6K}]$ 46% Axial | $[(70/0/-70/0)_2/70/0/-70]_S$ |
| 3 | $[0_{75K},\pm70_{15K}]$ 46% Axial | $[(70/0/-70/0)_2/70/0/-70]_S$ |
| 4 | $[0_{6K},\pm45_{15K}]$ 12% Axial | $[(\pm45)_2/0/(\pm45)_3/0/(\pm45)_3/0/(\pm45)_2]_T$ |

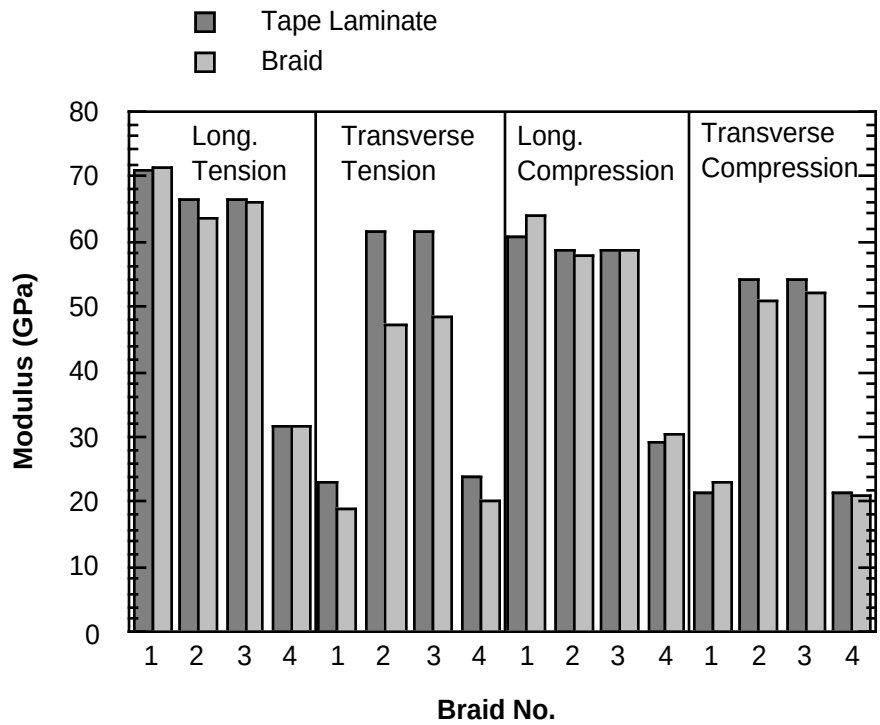


Figure 3-1. The Moduli of 2D Braids and Equivalent Tape Laminates

## 3.4 In-Plane Strength

Unnotched tensile and compressive strength are usually lower in quasi-laminar textiles than in equivalent tape laminates. Part of the reason for this is the tow architecture in textiles, which imparts waviness to tows and generates off-axis local stresses; and part is due to damage sustained by fibers in the rigors of textile manufacture.

The role of waviness in the compressive failure of polymer matrix composites is well established. Compressive failure when loads are aligned with one set of tows occurs via kink band formation (see Sect. 4). The critical load for kinking falls in inverse

proportion to the maximum misalignment angle of a wavy tow. Since waviness in textiles is usually higher than in tape laminates, the compressive strength is likely to be lower. However, it need not be much lower. In 3D architectures that permit nominally straight in-plane tows (e.g. the interlock weaves of Sect. 2.3.1.6), waviness can be controlled by high quality processing.

How waviness might lower tensile strength is less clear, but some experiments suggest that it does. Unfortunately, verified models are unavailable for estimating waviness effects on tensile strength; and, in most data sets for tensile strength, it is difficult to identify trends with degree of waviness amidst the noise of the data. Knockdowns due to fiber damage are much more important in tension than they are in compression (Sect. 4) and will always give some scatter in strength.

3D textiles are often equal or superior in notched strength to equivalent tape laminates. The large strain to failure of many 3D textile composites allows the development of extensive damage process zones next to stress concentrators, which decreases notch sensitivity. This superiority is not generally shared by 2D textiles, which lack some of the energy absorbing mechanisms present in 3D textiles (Sect. 4).

### *3.4.1 2D Weaves*

The ultimate tensile strengths of woven graphite/epoxy laminates and equivalent tape laminates are compared in Figure 3-2 (from [3.4] and [3.5]). The data represent 5-harness satin weave fabric manufactured with 3k yarns of carbon and consolidated with two resin systems. The woven laminates had a fiber volume fraction approximately 10% lower than in the tape laminates and a higher areal weight, and were accordingly 12-17% thicker. The ratio of the fabric strength to the tape laminate strength appears in parenthesis above each pair of bars.

The unnotched strength of the textiles (Fig. 3-2(a)) is significantly lower (15-23%) when the load is aligned with the 0° fiber axis. For a ±45° laminate, the difference disappears. Tensile axial tow strength, which is fiber dominated, is most affected by waviness and fiber damage. Shear strength, which is resin dominated, is affected less. The quasi-isotropic laminates have knockdowns similar to the 0/90° laminates. Notched strength (Fig. 3-2(b)) shows similar trends, although the knockdowns for the 0/90° laminates are greater (30-33%).

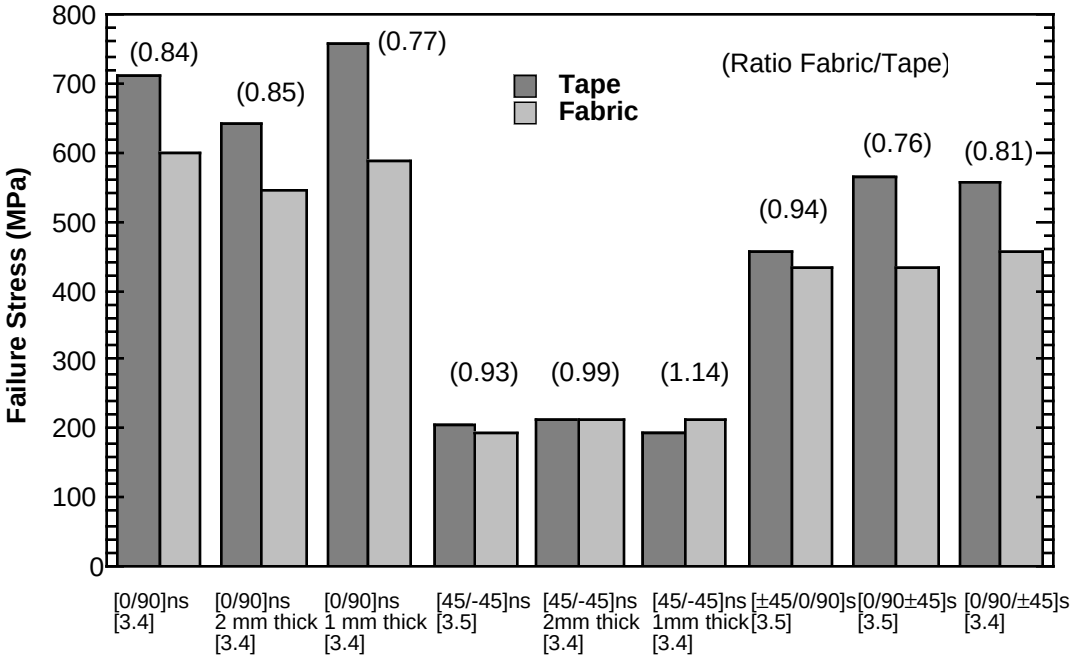


a) Unnotched

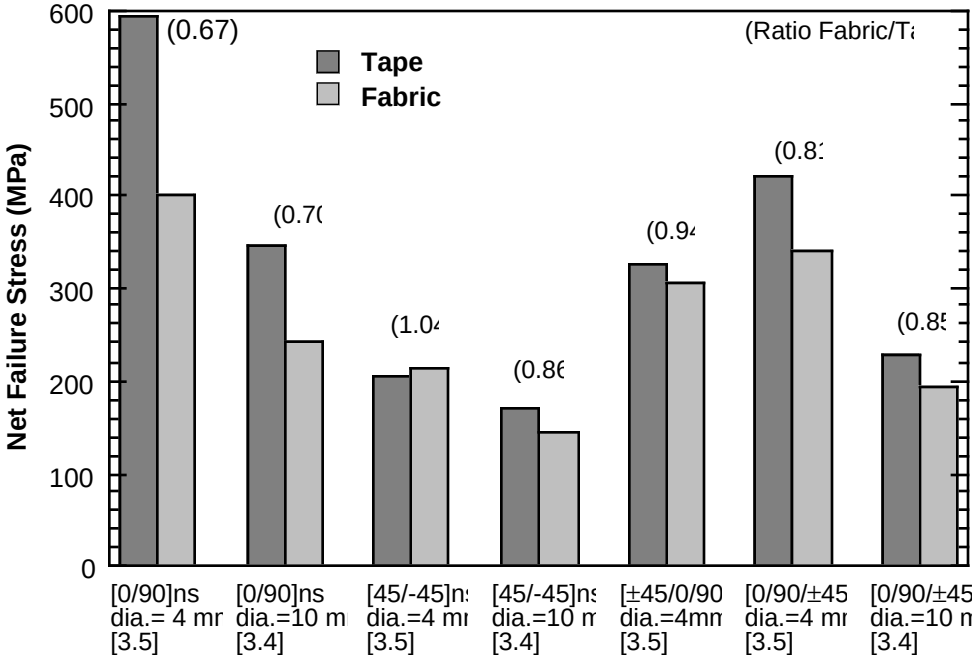


b) Notched

Figure 3-2. Comparison of (a) unnotched and (b) notched tensile strengths of 5-harness satin weave laminate and equivalent tape laminate. Material 1: Gr/MY720 epoxy. Material 2: T300/Ciba Geigy BSL914C. Notched strengths are from open hole tension tests, with hole diameters as shown.

While crimp effects on shear are small, they can sometimes give consistent variations. Figure 3-3 shows that the length of the float (the uncrimped length of yarn between cross-over points) in satin weaves affects shear strength. In this figure, the Oxford weave has the shortest float, followed by the 5-harness satin, and the 8-harness satin. The shear strength increases as the float length increases.

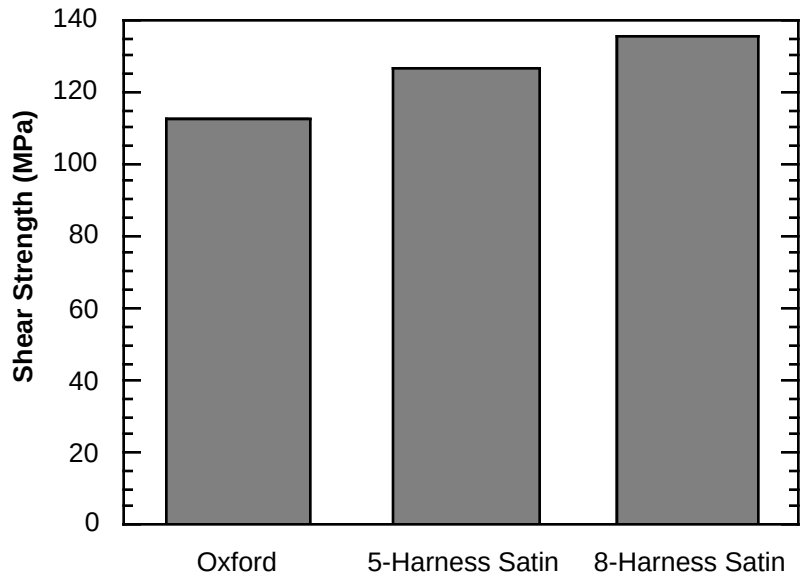


Figure 3-3. Comparison of in-plane shear strengths of various T300/934 weaves, showing effect of crimp. (From [3.6].)

### *3.4.2 2D Braids*

As for 2D weaves, the relationship between fiber architecture and strength for 2D braids must also involve the degree of waviness of the primary load bearing tows. In addition, braids introduce several further variables, whose roles are still poorly understood. These include the relative sizes of inlaid tows and braider tows, the spacing of inlaid tows, and the size of the unit cell.

The tensile strengths of two triaxial carbon/epoxy braids and equivalent tape laminates are compared in Fig. 3-4. The braid notation is defined in Section 2.3.1.3. The unnotched strength of the braids is 10-30% less than that of the tape laminates. However, the notched strengths are much closer, with the braids in one case even being superior. The braids overall are considerably less notch sensitive.

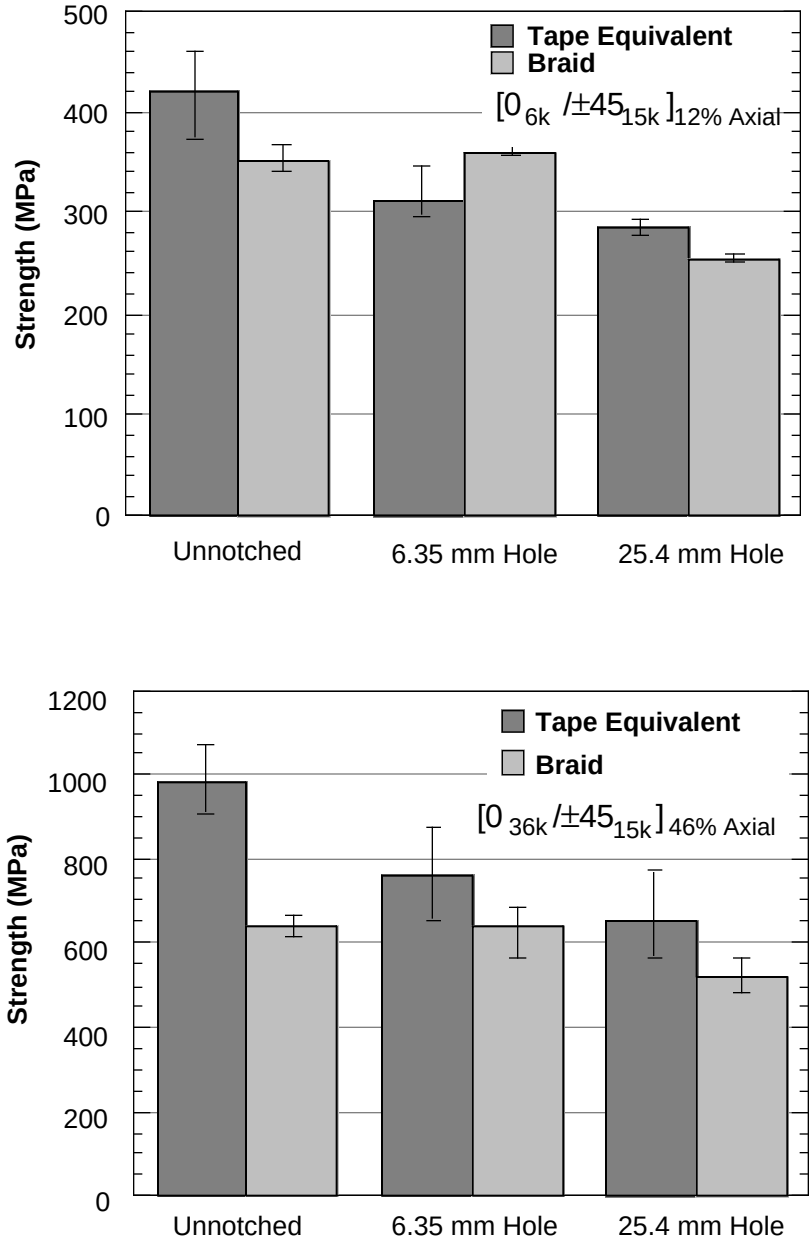


Figure 3-4. Comparison of unnotched and open hole tensile strengths for two triaxial braids and equivalent tape laminates (from [3.7]).

Strength knockdowns for unnotched triaxial braids have also been estimated by other means. Aligned axial tows in triaxial glass/urethane braided composites are found to fail at about 70% of the strain to failure of unidirectional tape laminates, indicating a 30% reduction in strength for the tows in the braided architecture [3.1]. This reduction is consistent with Fig. 3-4.

Data for triaxial braids occasionally show variations that are not readily correlated with architecture or waviness. For example, Table 3.2 (from [3.8]) shows that the tensile strengths for {$[0°_{18k}/\pm 66.5°_{6k}]$37.6% Axial} and {$[0°_{18k}/\pm 70°_{6k}]$34% Axial} braids differ by far more (30%) than the small differences in their fiber distributions would imply. No significant differences in the degree of waviness were observed on cut sections [3.9]. It is possible that the small change in orientation and packing of the bias tows caused more damage during braiding to the axial tows in the braid with 70° bias orientation. Further research must define the process parameters involved, so that consistent strength can be achieved. Bringing quality control to the levels common in tape laminates remains a challenge in textile processing, although well made textiles show that it is an attainable goal.

**Table 3.2 Comparison of Unnotched Tensile Strengths for Various AS4/1895 Triaxial Braids.**

| BRAID | Longitudinal Tension | | Transverse Tension | |
|---|---|---|---|---|
| | Strength (MPa) | Ultimate Strain, % | Strength (MPa) | Ultimate Strain, % |
| $[0°_{24k}/\pm 63°_{12k}]_{31.5\%}$ | 432 ± 25 | 1.16 ± 0.13 | 243 | 0.67 |
| $[0°_{18k}/\pm 66.5°_{6k}]_{37.6\%}$ | 556 ± 10 | 1.36 ± 0.07 | 288 ± 25 | 0.67 ± 0.12 |
| $[0°_{18k}/\pm 70°_{6k}]_{34\%}$ | 394 ± 10 | 0.96 ± 0.12 | 321 ± 39 | 0.70 ± 0.14 |

### *3.4.3 Stitched Laminates*

The unnotched and open hole tension strengths of some typical stitched and unstitched laminates are compared in Figure 3-5, while Fig. 3-6 shows similar data for compression, including compression after impact (CAI). The results show that stitching hardly affects tensile strength, but reduces the unnotched compression strength by 10-20%. However, stitching dramatically improves the CAI strength, being even more effective than the toughened resin system IM7/8551-7.

Compression strength is reduced by stitching because the stitching misaligns in-plane fibers near the surface [3.10]. Misalignment always facilitates fiber kinking (Sect. 4). If it affects entire plies of fibers, it will also soften those plies and increase the stress born by straighter plies. On the positive side, stitching provides preform debulking before the fabric is placed into a tool, which helps maximize fiber volume fraction.

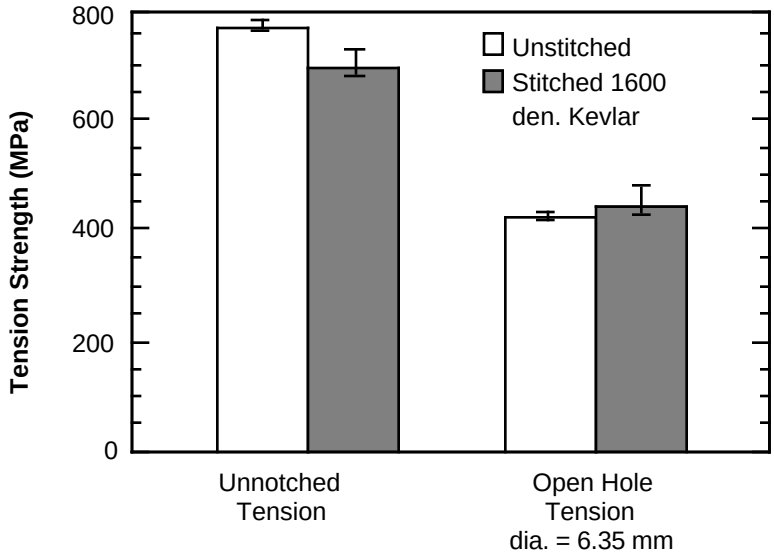


Fig. 3-5. Tensile strengths of stitched and unstitched IM7/3501-6 laminates. Stitching with 0.125 in. (3.1 mm) pitch (between penetrations within a row) and 0.20 in. (5.0 mm) spacing between the stitching rows. (from [3.10])

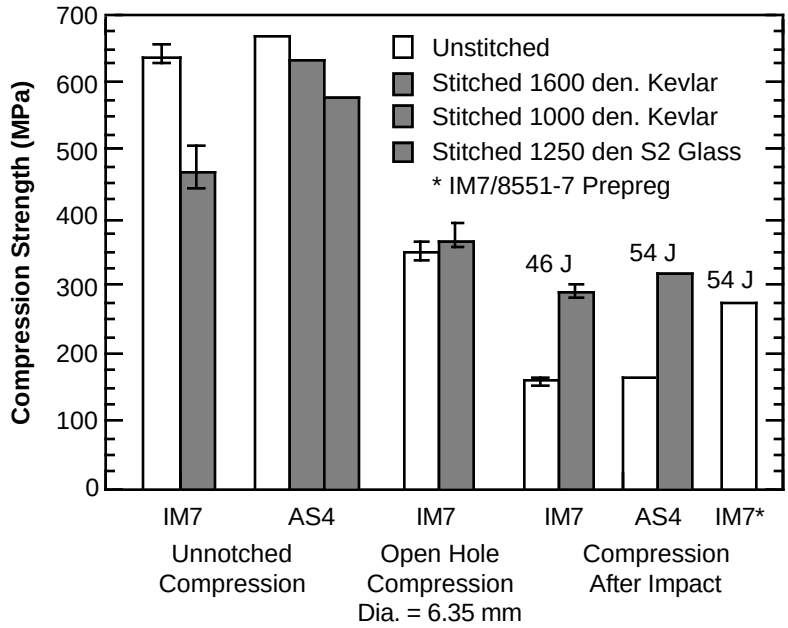


Fig. 3-6. Compression strengths and CAI data for stitched and unstitched laminates (from [3.10]).

### *3.4.4 3D Interlock Weaves*

Substantial data exist for the tensile and compressive strengths of 3D interlock weaves when loads are aligned with either stuffers or fillers, although no data are available for equivalent tape laminates. Using instead strength estimates based on the strengths of

unidirectional tapes reduced according to the volume fractions of stuffers or fillers, it is characteristically found that tow strengths are knocked down by about 30% [3.11-3.13].

## 3.5 Out-of-Plane Strength; Delamination and Impact Resistance

The great weakness of tape laminates is their vulnerability to delamination. Delamination failure can be caused in undamaged laminates by excessive through-thickness loads, which arise whenever the laminate is attached to some other structural member, such as a stiffener, near holes or edges, and under in-plane loads if the laminate forms a curved part. Once a laminate is damaged by impact and contains even a limited delamination crack, the critical through-thickness stress for failure drops dramatically, since the composite relies on the matrix toughness alone to resist delamination crack growth. A delamination crack of length, $a$, grows essentially as a Griffith crack, with the critical through-thickness stress falling as $a^{-1/2}$ to arbitrarily small values. Under in-plane loads, a partially delaminated tape laminate will still fail all too readily. It has poor resistance to buckling of the plies in delaminated areas, which leads to unstable delamination crack growth and failure. The critical buckling stress again falls as $a^{-1/2}$.

Through-thickness reinforcement in a quasi-laminar textile composite changes the picture entirely. Even if delamination flaws exist in advance, through-thickness reinforcement will arrest their growth as long as the stress remains above some critical value, $\sigma_1$, which is a material constant for the composite and independent of the delamination crack length, $a$. By proper design, delamination crack growth driven by through-thickness loads in curved parts and buckling of delaminated layers under in-plane compression can thus be eliminated. Some bounding formulae for the minimum required volume fractions of through-thickness reinforcement are provided in Sect. 4. The required volume fractions turn out to be at most a few percent for most applications [3.13-3.15].

## 3.6 Work of Fracture and Notch Sensitivity

Many textile composites, especially those with 3D reinforcement but also some with 2D reinforcement, have very high values of work of fracture and are exceptionally notch insensitive. Work of fracture values exceeding 1 MJ/m$^2$ have been reported for 3D interlock weaves [3.16], which are an order of magnitude higher than values for tape laminates or high toughness alloys. High work of fracture generally translates into notch

insensitivity. Around any stress concentrator, such as a round hole or sharp notch, a damage band forms in a ductile material, redistributing stress in such a way as to minimize stress concentration. The size of the damage band dictates the notch sensitivity. It has a characteristic length, $l_{ch}$, given to order of magnitude by

$$l_{ch} = E \ W_f \ / \ \sigma_c^2 \tag{3.2}$$

where $W_f$ is the work of fracture and $\sigma_C$ is the critical stress for the onset of damage. When the notch size, $c_o$, is much greater than $l_{ch}$, the strength of the part falls as $c_o^{-1/2}$. When the notch size, $c_o$, is much smaller than $l_{ch}$, the material is notch insensitive: the strength falls only as the net section stress rises. For tape laminates, $l_{ch}$ ~ 1 mm. For 3D interlock weaves, $l_{ch}$ ~ 10-100 mm [3.16].

Two factors in these high measures of damage tolerance have already been identified. First, the large tow diameter typical of most textiles favor crack deflection and increase the pullout lengths of broken tows that continue to carry load across the primary fracture plane. (It is fortuitous that large diameter tows also lower production costs.) Second, the wrapping of through-thickness tows around in-plane tows clamps the latter together even after they have failed, raising pullout stresses to unusually high values. These mechanisms are discussed in more detail in Sect. 4.

High work of fracture and notch insensitivity will create many opportunities for textile composites in applications demanding exceptional damage tolerance. These opportunities have only begun to be explored.

## References

3.1 M. S. Dadkhah, J. G. Flintoff, T. Kniveton, and B. N. Cox, "Simple Models for Triaxially Braided Composites," *Composites*, **26**, 91-102 (1995).

3.2 B. N. Cox and M. S. Dadkhah," The Macroscopic Elasticity of 3D Woven Composites," *J. Comp. Mater.*, **29**[6], 785-819 (1995).

3.3 P. J. Minguet, M. J. Fedro, and C. K. Gunther, *Test Methods for Textile Composites*, NASA Contractor Report 4609, Boeing Defense and Space Group, Philadelphia, 1994.

3.4 P.T. Curtis, and S.M. Bishop, “An Assessment of the Potential of Woven Carbon Fibre-Reinforced Plastics for High Performance Applications,” *Composites* **15**[4], 259-265 (1984).

3.5 P.T. Curtis, and B.B. Moore, “A Comparison of the Fatigue Performance of Woven and Non-Woven CFRP Laminates,” proceedings, ICCM V, San Diego, 1985, pp. 293-314.

3.6 D. F. Adams, and D. E. Walrath, “In-Plane and Interlaminar Iosipescu Shear Properties of Various Graphite Fabric/Epoxy Laminates,” *J. of Composites Technology & Research* **9**[3], 88-94 (1987).

3.7 T.L. Norman, D. Gaskin, and M. Patrick, “Failure of Notched 2D Braided LSS and LLS Textile and Tape Equivalent Composite Laminates,” presented at the NASA Textile Mechanics Working Group Meeting, March 9-11, 1994, NASA Langley Research Center, Hampton Va.

3.8 J.E. Masters, R.L. Foye, C.M. Pastore, and Y.A. Gowayed, “Mechanical Properties of Triaxially Braided Composites: Experimental and Analytical Results” *J. of Composites Technology & Research* **15**[2], 112-122 (1993).

3.9 J.E. Masters, R.A. Naik, P.J. Minguet, “Effects of Preform Architecture on Modulus and Strength of 2-D Triaxially Braided Textile Composites,” in *Mechanics of Textile Composites Conference*, ed. C. C. Poe, Jr., and C. E. Harris, NASA Conference Publication 3311, Part 2, pp 349-378.

3.10 D.H. Morris, and S.T. Burr, “Quarterly Progress Report No. 10: Damage Initiation and Growth in a Braided Composite Subjected to Fatigue Loading”, Grant No. NAG-1-343, NASA Langley Research Center.

3.11 B. N. Cox, M. S. Dadkhah, W. L. Morris, and J. G. Flintoff, "Failure Mechanisms of 3D Woven Composites in Tension, Compression, and Bending," *Acta Metallurgica et Materialia*., **42** (1994) 3967-84.

3.12 K. Pochiraju and T.-W. Chou, Final Report on Textile Composites Modeling, ACT Program, NASA Langley, 1994.

3.13 B. N. Cox, “Fundamental Concepts in the Suppression of Delamination Buckling by Stitching,” in *Proc. 9th DoD/NASA/FAA Conf. on Fibrous Composites in Structural Design*, Lake Tahoe, Nevada, November 1991, ed. J. R. Soderquist, L. M. Neri, and H. L. Bohon (U.S. Dept. Transportation, 1992) pp. 1105-1110.

3.14 B. N. Cox, "Delamination and Buckling in 3D Composites," *J. Comp. Mater.*, **28** (1994) 1114-26.

3.15 B. N. Cox, R. Massabó, and K. Kedward, "The Suppression of Delaminations in Curved Structures by Stitching," *Composites*, in press.

3.16 B. N. Cox, M. S. Dadkhah, and W. L. Morris, "On the Tensile Failure of 3D Woven Composites," *Composites*, in press.

# 4. FAILURE MECHANISMS

In Section 2, textile composites were categorized as quasi-laminar and nonlaminar, depending on whether or not they can be considered as laminates modified by the inclusion of relatively few through-thickness fibers. This distinction is particularly useful in discussing failure mechanisms. Through-thickness reinforcement was in most cases introduced to combat undesirable failure mechanisms in 2D laminates. The suppression of these mechanisms should often still be described in the language of laminate mechanics, with the effects of the through-thickness reinforcement treated as a perturbation. The reader is therefore encouraged to review the categorization in Section 2 before proceeding here.

However, the terms quasi-laminar and nonlaminar should be used with care. Some textiles may appear geometrically and behave elastically as obvious quasi-laminates, yet show stress-strain characteristics and mechanisms of stress redistribution and damage accumulation that have no parallel in 2D laminates. A prime example is 3D interlock weaves, which show extraordinary damage tolerance and other properties related to the work of fracture by mechanisms that are intimately associated with their 3D nature, as will be seen in the following.

## 4.1 Shear

Axial shear failure in bundles of fibers in a polymer matrix begins with arrays of ogive microcracks aligned between pairs of fibers (Fig. 4-1 and [4.1,4.2]). These cracks grow and sometimes coalesce amidst considerable microplasticity, which probably involves crazing and fibril tearing. At higher strains, the damaged matrix divides into pieces of rubble. The corresponding macroscopic constitutive behaviour can be measured conveniently and fairly representatively by loading ±45° laminates in uniaxial tension. Since the deviatoric stresses within such a specimen are pure shear within all plies, the specimen stress/strain response is proportional to that of a single ply under axial shear. Viewed over the range of strains relevant to ultimate failure, the measured response is often approximately linear/perfectly plastic, with plasticity occurring above a threshold stress, $\tau_c$ (Fig. 4-2(a) and [4.1,4.2]).

For composites in which the fibers have much higher modulus than the matrix, the shear behaviour represented by Fig. 4-2(a) is controlled entirely by the properties of the matrix deforming under the geometrical constraints imposed by the fibers [4.3,4.4]. Thus $\tau_c$ should be regarded primarily as a matrix property, with some dependence on parameters

of the fiber arrangement such as volume fraction. Little is known about variations of $\tau_c$ with volume fraction, but the available evidence suggests they are small for the ranges of volume fraction typical of aerospace composites. Representative values of $\tau_c$ are 75 MPa for the aerospace resin Shell 1895 [4.1] and 30 MPa for automotive urethanes [4.2].

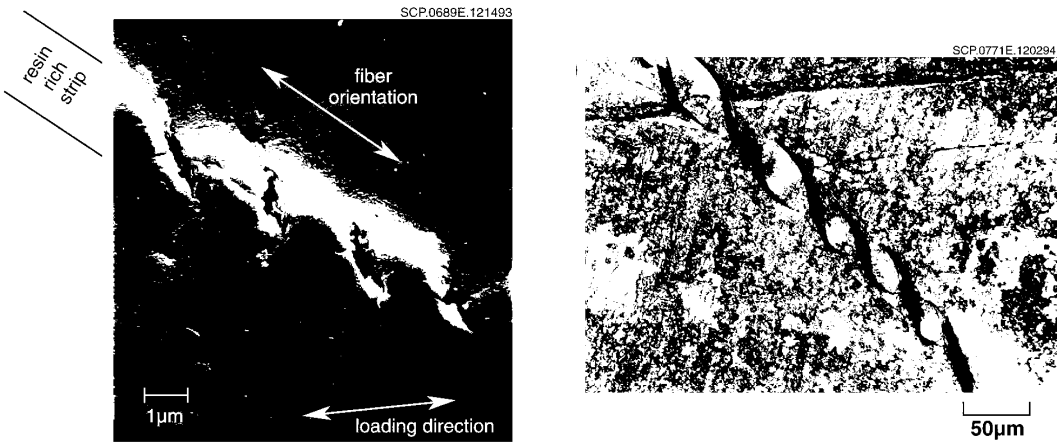


(a) (b)

Figure 4-1. Arrays of ogive microcracks in (a) an AS4/1895 tape laminate (from [4.1]) and (b) a glass/urethane triaxial braid (from [4.2]). The fiber direction is parallel to the bands of microcracks.

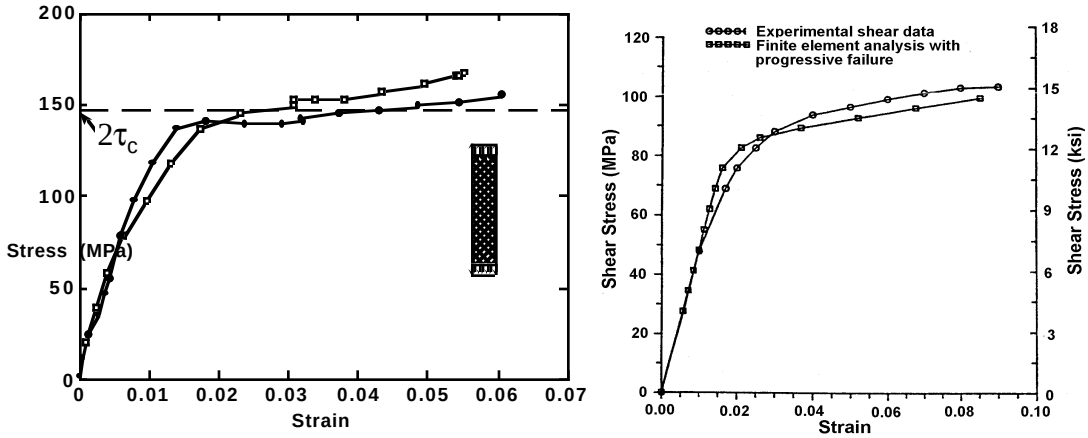


(a) (b)

Figure 4-2. Typical stress-strain response of a polymer composite when the deviatoric stress in plies is pure shear. (a) AS4/1895 tape laminate (from [4.1]). (b) AS4/3501-6 plain weave (from [4.5]).

Textile composites under shear loading show stress-strain properties very like Fig. 4-2(a). Figure 4-2(b) shows a typical curve for a short shear specimen of a plain woven, AS4/3501-6 laminate superimposed on a theoretical prediction based on a progressive

failure model (both from [4.5]). The model attributed nonlinearity in shear to degradation of the matrix stiffness. Once the matrix had yielded (critical maximum principal stress), the shear stiffness in the model was reduced to 20% of its original value. This approach does not specify the physical nature of the resulting cracks.

In assessing failure mechanisms in textile composites beyond the proportional limit, the possibility of shear failure can usually be predicted quite well by comparing the axial shear stress within individual plies or tows with $\tau_c$. In computing the stress-strain response, reasonable results can usually be obtained by regarding individual plies or tows as elastic/perfectly plastic in axial shear.

## 4.2 Monotonic Compression

Quasi-laminar textile composites almost always fail under aligned, monotonic compression by one of two mechanisms: kink band formation; and delamination, which is often followed by Euler buckling.

Kind band formation is illustrated by Fig. 4-3. It is a local shear instability in which a bundle of fibers rotates and ruptures, causing almost total loss of axial strength for the bundle. The bulk of data confirms that Argon's Law [4.6,4.7]

$$\sigma_c = \tau_c/\phi \tag{4.1}$$

is a serviceable approximation for kink band formation in polymer composites, where $\sigma_k$ is the critical axial stress for kinking, $\tau_c$ is the critical shear flow stress of Fig. 4-2(a), and $\phi$ is the misalignment angle of the fibers with respect to the applied load (measured in radians). As Eq. (4.1) shows, the crucial manufacturing issue in optimizing compressive strength is minimizing the misalignment angle; or, in other words, minimizing fiber or tow waviness.

Fiber defects have a marginal effect on the dynamics and kinetics of shear flow and fiber rotation; and therefore a negligible effect on the critical stress for kink band formation in compression. In contrast, the tensile strength of tows is strongly influenced by fiber defects and therefore handling damage during processing (see Sect. 4.3).

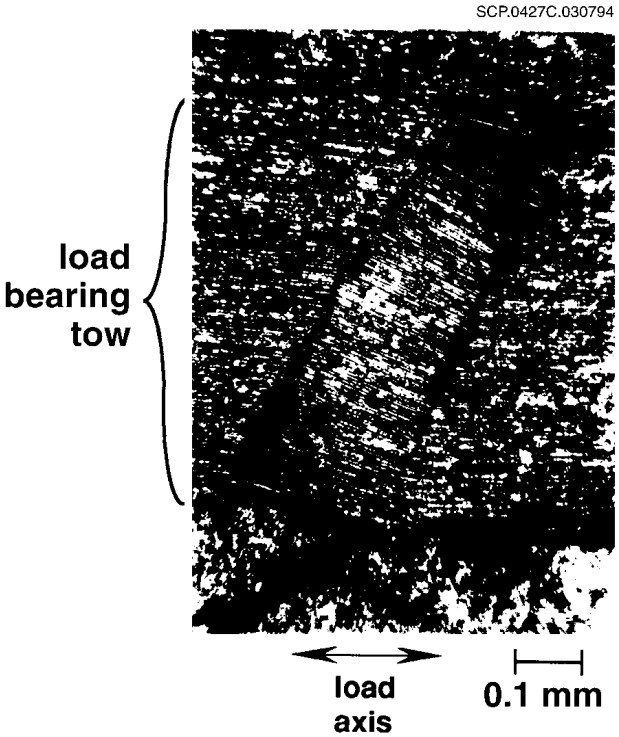


Figure 4-3. Micrograph of a typical kink band in an aligned tow in an AS4/1895 3D interlock weave (from [4.1]).

Delamination has been the most serious weakness of conventional tape laminates, especially around edges or in association with impact damage. When a stress singularity at an edge or an impact event causes limited delamination, failure can ensue via Euler buckling of the delaminated plies under in-plane compression; or by delamination crack growth under shear induced by bending. In the absence of through-thickness reinforcement, the critical load for buckling and delamination crack growth under in-plane compression falls in inverse proportion to the size of the delamination to arbitrarily small values; as does the critical load for delamination crack growth in bending. In either case, resistance to delamination crack growth depends entirely on the fracture resistance of the matrix. Well established, low-cost polymer matrices are generally not very tough. Even toughened polymers and thermoplastics, which are usually relatively expensive, provide only modest increases in toughness.

In quasi-laminar textile composites such as stitched laminates or 3D interlock weaves, delamination resistance is greatly enhanced by through-thickness reinforcement. The through-thickness reinforcement does not entirely eliminate delamination, especially during impact, but by suppressing buckling under subsequent compressive loads, it eliminates the driving force for delamination crack growth under in-plane compression; and

by bridging the delamination crack, it greatly increases resistance to shear loads (Sect. 4.5). The minimum load for buckling or delamination crack growth does not fall indefinitely with increasing delamination size, but approaches a constant value which depends on the parameters of the through-thickness reinforcement [4.8-4.11]. Given adequate provision of through-thickness reinforcement, ultimate failure must revert to the kink band mechanism, which is largely unaffected by delaminations, and the compressive strength is then usually close to that of pristine material.

Thus a transition exists in failure mechanism from delamination to kinking depending on the efficacy of the through-thickness reinforcement. Rough estimates of the minimum volume fraction, $V_t$, of through-thickness reinforcement required to suppress buckling and assure failure by kinking can be deduced from the theory of buckling plates on an elastic foundation [4.8-4.10]

$$V_t = \frac{\sigma_k^2}{E_x E_t V_x \cos^2\theta} \qquad \text{(mid-plane delamination)} \qquad (4.2a)$$

$$V_t = \frac{\sigma_k^2}{E_x E_t V_x \cos^2\theta}\frac{t}{h} \qquad \text{(surface delamination)} \qquad (4.2b)$$

where $\sigma_k$ is the applied stress at which kinking occurs, $E_x$ and $E_t$ are the stiffnesses of the in-plane and through-thickness fibers; $V_x$ is the volume fraction of aligned, in-plane fibers; and the dimensions $h$ and $t$ and the angle $\theta$ are defined in Fig. 4-4. Values found for $V_t$ from Eq. (4.2) are ~ $10^{-3}$, considerably less than the volume fractions of stitching or interlock fibers in current composites. Equation (4.2) is based on the simplistic assumption that the through-thickness reinforcement behaves as a linear spring with strain uniformly distributed through the thickness of the composite. If loads were transferred by shear into the surrounding laminate, the through-thickness reinforcement would provide a stiffer foundation and even lower volume fractions would be required. Thus, for this particular transition in failure mode and provided the through-thickness reinforcement remains intact, Equation (4.2) should be a conservative estimate. However, if through-thickness reinforcement is damaged, perhaps by impact, or crimped during manufacture, then buckling will occur much more readily. Design rules for such situations have not yet been established.

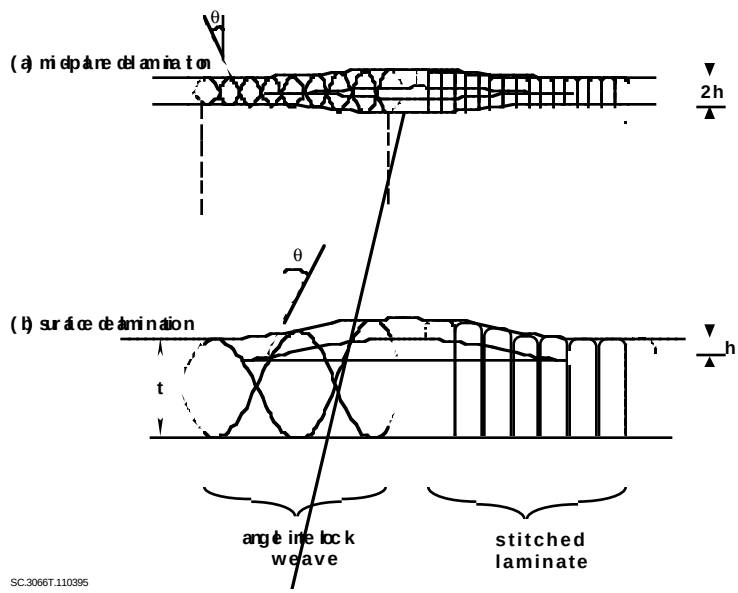


Figure 4-4. Schematic of buckling under in-plane compression following delamination due to impact.

### *4.2.1 2D Weaves and Braids*

Under aligned compression, 2D weaves and braids without prior damage typically fail by a combination of shear plasticity and delamination [4.2,4.12]. Shear failures may appear as kink bands, although the evidence for kinking is often obscured by the extent of damage that immediately ensues tow failure. Nevertheless, clear evidence exists for kinking in plain and satin weaves [4.12-4.14] and in nominally straight axial tows in triaxial braids [4.2,4.15]. Large scale delaminations occur between plies [4.12]. Localized delaminations may occur between tows within the same ply, especially along the float in 2D weaves (Fig. 4-5).

Representative compression strength data for four carbon/epoxy triaxial braids are shown in Table 4.1 [4.16]. The braid with a low percentage of axial yarns, $\{[0_{6k}/\pm 45_{15k}]12\%\ \text{Axial}\}$, failed by extensive shear cracking in the bias rovings with a very nonlinear stress-strain curve similar to Fig. 4-2 (see also similar data in [4.2,4.14,4.17]). The strength of the remaining, axially dominated braids was controlled by splitting and buckling of the axial fiber bundles, which presumably involved kink bands like those reported in [4.2,4.14,4.15]; and the stress-strain curves were nearly linear to failure.

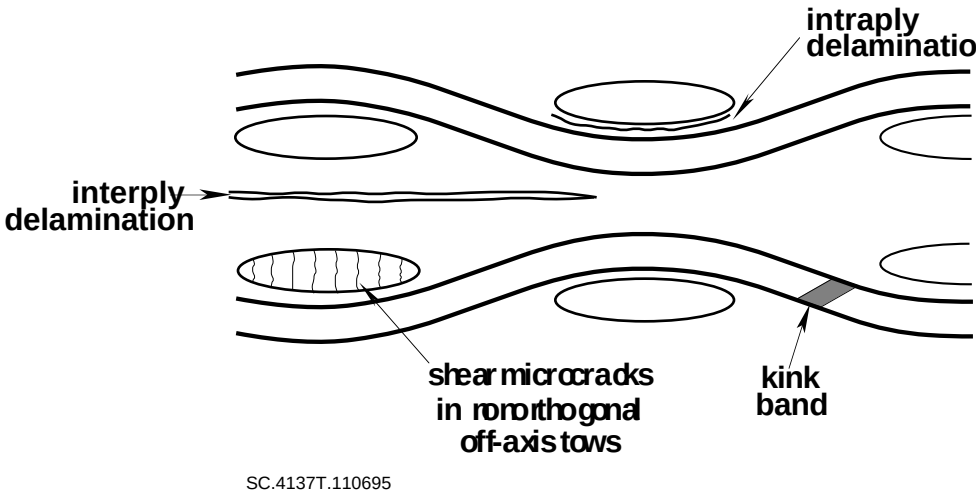


Figure 4-5. Schematic of delamination and shear failure events in a typical 2D weave.

Because tows in 2D weaves pass over and under one another, the primary load bearing fibers suffer unavoidably large misalignments with respect to the applied load axis. Therefore, axial shear stresses are high under nominally aligned loads and the critical load for plasticity (probably leading to kinking) is relatively low. In triaxial braids, the axial tows can be straight in principle, but in practice they are much more wavy than plies in a tape laminate [4.2]. Critical loads for kinking are again relatively low [4.2,4.17].

**Table 4.1 Compression Data for Gr/Ep Triaxial Braids (from [4.16]).**

| Braid | Modulus (GPa) | Ultimate Strength (MPa) | Ultimate Strain (%) |
|---|---|---|---|
| $[0_{6k}/\pm45_{15k}]_{12\%}$ | 32.4 ± 1.0 | 353 ± 37 | 1.56 ± 0.22 |
| $[0_{36k}/\pm45_{15k}]_{46\%}$ | 69.7 ± 1.8 | 621 ± 17 | 1.03 ± 0.04 |
| $[0_{30k}/\pm70_{6k}]_{46\%}$ | 62.0 ± 0.3 | 503 ± 43 | 0.86 ± 0.08 |
| $[0_{75k}/\pm70_{15k}]_{46\%}$ | 63.4 ± 2.1 | 439 ± 752 | 0.77 ± 0.14 |

Once kinking or other shear failure occurs, inter-ply delamination usually ensues immediately. If inter-ply delamination is already present, as after impact, failure may occur via delamination crack growth and Euler buckling without kink band formation. Because the delamination stress following impact or the kinking stress otherwise is low, 2D weaves and braids appear to be inferior choices for applications involving significant in-plane compression.

### *4.2.2 Stitched and Stitched-Knitted Laminates*

Stitching, either alone or in combination with weaving (usually uniweave plies) or knitting, is very effective in suppressing delamination. In the absence of delamination, failure in monotonic compression commonly occurs via kink band formation [4.18]. The critical stress for kinking is generally much higher than in 2D weaves and braids, because the in-plane fibers in stitched uniweave or stitched-knitted laminates tend to be better aligned. Stitched uniweave and stitched/knitted laminates are good candidates for applications involving compression.

When a kink band forms in a stitched laminate, it propagates unstably through the thickness of the specimen [4.18]. The load-bearing capacity of the material drops immediately to zero; the material exhibits brittle failure.

### *4.2.3 3D Weaves*

Under aligned loads, 3D interlock weaves also fail by kink band formation [4.1,4.18]. However, the failure is generally not nearly as brittle as in a stitched laminate. Each kink band that forms is confined to a single aligned tow and does not spread catastrophically into neighboring tows. Ultimate failure is only achieved by the cumulative effect of many distinct kinking events, which may be spread over a substantial volume of the composite. Strains to ultimate failure of 3-15% have been measured, depending on the details of the architecture and the test configuration [4.1,4.18].

Misaligned tow segments constitute geometrical flaws, with the strength or critical local stress for each flaw depending on the misalignment angle via Eq. (4.1). The statistics of kink formation depend on how these flaws are distributed in strength and space. Broader distributions favour delocalized kinking sequences and high strain to failure [4.18].

The peak compressive stress also depends on the statistics of the misalignment fluctuations in the aligned tows. The highest values of misalignment tend to be somewhat higher than in tape laminates, at least in current 3D interlock weaves [4.1]. The peak load is commensurately lower than in equivalent tape laminates.

Local delaminations are frequently observed in 3D weaves under compression. But delamination crack growth is limited and Euler buckling of delaminated tows is not a failure path provided the through-thickness reinforcement is not heavily crimped during

fabrication. With this proviso, delamination is not the strength limiting mechanism even after impact [4.19].

### *4.2.4 3D Braids*

Detailed observations of the mechanisms of failure in 3D braids have not been reported. Experiments have been conducted in load control rather than displacement control, which frustrates attempts to identify kink bands post mortem. However, if the braid architecture contains significant proportions of nominally straight, aligned tows, it is very likely that their kinking will be the primary mechanism of composite failure. By delocalizing mechanisms similar to those operating in 3D interlock weaves, one might again expect very high strains to ultimate failure in favourable cases.

## 4.3 Monotonic Tension

Under aligned tension, almost all load is borne by the aligned fibers. Their rupture is the primary failure mechanism and determines ultimate strength. However, depending on the fiber architecture, tensile or shear failures of the matrix can cause nonlinearity at much lower loads.

Tow rupture strengths in weaves or braids are usually ~30-50% lower than would be expected from the properties of pristine fibers or comparable unidirectional tape laminates (Sect. 3). For example, AS4 carbon tows with an internal volume fraction of 70% apparently have rupture strengths near 1.5 Gpa in 3D interlock weaves [4.1]. The manufacturer quotes 4 GPa for the strength of AS4 fibers[1] while data for equivalent tape laminates [4.17] imply tow ply strengths exceeding 2 GPa.

Unidirectional composites have lower strengths than implied by bare fiber strength data because flaws on neighbouring fibers in a composite are coupled by the matrix. When one fiber fails in a bundle of bare fibers, the load it sheds is picked up equally by all surviving fibers, without any small group of them bearing excessive loads. This favours higher bundle strength. When one fiber fails in a polymer composite, in contrast, there is a significant stress concentration acting on its neighbours [4.20]. Nearby flaws in separate fibers are thus grouped into larger flaws and composite strength tends to be lower.

Various mechanisms can be conjectured to explain why tow strengths in textiles are even lower still. 1) The rigours of textile processing are always likely to damage tows. 2)

[1] Data sheets of Hercules Inc., Wilmington, Delaware.

Tow waviness creates fluctuations in the stiffness of short segments of tows, which results in uneven load distributions. For the waviness typical of 3D interlock weaves, for example, this will cause strength knockdowns of up to 10% [4.21]. 3) Misaligned or pinched tows may be weaker than straight tows. 4) Lateral loads imposed on tows by neighbouring interlaced tows may reduce their strength.

One common manifestation of shear plasticity under tensile loads is plastic straightening of wavy tows. The criterion for the onset of tow straightening is essentially the same as that for kink band formation under compression. The resolved axial shear stress, which is proportional to the local misalignment angle, $\phi$, must exceed $\tau_c$, the shear flow stress, leading again to Eq. (1), with $\sigma_p$, the critical axial stress for shear plasticity, replacing $\sigma_k$. Since tow misalignment is a continuously varying random variable, tow straightening commences at different stresses for different locations on the same tow.

Unlike kinking, tow straightening leads to hardening and can therefore propagate along a tow. Its progression can be estimated simply by calculating the local rotation of the tow, which leads to evolution in $\phi$ and therefore $\sigma_p$. Tow straightening ceases when the axial plastic strain equals the fractional difference between the initial arc length of the wavy tow and its projected length in the axial direction. The contribution to strain to failure from this source rises as the square of the average misalignment angle [4.22].

When a tensile load is not aligned with a primary group of tows, tow rupture may give way to failure by shear or transverse cracking [4.2,4.14,4.23]. For loading at ±45° with respect to two orthogonal sets of tows, which might be tows in the plain weave of Fig. 4-2(b) or in a 3D interlock weave, the problem reduces to one of deviatoric shear in those tows. The stress-strain response will be similar to those shown in Fig. 4-2. Figure 4-6(a) shows stress-strain curves for a plain weave composite loaded at various orientations. Response in the 0/90° orientation is nearly linear to failure, while considerable plasticity and high strains to failure are exhibited for off-axis loads. Figure 4-6(b) shows similar trends for open hole specimens. The failure stress for off-axis loads can be higher in the notched than in the unnotched specimen. The authors of Ref. [4.24] attribute this curious result to plastic tow straightening occurring near the hole. In tubular braided specimens, interesting lockup mechanisms can come into play when tows interfere with one another at very high strains, causing pronounced hardening. The hardening enables a form of cold drawing to progress along the entire specimen, with high levels of plastic work required to achieve ultimate failure [4.25].

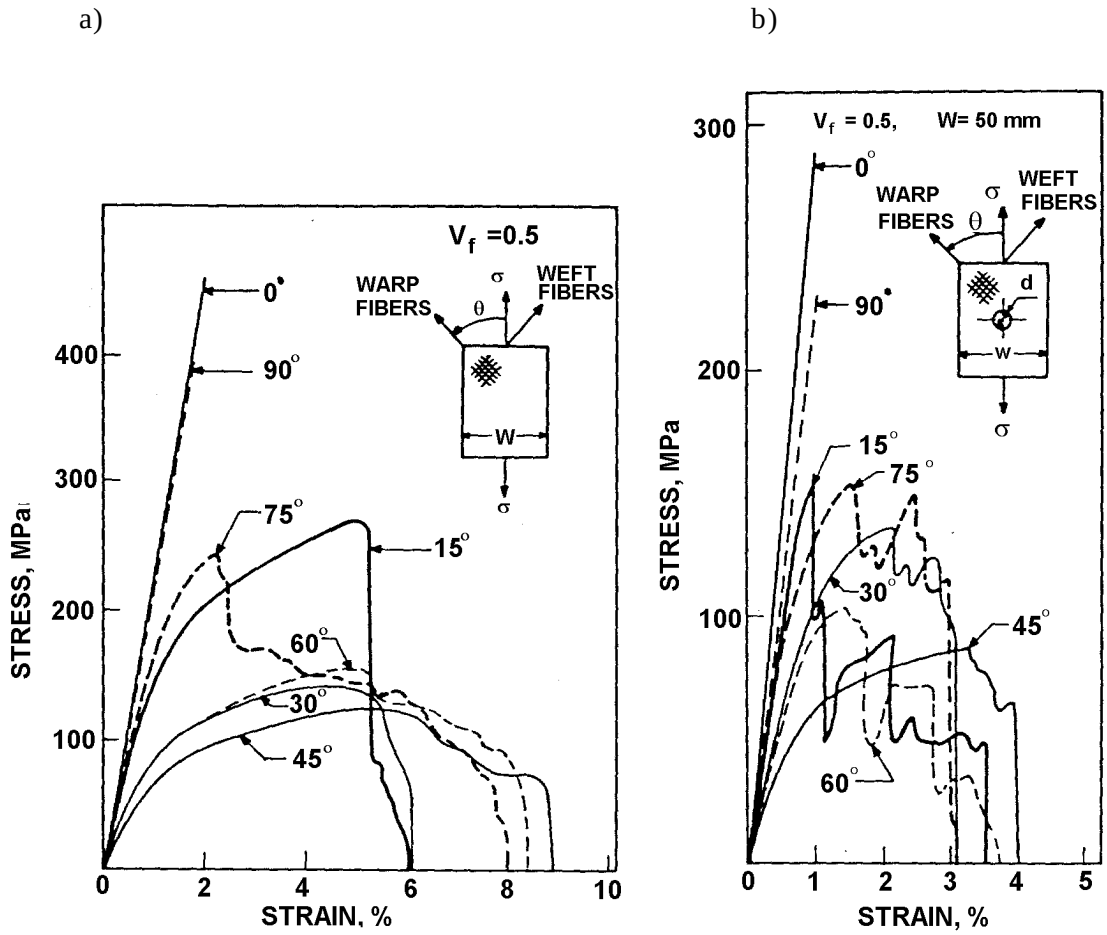


Figure 4-6. Stress-strain curves for plain woven carbon/eopxy laminate. (a) Unnotched. (b) Notched ($d$ = 4 mm). (From [4.24].)

The rest of this section will be directed mainly to failure mechanisms under loads aligned with a primary set of tows. This is the configuration of most interest for applications such as airframes where stiffness and strength are paramount.

### *4.3.1 2D Weaves and Braids*

In 2D woven laminates, including plain weaves, satin weaves, etc., the earliest softening under aligned loads is caused by microcracking within transversely oriented tows, around tows of both orientations, and between plies. The systems of microcracks are often complex [4.14], linked to irregularities in geometry, and difficult to correlate with estimates of local stresses (see Sect. 5). Plastic tow straightening is inhibited by the interlacing of tows.

In triaxial braids loaded along the axial tows, microcracking similar to that depicted in Fig. 4-1 usually occurs first in the bias rovings, where the dominant stress is shear [4.2]. At higher strains, plastic straightening of the aligned tows may generate further measurable nonlinearity prior to peak load. Whether plastic tow straightening is significant depends on the degree of waviness of the aligned tows, which depends strongly on architecture and processing.

### *4.3.2 Stitched, Stitched-Woven, and Stitched-Knitted Laminates*

The principal systems of microcracks in stitched prepreg, stitched uniweave, and stitched-knitted laminates are roughly periodic cracks normal to the applied load in the transverse plies; and shear cracks in off-axis plies. These crack systems are very similar to those found in tape laminates, although their shapes and spacing are influenced in a complicated way by the stitches. Ultimate failure accompanies rupture of the aligned plies, much as in a tape laminate. The stitching minimizes delamination during large strains, but this has a minor effect on the ultimate strength or strain to failure. Because the in-plane fibers lie in approximately flat plies, tow straightening is not evident.

### *4.3.3 3D Weaves*

In 3D interlock weaves, the first cracks observed usually run orthogonal to the applied load between transverse tows [4.1]. Cracks within the transverse tows are comparatively rare. Other cracks develop along the trajectories of warp weavers (interlock tows). At loads typically exceeding half the peak load (~500 MPa in typical graphite/epoxy composites), significant softening occurs because of plastic tow straightening. Although the stuffers and fillers (the in-plane load bearing tows) are nominally straight in interlock weaves, they tend in current materials to be substantially more wavy than the majority of plies in stitched-woven or stitched-knitted laminates. Plastic tow straightening may contribute 0.1-0.25% to the strain to peak load [4.22].

The strength limiting process in 3D interlock weaves is the rupture of aligned tows. Tows fail as discrete entities. When one tow fails, the damage does not generally propagate into neighboring tows. Rather, tow rupture sites are broadly distributed, leading to tow pullout over 5-10 mm lengths across the ultimate fracture plane [4.1,4.22].

Following the attainment of peak load, a sharp drop occurs in tensile tests, after which tow pullout sustains much smaller loads (Fig. 4-7). However, the load drop occurs at remarkable high strains, typically 2.5-4% for loads aligned with the stuffers in

specimens with gauge lengths of 20-30 mm. All the primary load bearing tows have failed well before this strain. Thus the composite possesses mechanisms for transferring loads around failure sites during substantial further straining. It is believed that the key factors are tow waviness or other irregularities and the clamping effect of the interlock tows, which act together to create a lockup effect which restricts sliding displacements of failed tows [4.22]. Because loads near the peak load (~ 1 GPa) are sustained over nonlinear displacements of ~ 1 mm, the work of fracture of interlock weaves can exceed 1 MJ/m$^2$.

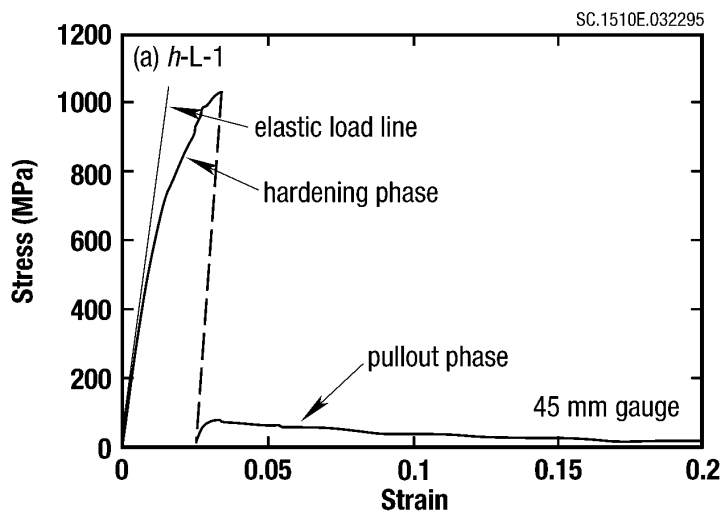


Figure 4-7. Stress-strain data for a 3D interlock weave tested in uniaxial tension aligned with the stuffers (from [4.22]).

## 4.4 Delamination under Through-Thickness Tension (Curved Structures)

Through-thickness tension arises in curved panels whenever the sense of in-plane moments creates in-plane compression, $\sigma^{(o)}$, on the outer surface of the panel (Fig. 4-8 and [4.26]). For polymer composites, the maximum magnitude of the tensile stress, $\sigma_o$, which occurs near the panel's midplane, can be written

$$\sigma_o = \sigma^{(o)} \frac{h}{r_m} \eta \left(\frac{h}{r_m}\right) \tag{4.3}$$

where $h$ is the half-thickness of the panel, $r_m$ is its median radius, and $\eta$ is a dimensionless function given approximately by $\eta \approx 1 + 0.6h/r_m + (h/r_m)^2$ [4.27,4.28].

In the presence of a delamination crack of length $2a$, which may be a pre-existing flaw or damage induced by impact, the stress $\sigma^{(o)}$ will cause failure if it exceeds the critical critical value, $\sigma_1$, for delamination crack growth. Since $\sigma_1$ falls as $a^{-1/2}$, the critical value of

$\sigma^{(o)}$ can be arbitrarily small for sufficiently severe flaws or damage. The maximum in-plane stress for which the part can be designed falls commensurately.

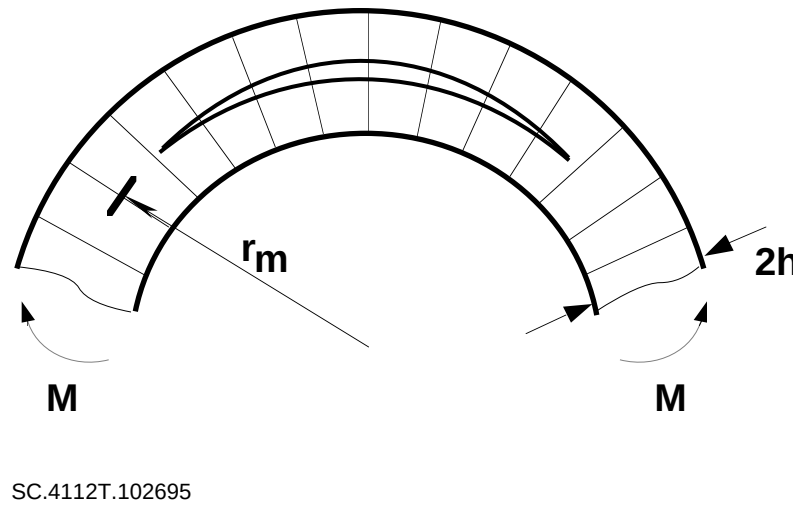


Figure 4-8. Stitching bridging a delamination crack in a curved part.

Through-thickness reinforcement such as stitching bridges delamination cracks, shields the crack tip from the applied load, and thus can suppress delamination crack growth. A simple, conservative bound to the effect of the stitches can be found by considering them to be linear springs of length equal to the panel thickness [4.28]. For such bridging springs, the critical stress for crack growth approaches a constant value, $\sigma_1$, independent of crack length for sufficiently long delaminations [4.28,4.29]. The stress, $\sigma_1$, can be related analytically to the properties of the stitches. Since $\sigma_1$ is a lower bound to the critical value of $\sigma_o$, a design rule can be deduced for the minimum volume fraction of stitching fibers required to suppress delamination crack growth. One way of expressing the rule is to require that $\sigma_o < \sigma_1$ as long as $\sigma^{(o)} < \sigma_c$, where $\sigma_c$ is the critical stress for in-plane failure. If delamination is suppressed, the latter will probably be via kink band formation. Then the volume fraction, $f_S$, of stitching fibers must satisfy [4.28]

$$f_s > \frac{\eta^2}{4}\,\sigma_c^2\,\frac{h^2}{r_m^2}\,\frac{h}{E_s G_{Ic}} \tag{4.4}$$

where $E_S$ is the modulus of the stitching fibers and $G_{Ic}$ is the critical Mode I strain energy release rate for a delamination crack in an unstitched laminate.

The strength of the stitches must also be sufficient to ensure that the through-thickness tension cannot rupture them. This enforces a second condition on the stitch density [4.28]:

$$f_s > \frac{\eta}{3}\frac{h}{r_m}\frac{\sigma_c}{\sigma_s} \tag{4.5}$$

where $\sigma_s$ is the strength of a stitching tow and it has been assumed that the fiber volume fraction within a stitch = 0.67. Which of Eqs. (4.4) and (4.5) is the more stringent condition depends on the relative curvature of the panel and the various material parameters involved. The possible failure modes for a curved part are mapped in Fig. 4-9.

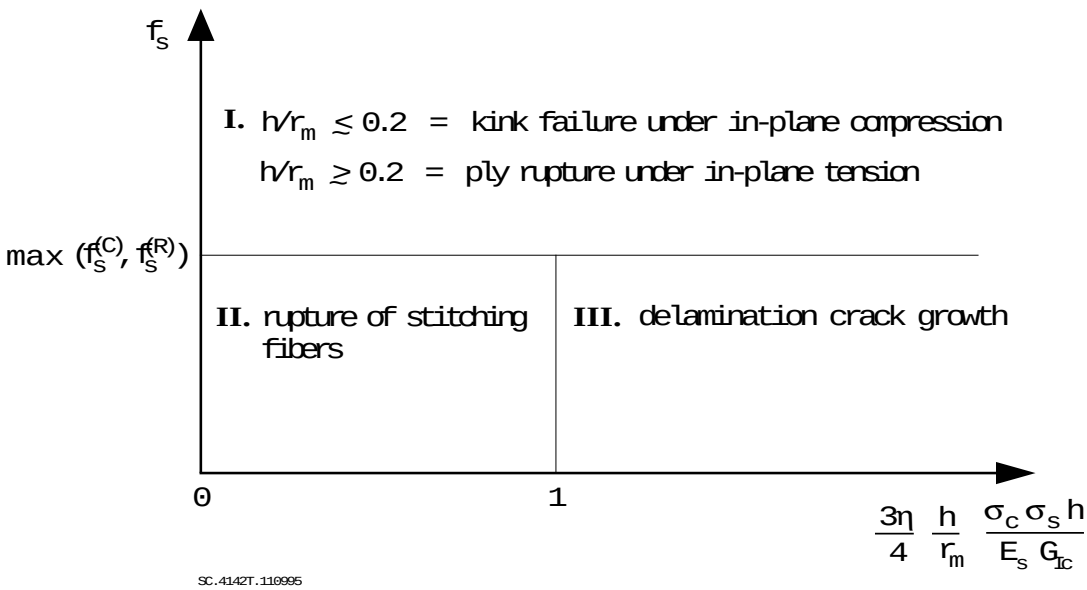


Figure 4-9. Map of failure modes for a curved panel. The transition from failure on the compressive side to failure on the tensile side in Domain I depends on the relative values of the critical stresses for tensile rupture and kinking. The critical value of $h/r_m$ shown corresponds to a tensile rupture stress that is 50% higher in magnitude than the kinking stress.

Through-thickness tension can also arise around joints and in thick, shaped sections. If these structures are built up from laminated plies, there is again severe risk of delamination. However, while textile composites may be the only practicable means of overcoming such delamination problems, experimental observations of failure mechanisms in parts of general shape with triaxial stresses are still being gathered.

## 4.5 Shear Delamination in Bending

When shear stresses are created by bending near a free edge or notch, delamination crack growth can ensue under pure Mode II or mixed mode conditions. In a 2D laminate, the crack growth is catastrophic for common loading configurations, with the critical stress falling with the length of the initial delamination length.

Through-thickness reinforcement changes the mechanics of Mode II delamination in a similar way to its effect on Mode I delamination, bridging the crack and imposing shielding shear tractions on the fracture surfaces. The resulting fracture behaviour has been well illustrated by models and tests of stitched laminates, especially using the end-notch flexure test configuration [4.30-4.32]. Provided the stitches remain intact, the critical applied load, $\tau_d$, for delamination crack propagation approaches a steady-state value, $\tau_{ss}$, which is independent of the delamination crack length for long enough cracks. Like the critical stress, $\sigma_1$, for bridged Mode I delaminations (Sect. 4.4), $\tau_{ss}$ is a material property of the composite. Since all delaminations must remain relatively short for smaller values of the applied shear stress, $\tau_{ss}$ can be used as a design limit. However, the stitching must also be strong enough to remain intact. If it fails, catastrophic delamination crack growth will resume, but the Mode II delamination toughness will still be enhanced by the work required to stretch and break the stitches [4.30,4.32].

## 4.6 Notch Sensitivity

Textile composites are generally remarkably notch insensitive. In both tension and compression, cohesive or nonlinear process zones form at the notch and redistribute loads in such a way as to reduce the stress concentration factor and minimize the degradation of ultimate strength. Stress concentration factors can also be limited by splitting cracks running from the notch root parallel to the load axis, which isolate the material ahead of the notch from the notch stress fields. Both of these mechanisms are familiar in tape laminates, but they can both be much more effective in textile composites.

### *4.6.1 Cohesive Zones*

The effectiveness of a cohesive zone in redistributing loads around a notch is determined by mechanisms that permit significant local displacements without complete loss of strength. The cohesive zone is characterized by the relation between the tractions, $p$, it supports and the displacement discontinuity, $2u$, it introduces into the elastic material

around it [4.33]. The notch sensitivity of the composite depends mainly on the strength of the tows and the work of fracture [4.34]

$$W_f = \int p \, du \quad . \tag{4.6}$$

Very few observations of the mechanisms in cohesive zones have been made in notched specimens. However, detailed observations during uniaxial tension tests of 3D interlock weaves [4.22], which were summarized in Sect. 4.3.3, are probably an excellent guide to what to expect in a notched specimen. The nature of the observed phenomena themselves also suggests that they are likely to be found in nearly all textile composites containing significant volume fractions of aligned tows.

Figure 4-10 shows a schematic of a cohesive zone as inferred from the observations for 3D interlock weaves. At the furthest distances from the notch, the earliest damage in the band consists of matrix cracking, for example transverse cracks between the orthogonally disposed tows in an interlock weave. Because this cracking occurs at relatively low loads and strains, it makes a relatively small contribution to $W_f$ and therefore to notch effects. Nearer the notch, the plastic straightening and rupture of aligned tows occurs. As far as these effects are confined to a band associated with the notch, they may be subsumed in the relation $p(u)$. (If damage is spread more or less uniformly over the whole composite, this is large scale yielding and the cohesive zone is no longer an appropriate depiction of events.) Tow rupture will define the maximum traction, $p_{max}$, supported by the cohesive zone. Following tow rupture, cohesive tractions will continue to be supported as the broken tows are pulled out of the composite across the eventual fracture plane. When the tows are fully pulled out, a traction free crack exists, which occurs first at the notch root.

Tow pullout lengths can be exceptionally large in textile composites. Part of the reason is the large tow diameters preferred in textiles to minimize manufacturing costs. When a single tow breaks, debonding from the surrounding composite occurs over a slip length, $l_s$, which scales as the ratio of the tow's area and circumference, i.e. as its diameter [4.1]. Pullout lengths also depend on the spatial distribution of flaws in the aligned tows. since tow strength is probably impaired by tow crimp and pinching, there is scope for designing a favourable distribution of flaws into the composite by controlling the extent to which aligned tows are impinged upon by other tows.

After tow failure in 3D interlock weaves, there is an interval where pullout of the broken tow ends is opposed by unusually strong friction, an effect dubbed lockup (Section 4.3.3; [4.22,4.35]). This peculiarity of textile composites is intimately linked to the

irregularity endemic to textile products. Lockup is the impingement of irregular features on neighbouring tows as they are dragged by one another during the pullout process. It is abetted by the through-thickness compression generated by the through-thickness reinforcement in a 3D composite when it is loaded in in-plane tension. Through-thickness compression forces sliding tows into close contact. Lockup allows the cohesive traction, $p$, to remain near its peak value, $p_{max}$, while displacement discontinuities $2u \sim 1$ mm are developed. The resulting contribution to $W_f$ is of the order of 1 $MJm^{-2}$ in some 3D interlock weaves. The characteristic length, $l_{ch}$, of the cohesive zone will correspondingly be ~ 100 mm. Notch sensitivity will be found only for notches exceeding this dimension, as discussed in Section 3.6. For tape laminates, $W_f \sim 100$ $MJm^{-2}$ and $l_{ch} \sim 3$ mm at most.

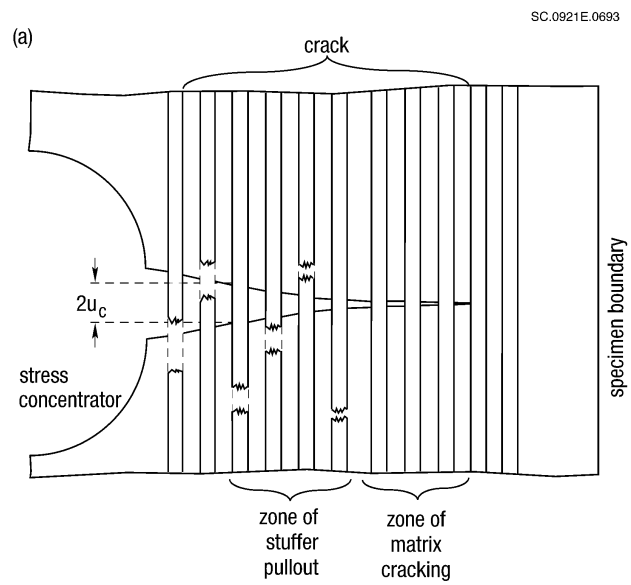


Figure 4-10. Schematic of a nonlinear damage band growing from a stress concentrator in a textile composite.

### *4.6.2 Splitting at a Notch*

The mechanics of splitting cracks running parallel to the load axis from notches have been much studied (e.g. [4.36]). A splitting crack will be energetically favoured when the toughness, $G_s$, of the material through which it must propagate is much lower than the composite toughness, $G_{Ic}$, for propagation of a mode I crack normal to the applied load. In a textile composite, $G_{Ic}$ is large; e.g., ~ 1 $MJm^{-2}$ for 3D angle interlock weaves, as discussed above. But the arrangement of fibers into discrete tows also lowers $G_s$, since it creates resin rich layers which are easy paths for fracture. The mechanics of splitting cracks in textile is a subject of current research.

## 4.7 Fatigue

Reported accounts of fatigue mechanisms in textile composites are few and incomplete. For 3D textile composites, even basic fatigue data, without any observations of mechanisms, are unavailable for some important loading conditions, especially non-aligned or multi-axial loads. This survey is correspondingly imperfect. Nevertheless, the available data do reveal some consistent mechanisms in many classes of textiles, inviting generalizations that may turn out to apply to all or at least most cases.

1. For cyclic loads aligned with one primary fiber orientation, the local failure events are much the same as they are in monotonic loading, viz. microcracking; delaminations, including interply and intraply delaminations in 2D composites; kink band formation; and tow rupture.

2. In high cycle fatigue, microcracking tends to be less abundant than in monotonic loading, because damage accumulates inside aligned tows at a few favourable locations at stresses below the threshold for damage elsewhere. The favourable locations are determined by the textile architecture and by geometrical imperfections (especially tow misalignments).

3. At least in 3D interlock weaves, fatigue damage accumulates more rapidly on the compressive phase of the loading cycle.

4. In parallel with their damage tolerance in monotonic loading, 3D textiles gradually accumulate spatially distributed fatigue damage. In strain control, they may have extensive life beyond the first tow failures or the first significant loss of stiffness.

### *4.7.1 2D Weaves and Braids*

Observations for triaxial braids are available for tension-tension fatigue only [4.15]. For loading aligned with the axial tows, fatigue damage commences with tensile microcracking in resin pockets and microcracking within bias tows that may be driven by either tension or shear, depending on the bias angle. The composite stiffness declines rapidly during this phase. After further cycles, the decline in stiffness slows, but axial tows become disbonded from the bias tows, eventually splitting and rupturing.

### *4.7.2 3D Interlock Weaves*

Just as under monotonic loading, the principal failure mechanism for interlock weaves subject to aligned cyclic compression is kink band formation [4.37]. The kinks form in segments of nominally straight tows that have unusually high misalignment (e.g., Fig. 4-11). Fatigue damage accumulation apparently consists of damage to the resin within individual tows. This may either allow rotation of fibers and an increase of the misalignment angle, $\phi$, of the affected segment; or a gradual lowering of the critical shear flow stress, $\sigma_c$ [4.37,4.38]. Some evidence indicates that the latter is more likely in interlock weaves [4.37]. In either case, the criterion for kink band formation, Eq. (4.1), will eventually be satisfied and kink failure will occur in the tow.

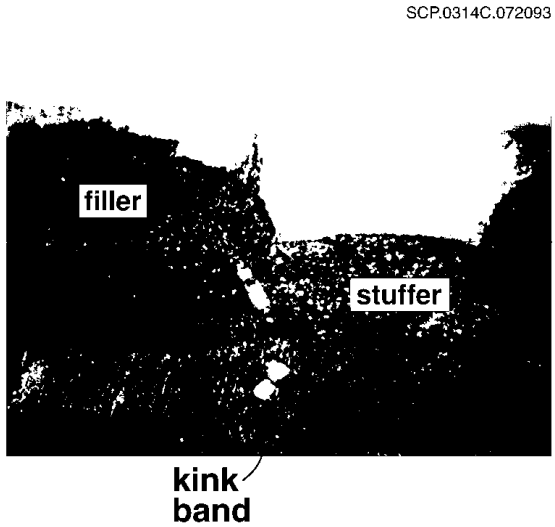


Figure 4-11. A kink band formed in fatigue in a misaligned segment of a stuffer in an AS4/1895 layer-to-layer interlock weave (from [4.37]).

Just as in monotonic loading, a kink failure in one tow does not usually propagate unstably into neighbouring tows. The failed tow debonds from the surrounding composite via a peripheral matrix crack, minimizing local stress concentrations. Since misaligned segments, which act as geometrical flaws, tend to be broadly distributed in space in 3D interlock weaves, subsequent kinking tends to occur elsewhere in the composite [4.18]. Ultimate failure under strain control might involve a widely distributed accumulation of separate kink events.

## References

4.1 B. N. Cox, M. S. Dadkhah, and W. L. Morris, "Failure Mechanisms for 3D Woven Composites in Tension, Compression, and Bending," *Acta Metall. Mater.* **42** (1994) 3967-84.

4.2 M. S. Dadkhah, W. L. Morris, T. Kniveton, and B. N. Cox, "Simple Models for Triaxially Braided Composites," *Composites* **26**, 91-102 (1995).

4.3 N. A. Fleck, "Brittle Fracture due to an Array of Microcracks," *Proc. Roy. Soc. London* **A432**, 55-76 (1991).

4.4 Z. C. Xia and J. W. Hutchinson, "Mode II Fracture Toughness of a Brittle Adhesive Layer," *Int. J. Solids Structures* **31**, 1133-1148 (1994).

4.5 D.M. Blackketter, D.E. Walrath, and A.C. Hansen, "Modeling Damage in a Plain Weave Fabric-Reinforced Composite Material," *J. of Composites Technology & Research* **15**[2], 136-142 (1993).

4.6 A. S. Argon, in *Treatise on Materials Science and Technology*, Vol. 1, Academic Press, New York.

4.7 B. Budiansky and N. A. Fleck, "Compressive Failure of Fibre Composites," *J. Mech. Phys. Solids* **41**, 183-211 (1993).

4.8 M. Hetényi, *Beams on Elastic Foundation*, University of Michigan Press, Ann Arbor, Michigan, 1946.

4.9 B. N. Cox, "Fundamental Concepts in the Suppression of Delamination Buckling by Stitching," in *Proc. 9th DoD/NASA/FAA Conf. on Fibrous Composites in Structural Design*, Lake Tahoe, Nevada, November 1991, ed. J. R. Soderquist, L. M. Neri, and H. L. Bohon (U.S. Dept. Transportation, 1992) pp. 1105-1110.

4.10 B. N. Cox, "Delamination and Buckling in 3D Composites," *J. Comp. Mater.*, **28** (1994) 1114-26.

4.11 Shu and Y.-W. Mai, "Effect of Stitching on Interlaminar Delamination Extension in Composite Laminates," *Comp. Sci. and Tech.* **49**, 165-71 (1993).

4.12 A. G. Evans and W. F. Adler, "Kinking as a Mode of Structural Degradation in Carbon Fiber Composites," *Acta Met.* **26**, 725-38 (1978).

4.13 K. L. Reifsnider and F. Mirzadeh, "Compressive Strength and Mode of Failure of 8H Celion 3000/PMR15 Woven Composite Material," *J. Comp. Tech. Res.* **10**, 156-64.

4.14 M. Karayaka and P. Kurath, "Deformation and Failure Behaviour of Woven Composite Laminates," *J. Eng. Mater. Tech.* **116**, 222-32 (1995).

4.15 S. T. Burr and D. H. Morris, "Characterization of 2-Dimensionally Braided Composites Subject to Static and Fatigue Loading," in *Mechanics of Textile Composites Conference*, ed. C. C. Poe, Jr. and C. E. Harris, NASA Conference Publication 3311 (NASA, 1995).

4.16 J. E. Masters, R. L. Foye, C. M. Pastore, and Y .A. Gowayed, “Mechanical Properties of Triaxially Braided Composites: Experimental and Analytical Results” *J. of Composites Technology & Research* **15**[2], 112-122 (1993).

4.17 P. J. Minguet and C. K. Gunther, *A Comparison of Graphite/Epoxy Tape Laminates amd 2-D Braided Composites Mechanical Properties*, NASA Contractor Report 4610, Boeing Defense and Space Group, Philadelphia, Pennsylvania, 1994.

4.18 B. N. Cox, M. S. Dadkhah, W. L. Morris, and J. Zupon, "Mechanisms of Compressive Failure in 3D Composites," *Acta Metall. Mater.* **40**, 3285-3298 (1992).

4.19 B. N. Cox, *Failure Models for Textile Composites*, NASA Contractor Report 4686, Rockwell Science Center, Thousand Oaks, California, 1995.

4.20 J. M. Hedgepeth and P. Van Dyke, "Local Stress Concentrations in Imperfect Filamentary Composite Materials," *J. Comp. Mater.* **1**, 294-309 (1967).

4.21 J. Xu, B. N. Cox, M. A. McGlockton, and W. C. Carter, "A Binary Model of Textile Composites - II. The Elastic Regime," *Acta Metall. Mater.* **43**, 3511-24 (1995).

4.22 B. N. Cox, M. S. Dadkhah, and W. L. Morris, "On the Tensile Failure of 3D Woven Composites," *Composites*, in press.

4.23 A. Fujita, Z. Maekawa, H. Hamada, and A. Yokoyama, "Mechanical Behavior and Fracture Mechanism in Flat Braided Composites. Part 1: Braided Flat Bar," *J. Reinf. Plastics Comp.* **11**, 600-17 (1992).

4.24 N. K. Naik, P. S. Shembekar, and M. V. Hosur, "Failure Behaviour of Woven Fabric Composites," *J. Comp. Tech. and Res.* **13**[1], 107-16 (1991).

4.25 A.-M. Harte and N. A. Fleck, private communication, 1995.

4.26 S. P. Timoshenko and J. N. Goodier, *Theory of Elasticity* (McGraw-Hill, New York, 1951).

4.27 T. J. Lu, Z. C. Xia, and J. W. Hutchinson, " Delamination of Beams under Transverse Shear and Bending," *Mater. Sci. Eng.* **A188**, 103-12 (1994).

4.28 B. N. Cox, R. Massabò, and K. Kedward, “The Suppression of Delaminations in Curved Structures by Stitching,” *Composites*, in press.

4.29 T.-J. Lu and J. W. Hutchinson, "Role of Fiber Stitching in Eliminating Transverse Fracture in Cross-Ply Ceramic Composites," *J. Amer. Ceram. Soc.* **78**, 251-3 (1995).

4.30 L. K. Jain and Y.-W. Mai, “On the Effect of Stitching on Mode I Delamination Toughness of Laminated Composites,” *Composites Science and Technology* **51**, 331-45 (1994).

4.31 B. V. Sankar and S. K. Sharma, "Effects of Stitching on Fracture Toughness of Uniweave Textile Graphite/Epoxy Laminates," in *Mechanics of Textile Composites Conference*, ed. C. C. Poe, Jr., and C. E. Harris, NASA Conf. Publ. 3311, October, 1995.

4.32 R. Massabò and B. N. Cox, "Concepts for Bridged Mode II Delamination Cracks," submitted to *Mechanics of Materials*.

4.33 B. N. Cox and D. B. Marshall, “Concepts for Bridged Cracks in Fracture and Fatigue,” *Acta Metall. Mater.* **42**[2], 341-63 (1994).

4.34 G. Bao and Z. Suo, “Remarks on Crack Bridging Concepts," *Appl. Mech. REv.* **24**, 355-66 (1992).

4.35 B. N. Cox, “Lockup, Chains, and the Delocalization of Damage,” *J. Mater. Sci.*, in press.

4.36 K. S. Chan, M. Y. He, and J. W. Hutchinson, "Cracking and Stress Redistribution in Ceramic Layered Composites," *Mater. Sci. Engng* **A167**, 57-64 (1993).

4.37 M. S. Dadkhah, B. N. Cox, and W. L. Morris, "Compression-Compression Fatigue of 3D Woven Composites," *Acta Metall. Mater.* **43**[12], 4235-45 (1995).

4.38 W. S. Slaughter and N. A. Fleck, "Compressive Fatigue of Fiber Composites," *J. Mech. Phys. Solids* **41**[8], 1265-84 (1993).

# 5. PREDICTION OF ELASTIC CONSTANTS AND THERMAL EXPANSION

## 5.1 Concepts

The great challenge in modeling the elastic properties of textile composites is dealing sufficiently well with the very large variations in stress and strain that can occur within a textile even under uniform applied loads. A textile composite is a highly heterogeneous structure. It may be viewed (and is often modeled) as a three-dimensional tessellation of grains, each of which is an approximately unidirectional composite and therefore transversely isotropic, with the plane of isotropy lying normal to the local fiber direction. In polymer composites, the anisotropy factor for each grain is high, with $E_{\text{axial}}/E_{\text{transverse}} \approx 20$ for typical graphite/epoxy. The distribution of stresses among the different grains therefore depends very strongly on their relative sizes and orientations and on the degree of order in their organization. In other words, it depends on the textile architecture.

All models deal with this difficult situation by simplifying the description of the textile geometry and restricting the allowable internal stress variations. Models can be categorized into a few main groups according to how this is done. In choosing a particular model for some class of composites, the user should first ask whether the simplifying steps are valid for the given architecture. The following discussion of essential concepts will provide a guide to answering this question.

### *5.1.1 Isostrain and Isostress*

In infinite 2D laminates, uniform in-plane loads cause identical in-plane strains in each ply. Thus laminate theory for non-bending plates is based on an isostrain condition for the in-plane coordinates. The analysis of macroscopic elasticity is reduced to the simple analysis of a few macroscopic stress or strain components. Bending flat laminar plates causes a gradient in the in-plane strains through the thickness, but since the gradient is uniform, the relationship between stresses and strains in different plies remains trivial [e.g., 5.1].

If an infinite 2D laminate is subjected to a uniform through-thickness load, identical through-thickness stresses arise in each ply and an isostress condition exists for the through-thickness coordinate. Of course, through-thickness loads are always nonuniform (unless they are zero); but if they vary slowly over distances comparable to

the thickness of a single ply, isostress conditions may be considered to prevail locally in estimating the lumped stiffness of many plies.

The isostress or isostrain assumption works in 2D laminates because of translational invariances in the laminar structure. For example, when an observer scans along the load axis in Fig. 5-1, the composite he sees does not change. This translational invariance implies that planes normal to the load axis have no cause to deform under the load; they remain plane and the isostrain condition prevails. Translational invariance along two orthogonal in-plane axes is required for isostrain conditions to hold under in-plane shear; for isostress conditions to exist locally under through-thickness loads; and for strain gradients to be uniform in bending.

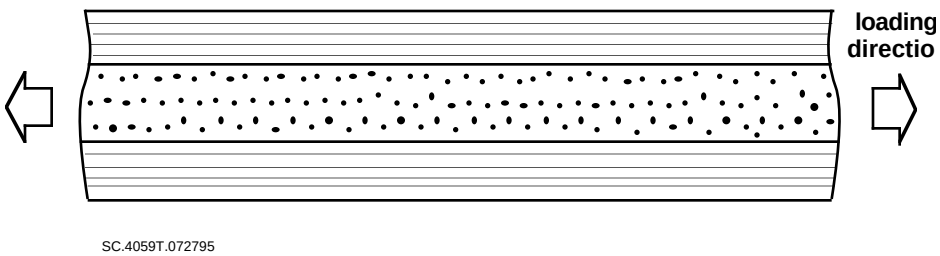


Figure 5-1. Translationally invariant 2D laminate.

Textile composites are frequently analyzed by assuming an isostrain or isostress condition. Under combined in-plane and bending loads, quasi-laminar textile composites are also usually represented by laminate theory. *Whether these steps are valid will be determined by the extent to which the textile composites are translationally invariant on the scale over which stress variations are being modeled.*

### *5.1.2 Tow Properties*

With no exception known to the writers, it is always adequate in modeling the *elastic* properties of textile composites to regard tows as being internally homogeneous. The fibers and resin within tows need not be modeled separately. Furthermore, in every case studied, the distributions of the fibers in any two directions normal to the tow axis are equivalent, whatever the tow aspect ratio. Therefore, in the absence of twist, the tows are transversely isotropic over any gauge length significantly greater than the fiber diameter.

Thus tow properties can be equated to the macroscopic properties of an equivalent unidirectional composite. Various closed form approximations for estimating the latter

from the fiber volume fraction and the fiber and matrix properties are available in the literature. The simplest are rules of mixtures (e.g., [5.1,5.2]). Better models offer more realistic partitioning of stress between fibers and resin [5.3-5.7]. The main features of some important models are compared in Table 5.1 and some tow properties computed for AS4/1895 are shown as functions of fiber volume fraction in Fig. 5-2. Each model predicts five elastic constants corresponding to the five degrees of freedom allowed by transverse isotropy. Only Hashin's model admits anisotropy in the fibers themselves; all the other models assume the fibers and resin are separately isotropic. Assuming glass fibers are isotropic is very plausible. But the anisotropy in common carbon fibers is substantial and Hashin's model should then be preferred [5.8].

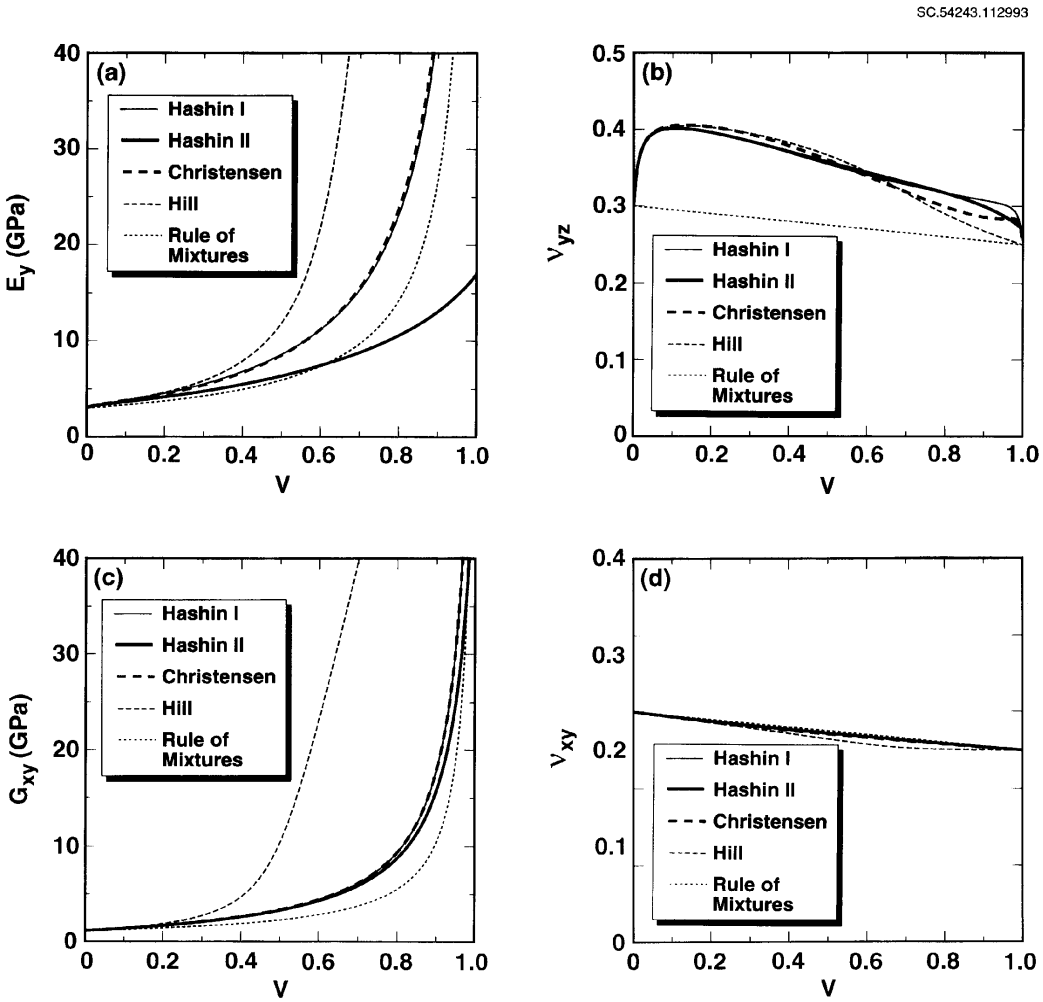


Figure 5-2. Comparison of the elastic constants predicted for tows in an AS4/1895 composite using various models from the literature (Table 5.1). Hashin I: assuming the same isotropic fiber elastic constants as in the other models. Hashin II: using anisotropic fiber elastic constants for AS4 fibers.

**Table 5.1 Some Models of Unidirectional Fiber Composites**

| Model | Remarks |
|---|---|
| 1. Rule of Mixtures [5.1, 5.2] | Simplistic stress partitioning |
| 2. Hill [5.4] | Inaccurate for polymer composites |
| 3. Christensen [5.5] | Accurate for isotropic fibers only |
| 4. Van Fo Fy [5.7] | Accurate for isotropic fibers only<br>Relatively cumbersome |
| 5. Hashin [5.3] | Bounds only; but narrowly spaced for unidirectional composites<br>Allows fiber anisotropy |

Computer codes for the micromechanical models in [5.3-5.7] can be found as FORTRAN subroutines in program **WEAVE** (Section 8).

Properties computed for AS4/epoxy and other carbon/polymer systems are compared in Table 5.2 (computed by Dr. R. Naik using a finite element model and the constituent data of Table 2.1).

**Table 5.2 Estimated Mechanical Properties of Tows**

| Fiber | Matrix | $V_f$ | $E_{11}$ (GPa) | $E_{22}$ (GPa) | $\nu_{12}$ | $\nu_{23}$ | $G_{12}$ (GPa) | $G_{23}$ (GPa) |
|---|---|---|---|---|---|---|---|---|
| AS4 | Epoxy | 0.65 | 154 | 11.8 | 0.32 | 0.42 | 5.2 | 4.1 |
| AS4 | Epoxy | 0.70 | 165 | 12.8 | 0.32 | 0.42 | 6.0 | 4.5 |
| AS4 | Epoxy | 0.75 | 177 | 13.8 | 0.32 | 0.41 | 7.0 | 4.9 |
| AS4 | Epoxy | 0.80 | 188 | 15.0 | 0.31 | 0.4 | 8.2 | 5.4 |
| IM6 | Epoxy | 0.65 | 177 | 10.3 | 0.35 | 0.45 | 5.2 | 3.6 |
| IM6 | Epoxy | 0.70 | 190 | 11.0 | 0.35 | 0.44 | 5.9 | 3.8 |
| IM6 | Epoxy | 0.75 | 203 | 11.8 | 0.35 | 0.44 | 6.8 | 4.1 |
| IM6 | Epoxy | 0.80 | 216 | 12.5 | 0.35 | 0.43 | 8.0 | 4.4 |
| AS4 | PEEK | 0.65 | 154 | 12.4 | 0.34 | 0.49 | 4.8 | 4.1 |
| AS4 | PEEK | 0.70 | 165 | 13.4 | 0.33 | 0.48 | 5.5 | 4.6 |
| AS4 | PEEK | 0.75 | 177 | 14.4 | 0.33 | 0.46 | 6.4 | 4.9 |
| AS4 | PEEK | 0.80 | 188 | 15.4 | 0.32 | 0.45 | 7.6 | 5.7 |
| AS4* | ~ | ~ | 234 | 22.4 | 0.3 | 0.35 | 22.1 | 8.3 |
| IM6* | ~ | ~ | 269 | 17.2 | 0.34 | 0.39 | 20.7 | 6.2 |
| ~ | Epoxy** | | 4.0 | | 0.37 | | | |
| ~ | PEEK** | | 3.6 | | 0.42 | | | |

*Bare fiber bundle properties (strength gauge length dependent)

**Neat resin properties

In reality, the tows in textile composites do usually have more complicated internal structure than unidirectional composites. Fibers within single tows follow tortuous, tangled paths, rather than being perfectly aligned. Large filament count tows are formed by combining several smaller tows, which usually leaves resin rich internal boundary layers. The smaller tows may also be twisted separately and the larger tow they form may be twisted as a whole, either deliberately or inadvertently. The tow will then not strictly be transversely isotropic. Yet these complications will not violate overall symmetry significantly. Minor deviations from transverse isotropy in individual tows will not alter the symmetry of the tow architecture on the scale of the textile. Local biases cancel one another out over larger scales. The effects of twist and other fiber irregularities within tows on macroscopic elasticity are never more than a modest reduction in the effective axial stiffness of a tow; perhaps ~ 1%. They are generally insignificant compared to the effects of tow waviness (Section 3).

### *5.1.3 Fiber Packing and Resin Pockets*

Because textile composites are manufactured with relatively large fiber tows which curve around one another in complex patterns, they contain significant volumes of resin pockets. The density of fibers, $V_t$, within tows is therefore higher (typically $0.65 \leq V_t \leq 0.7$) than the fiber density, $V$, averaged over representative volumes of the composite (typically $0.5 \leq V \leq 0.6$). It is the latter density that is measured by standard tests of fiber volume fraction, e.g. measuring the areal weight of preforms; or measuring the fiber content of composites by matrix dissolution [5.9].

Direct measurement of the volume of resin held in resin pockets requires painstaking sectioning of specimens. In engineering design situations, it will probably always be the case that resin pockets will be incompletely characterized. The volume fraction of fibers within tows will therefore not be known exactly.

Nevertheless, in textile composites designed for high stiffness, this uncertainty will always have a negligible effect on computed macroscopic properties. In high stiffness applications, a good fiber architecture is one in which all critical elastic moduli are fiber dominated; in other words, nearly straight fibers are so oriented that any extensional or shear strain is opposed by the axial extension or compression of fibers. Now the axial stiffness of a tow is very nearly proportional to the fiber volume fraction, $V_t$, assumed to exist within it; while the fraction of the whole composite constituted by the tow is *inversely* proportional to $V_t$ for fixed fiber counts. Therefore, the contribution

of the tow to composite stiffness is nearly independent of $V_t$. The critical characteristic is simply the total number of fibers in the tow, not their density of packing [5.8].

In the looping geometry of knitted fabrics made of yarns of approximately equal weight[1], on the other hand, all yarns have significant curvature over most of their lengths. Macroscopic properties are not fiber dominated, but depend more strongly on the response of tow segments to local transverse and shear stresses. Because transverse and shear tow moduli depend nonlinearly on the assumed value of $V_t$ (Fig. 5-2), the composite elastic constants can be influenced by the assignment of $V_t$ to a modest degree [5.10].

### *5.1.4 Unit Cells and Periodic Boundary Conditions*

Many textile processes yield patterns of interlaced tows or yarns that repeat in one or two directions; they are periodic. A large volume of such a structure can be generated in a model by stacking together unit cells, each of which represents the tows in one period or cycle. (The term unit cell has been borrowed from crystallography, e.g. [5.11].) The response of the textile composite to external loads can then be computed by analyzing the behavior of a single unit cell with suitable boundary conditions.

For any periodic structure, there are infinitely many ways of choosing a unit cell. For example, if a cuboid aligned with the axis system ($x_1$, $x_2$, $x_3$) is one possible unit cell, then so too is the rhombohedron obtained by shearing the faces normal to any one of these axes in the direction of either of the other two axes through a displacement equal to a multiple of its original length (Fig. 5-3). Equally, either unit cell outlined in Fig. 5-3 will remain a unit cell if it is displaced to the right or left by *any* distance.

Under uniform external loads, the stress and strain distribution in a periodic textile composite must also be periodic. The analysis of a single unit cell should therefore be subject to periodic boundary conditions for stresses or strains. The solutions obtained for different unit cells chosen to represent the same periodic structure should in principle be the same, although small differences may arise in practice because of inconsistent approximations in the numerical methods used, especially in the definition of computational grids. The choice of unit cell is usually guided by other symmetry properties of the textile. For example, choosing the unit cell to be symmetric about a

[1] When warp knitting is used to tie together heavy yarns (e.g., of carbon fibers) with a light thread (e.g., of polyester), the heavier yarns are often kept as straight as possible by design. Generalizations intended for fabrics with highly curved yarns are then inapplicable.

plane of mirror symmetry in the textile allows the use of a reduced cell in calculations, halving the size of the problem that has to be solved (solid line rectangle in Fig. 5-3).

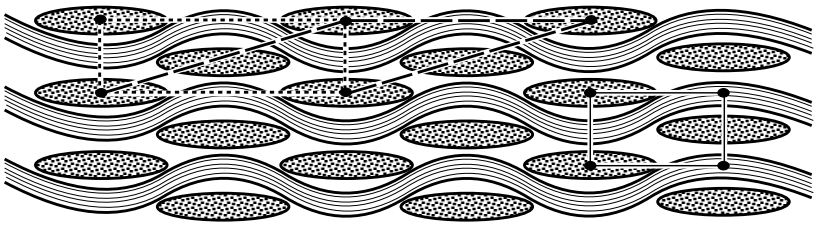


Figure 5-3. Alternative unit cells (short and long dash lines at upper left) in a plane woven laminate. The smaller, solid-lined rectangle (lower right) shows a reduced cell that takes advantage of reflection symmetry about a vertical plane.

The interior of the unit cell is often modeled in fine detail. In typical unit cell calculations, grids are defined to replicate each tow segment bounded by the cell and each resin pocket between tows. Interior stresses and strains are computed by a finite element simulation subject to periodic boundary conditions on the cell walls. Since the unit cell is a 3D structure with heterogeneous and highly anisotropic components, even a mildly complex textile architecture requires a large number of interior elements. Unit cell calculations are usually computationally intensive. The output of unit cell calculations includes both the spatially averaged response of the cell and details of stress distributions among tows and resin pockets.

Some workers have minimized computational cost by introducing simplified models of tow segments within the unit cell. For example, tow segments can be represented crudely as bending or shearing beams; or the unit cell of a quasi-laminar textile can be modeled by a variant of laminate theory. The properties of the unit cell are then computed relatively easily. However, the quality of calculations of the details of interior stress distributions is impaired.

When external loads are nonuniform, periodicity no longer exists in stresses and strains; and periodic boundary conditions are no longer correct for the unit cell. The strain in one cell of the composite has no simple relation to the strain in any of its neighbors (Fig. 5-4). One approach to modeling such cases is to calculate and store the response of a unit cell to uniform strains and uniform strain gradients; and then compute the response of an assembly of such cells when the strains and strain gradients are constrained to be compatible. In other words, the averaged response of the unit cell is

used to define a special element for a finite element calculation on a coarser scale. But the coarser finite element calculation should not be categorized as a unit cell calculation.

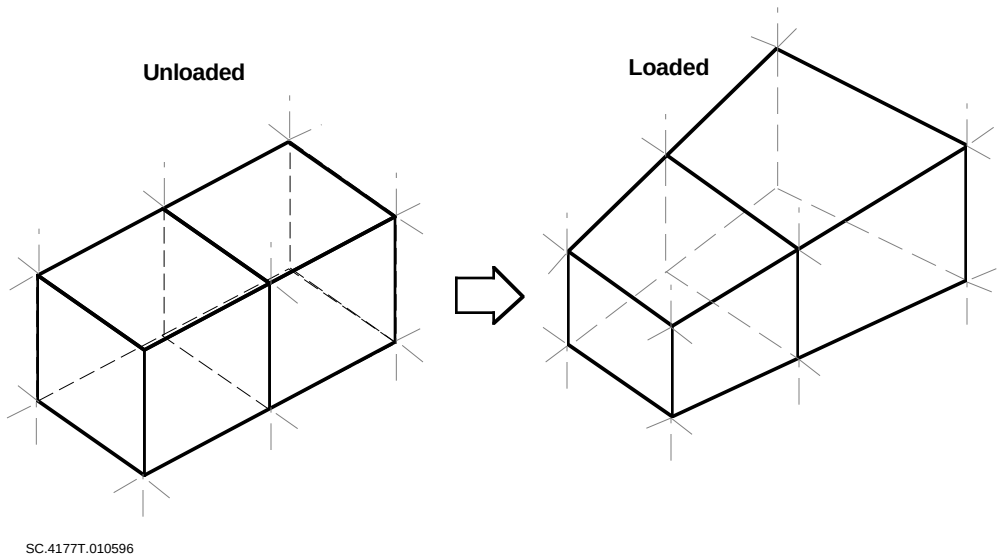


Fig. 5-4. Nonperiodic strains in a periodic structure under nonuniform external loads. Schematic of two unit cells in a larger array.

Several other factors limit the usefulness of the unit cell approach. If the textile architecture is periodic but complicated, the unit cell can become prohibitively large. In a 2D plain weave, a computational cell can be defined that contains just a handful of tow segments (e.g. Fig. 5-3). In a 3D interlock weave, in contrast, the unit cell may contain segments of ~100 tows. One example is the angle interlock woven panel of Fig. 5-5, in which the phase of the warp weavers is staggered in the filler direction. This architecture has a period of ten fillers in the stuffer direction and ten stuffers in the filler direction. The unit cell also contains ten warp weavers; and, because of the absence of translational invariance in the through-thickness direction, it must span from top to bottom of the panel. In all, it contains segments of 140 different tows. Finite element calculations of such a cell, with grids fine enough to represent the details of each tow's geometry, are not viable. To proceed, further assumptions about the distributions of stresses must be made to break the cell down into smaller constituents.

### *5.1.5 Macroscopic Length Scales*

The analysis of a structure is greatly simplified if the structural material can be treated as homogeneous over length scales comparable to any feature of the structure. Identifying the minimum length scales for homogeneity defines the term macroscopic in discussing elastic or other mechanical properties. A measured elastic constant is only a

meaningful material property if it is measured over gauge lengths that are macroscopic according to this definition. If the property is measured over smaller gauges, unacceptable variance will occur in the measurement. In textile composites, macroscopic length scales are unusually large and their consideration is therefore unusually important.

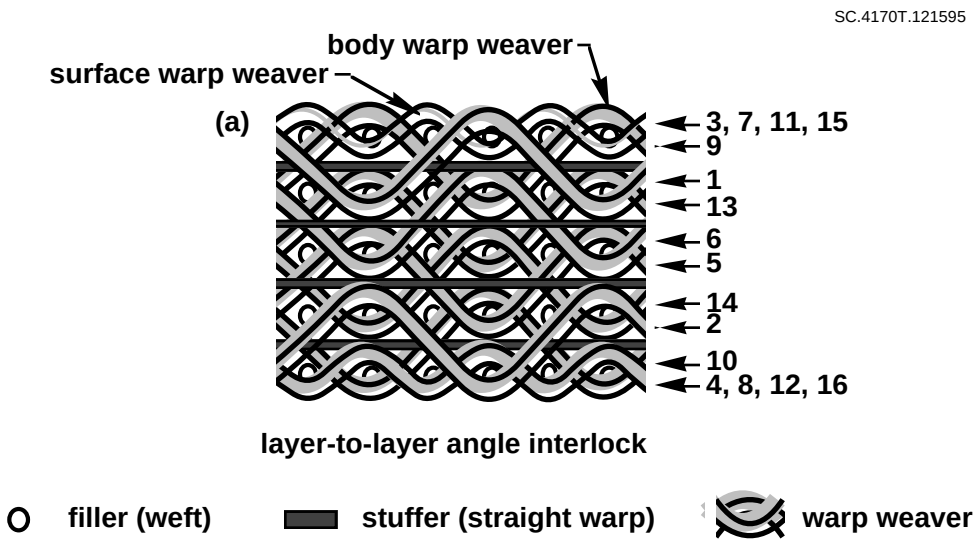


Figure 5-5. Schematic of a 3D interlock weave. The numbers at the right show the sequence of occurrence of warp weaver tows encountered on progressing into the plane of the figure.

Let $\lambda_i$, i=1,2,3, denote macroscopic length scales along three linearly independent directions. Almost always, the three $\lambda_i$ will take different values. An effective empirical definition of macroscopic length scales is that all sets of measurements of elastic constants or strains over different gauge lengths greater than $\lambda_i$ will have the same variance. Some experiments demonstrating the convergence of variance as the gauge length is increased were discussed in Section 3.

It would also obviously be useful to be able to estimate the $\lambda_i$ from the geometry of a textile composite alone, avoiding the expense of the empirical approach. Unfortunately, because of the complexity and variety of textiles, there is no single definition applicable to all cases. The following remarks are therefore a guide to a decision that must be made on a case by case basis.

If the textile is periodic, each $\lambda_i$ could be identified with the width of the unit cell in that direction. If the geometry is ideal and the loads uniform, measurements of strain

over gauge lengths that are different integral multiples of the unit cell width must give equal results. Measurements over nonintegral multiples of the cell width will show gauge length dependence, but the variations will fall inversely with the number of unit cells spanned by the gauge. In 2D braids, for example, variations in elastic modulus are a few percent at most if the gauge length exceeds three unit cell widths (Fig. 5-6). But this definition of $\lambda_i$ can also be an unnecessarily conservative rule. If the textile architecture is very complex, the unit cell will be large (e.g., Fig. 5-5). Yet large unit cells are often divisible into subunits whose elasticity is similar but not identical; then homogeneity may exist to a satisfactory degree over gauge lengths comparable to the subunits. Since the degree to which subunits differ is continuously variable in many textile processes, no general rule of thumb is possible.

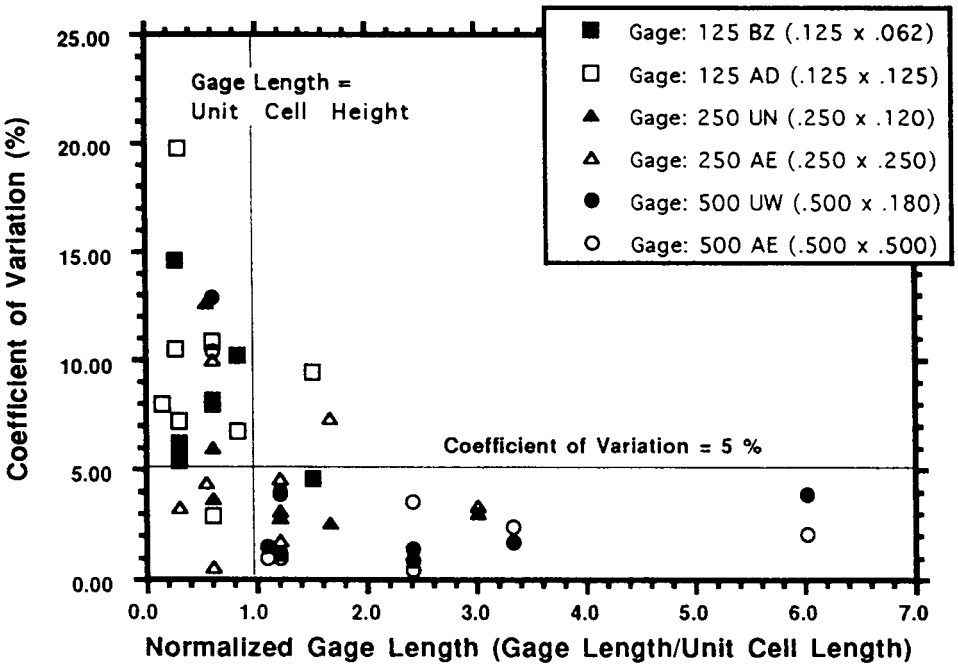


Figure 5-6. Coefficient of variation of Young's modulus measurements as a function of the size of the gauge used relative to the unit cell dimension in that direction (from [5.12]). Gauge sizes shown in inches in inset; 1 in. ≈ 25.4 mm.

Rather than being periodic, i.e. invariant under certain nonzero translations, a 2D laminate is invariant under translations of any size. It could be regarded as having a unit cell of vanishing size in the in-plane directions. Applying the definition of $\lambda_i$ suggested for periodic textiles, a 2D laminate therefore may be considered to be homogeneous in the in-plane directions over length scales that are vanishingly small. Similarly, a quasi-laminar textile, which may have a large unit cell on geometrical considerations alone, may be assigned vanishing values of $\lambda_i$ for in-plane directions if it is sufficiently

dominated by nominally straight in-plane tows. In a triaxial braid, for example, $\lambda_i$ in the direction of the axial tows may be effectively zero if the axial tows contain a sufficiently high fraction of all fibers.

### *5.1.6 Fundamentals of Heterogeneous Elastica*

The concept of homogeneous effective elastic properties existing over macroscopic length scales is based on some fundamental theorems regarding stresses and strains in heterogeneous materials. They are summarized here in the notation of Ref. [5.13].

Average Strain Theorem

Consider a heterogeneous body of volume $V$ consisting of an aggregate of different phases. If the displacements on its external surface, $S$, are

$$u_i(S) = u_i^0 \tag{5.1}$$

and displacement continuity is enforced on the internal boundary, $S_{12}$, between phases in such a way that

$$u_i^{(1)} = u_i^{(2)} \qquad \text{(on } S_{12}\text{)} \tag{5.2}$$

then the average strain, $\bar{\varepsilon}_{ij}$, in the body is

$$\bar{\varepsilon}_{ij} = \frac{1}{2V}\int_S \left(u_i^0 \hat{n}_j + u_j^0 \hat{n}_i\right) dS \tag{5.3}$$

where $\hat{n}$ is the unit normal to $S$. Further, if

$$u_i(S) = \varepsilon_{ij}^0 x_j \tag{5.4}$$

then

$$\bar{\varepsilon}_{ij} = \varepsilon_{ij}^0 \tag{5.5}$$

Average Stress Theorem

For an average stress, defined as

$$\overline{\sigma_{ij}} = \frac{1}{V}\int_V \sigma_{ij}(x)\ dV \tag{5.6}$$

the average stress theorem states that

$$\overline{\sigma_{ij}} = \frac{1}{V}\left[\int_S x_j T_i dS + \int_V x_j F_i dV\right] \tag{5.7}$$

where $T_i$ is a surface traction and $F_i$ a body force. If

$$\begin{aligned} T_i &= \sigma^0_{ij}\, n_j \\ F_i &= 0 \end{aligned} \tag{5.8}$$

then

$$\overline{\sigma}_{ij} = \overline{\sigma}^0_{ij} \tag{5.9}$$

<u>Average Virtual Work Theorems</u>

If the homogeneous displacements

$$u_i(S) = \varepsilon^0_{ij} x_j \tag{5.10}$$

are applied to the boundary, $S$, then the average virtual work, $J$, can be shown to be

$$J = \overline{\sigma}_{ij}\ \varepsilon^0_{ij}\ V \quad , \tag{5.11}$$

with summing implied over repeated indices. Alternatively, if on the bounding surface, $S$,

$$T_i = \sigma^0_{ij}\, n_j \tag{5.12}$$

then

$$J = \sigma^0_{ij}\ \overline{\varepsilon}_{ij}\ V \tag{5.13}$$

<u>Effective Elastic Moduli</u>

Assume that the displacement distribution within the heterogeneous body subject to the homogeneous boundary conditions of Eq. (5.10) is given by

$$u_i(x) = \varepsilon^0_{kl} u_i^{(kl)}(x) \quad . \tag{5.14}$$

Then the stress at any point is given by

$$\sigma_{ij}(x) = \varepsilon^0_{kl}\, C_{ijmn}(x)\, \varepsilon^{(kl)}_{mn}(x) \tag{5.15}$$

where

$$\varepsilon^{(kl)}_{ij}(x) = \frac{1}{2}\left(u^{(kl)}_{i,j} + u^{(kl)}_{j,i}\right) \quad . \tag{5.16}$$

Taking a volume average of Eq. (5.15) gives

$$\bar{\sigma}_{ij} = \bar{C}_{ijkl}\, \varepsilon^0_{kl} \tag{5.17}$$

where

$$\bar{C}_{ijkl} = \frac{1}{V} C_{ijmn}(x)\, \varepsilon^{(kl)}_{mn}(x)\, dV \tag{5.18}$$

(If the strain multipliers $\varepsilon^{(kl)}_{mn}$ are uniform and of value unity, then Eq. (5.18) reduces to the volume averaging of stiffness. This is the isostrain case.) From the average strain theorem, Eq. (5.5), Eq. (5.17) can be written as

$$\bar{\sigma}_{ij} = \bar{C}_{ijkl}\, \bar{\varepsilon}_{kl} \quad , \tag{5.19}$$

By a similar derivation, if an elastic body is subject to the homogeneous tractions of Eq. (5.12), then

$$\bar{\varepsilon}_{ij} = \bar{S}_{ijkl}\, \bar{\sigma}_{kl} \quad . \tag{5.20}$$

where $\bar{S}$ is the inverse of $\bar{C}$. Assuming homogeneous boundary conditions of either Eq. (5.10) or Eq. (5.12), it can be shown from the definition of $\bar{C}$ that strain and stress energies are given respectively by

$$U^{\varepsilon} = \frac{1}{2}\, \bar{C}_{ijkl}\, \bar{\varepsilon}_{ij}\, \bar{\varepsilon}_{kl}\, V$$

$$U^{\sigma} = \frac{1}{2}\, \bar{S}_{ijkl}\, \bar{\sigma}_{ij}\, \bar{\sigma}_{kl}\, V \quad . \tag{5.21}$$

Thus there is an exact correspondence between volume averaging and the definition of effective macroscopic properties based on energy expressions [5.14].

### *5.1.7 Orientation Averaging*

"Orientation Averaging" is based on two tenets: that the textile composite can be represented geometrically as a tessellation of grains of unidirectional composite; and that either isostress or isostrain conditions apply [5.15-5.19].

Grains are usually defined according to the ideal fabric geometry implied by geometrical models of the textile process. Irregularities such as pinching, waviness, or crimp are not modeled. Curved tow segments are usually divided into just a few grains in each of which the fiber orientation takes a single, spatially averaged value. Because curved tows are ubiquitous in textiles, the definition of grains is obviously not unique.

Each grain is assigned the elastic properties of a unidirectional composite using a model of the kind discussed in Section 5.1.2. Let $C^{(\alpha)}$ denote the stiffness matrix for grain $\alpha$; and $S^{(\alpha)}$ the corresponding compliance matrix. The components of $C^{(\alpha)}$ and $S^{(\alpha)}$ refer to an axis system aligned with the local fiber direction. Denote the composite stiffness matrix $C$ and the compliance $S$, both defined relative to a global coordinate system common to all grains. Then

$$C_{ij} \approx \sum_{\alpha} V_{\alpha}\, C_{ij}^{(\alpha)^*} \qquad \text{(isostrain conditions)} \qquad (5.22a)$$

or

$$S_{ij} \approx \sum_{\alpha} V_{\alpha}\, S_{ij}^{(\alpha)^*} \qquad \text{(isostress conditions)} \qquad (5.22b)$$

where $C^{(\alpha)*}$ and $S^{(\alpha)*}$ denote $C^{(\alpha)}$ and $S^{(\alpha)}$ respectively transformed into the global coordinate system:

$$C^{(\alpha)*} = T_{\sigma}^{-1}\, C^{(\alpha)}\, T_{\varepsilon} \qquad (5.23)$$

where $T_{\sigma}$ and $T_{\varepsilon}$ are the stress and strain transformation matrices, respectively, given by

$$T_{\varepsilon} = \begin{bmatrix} a_{11}^2 & a_{12}^2 & a_{13}^2 & a_{12}\,a_{13} & a_{11}\,a_{13} & a_{11}\,a_{12} \\ a_{21}^2 & a_{22}^2 & a_{23}^2 & a_{22}\,a_{23} & a_{23}\,a_{21} & a_{21}\,a_{22} \\ a_{31}^2 & a_{32}^2 & a_{33}^2 & a_{32}\,a_{33} & a_{33}\,a_{31} & a_{31}\,a_{32} \\ 2a_{21}\,a_{31} & 2a_{32}\,a_{22} & 2a_{23}\,a_{33} & (a_{22}\,a_{33}+a_{23}\,a_{32}) & (a_{23}\,a_{31}+a_{21}\,a_{33}) & (a_{21}\,a_{32}+a_{22}\,a_{31}) \\ 2a_{11}\,a_{31} & 2a_{12}\,a_{32} & 2a_{13}\,a_{33} & (a_{32}\,a_{13}+a_{33}\,a_{12}) & (a_{11}\,a_{33}+a_{13}\,a_{31}) & (a_{31}\,a_{12}+a_{32}\,a_{11}) \\ 2a_{11}\,a_{21} & 2a_{12}\,a_{22} & 2a_{13}\,a_{23} & (a_{12}\,a_{23}+a_{13}\,a_{22}) & (a_{13}\,a_{21}+a_{11}\,a_{23}) & (a_{11}\,a_{22}+a_{12}\,a_{21}) \end{bmatrix} \qquad (5.24)$$

where the $a_{ij}$ are the direction cosines between the local tow coordinate system and the global system; and

$$T_\sigma^{-1} = T_\varepsilon^T \quad , \tag{5.25}$$

which follows from orthogonality. (These transformations are well known results of tensor algebra [5.20,5.21].) For a tow whose axis is orientated at angles $\theta$ and $\beta$ with respect to the global system, as shown in Fig. 5-7, the $a_{ij}$ are given by

$$[a_{ij}] = \begin{bmatrix} \cos\theta\cos\beta & \sin\theta\cos\beta & \sin\beta \\ -\sin\theta & \cos\theta & 0 \\ -\cos\theta\sin\beta & \sin\theta\sin\beta & \cos\beta \end{bmatrix} \quad . \tag{5.26}$$

The tow is assumed to be transversely isotropic. Therefore, there is a degree of freedom in the definition of the local coordinate system. Without loss of generality, Eq. (5.26) refers to coordinate systems in which the 2 axis of the tow is perpendicular to the global $z$-axis.

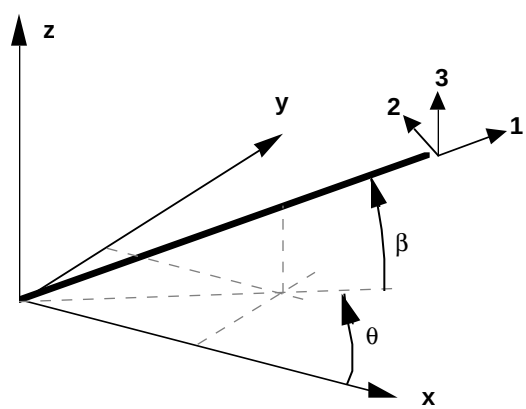


Figure 5-7. Coordinates for transformation of tow properties.

Orientation averaging preserves the symmetry inherent in the tessellation of grains over large gauge lengths. Thus, using an example common in flat textile sheets, if three orthogonal planes of symmetry exist in the pattern of grains, then the macroscopic stiffness and compliance tensors derived by orientation averaging will exhibit orthotropic symmetry (e.g., Fig. 5-8).

Whether either Eq. (5.22a) or (5.22b) is a good approximation depends on the textile architecture. Isostrain conditions apply when translational invariance obtains in the direction of the applied load. Isostress conditions apply when translational invariance

obtains normal to the applied load. From energy considerations, the isostress result, Eq. (5.22b), always provides a lower bound to the stiffness; the isostrain result, Eq. (5.22a), an upper bound.

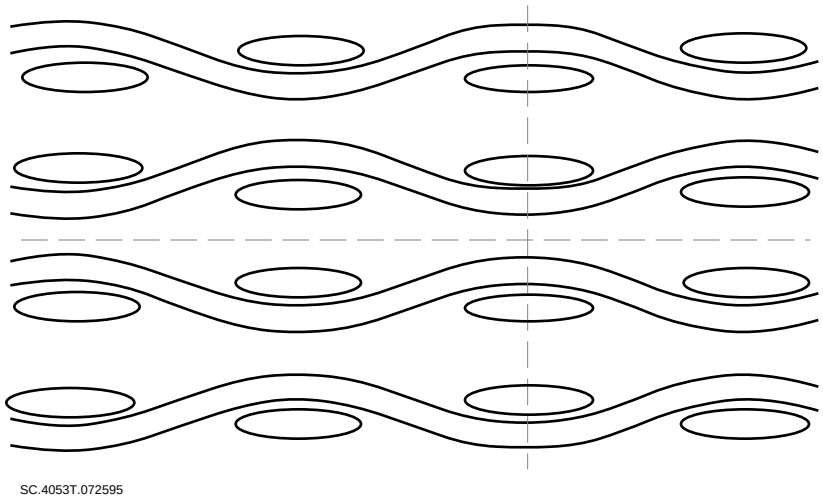


Figure 5-8. Three orthogonal symmetry planes (two marked by dashed lines and the third being the plane of the figure) in a stack of woven plies, implying orthotropy over gauge lengths that are larger than the ply thickness and the period of the weave.

Good design in airframes, which must be very stiff, requires positioning as many straight fibers as possible in the directions of the largest anticipated stresses. Isostrain conditions are then by far the better approximation.

In a 2D laminate, orientation averaging with isostrain conditions is equivalent to standard laminate theory for in-plane deformations. Thus orientation averaging models and models in which a textile is approximated geometrically as a laminate will yield similar results for quasi-laminar textiles [5.8,5.22].

### *5.1.8 Bending or Axial Shear?*

The response of a curved tow element to lateral loads is sometimes modeled as that of a simple beam that can bend but not shear. The beam may be anchored at points where the locus of the tow has extrema, usually at points where it is impinged upon by other tows (perhaps at the boundary of a unit cell). However, this modeling approach is valid only if the beam represents a tow segment whose length, $L$, is many multiples of its thickness, $2t$. If the tow segment is short, the primary contribution to its lateral deflection will be axial shear deformation, not bending.

Fig. 5-9 shows a simple paradigm for estimating the relative importance of bending and shear in a tow that is subject to lateral loads. Elementary calculations show that the bending and shear deflections, $v_b$ and $v_s$, are in the proportion

$$\frac{v_b}{v_s} = \chi\left(\frac{L}{2t}\right)^2 \frac{G_{xy}}{E_x} \quad . \tag{5.27}$$

where $E_x$ and $G_{xy}$ are the axial and shear moduli of the tow and $\chi$ is a geometrical factor of order unity. For carbon/epoxy, for example, $E_x/G_{xy} \approx 40$ [5.23]. Shear will dominate deflections for tow segments of aspect ratio less than 5; and in this case simple bending beam models should not be used. Simple bending beam models may be appropriate for satin weaves with long float or braids with flat tows, but they are inappropriate for plain weaves or 3D interlock weaves [5.23].

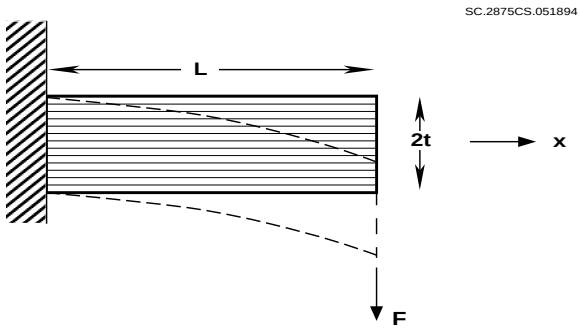


Figure 5-9. A simple paradigm for estimating the contributions of shear and bending to the deflection of a tow.

Axial shear deflections (i.e., shear deflections in a plane containing the beam axis) are admitted in thick beam models, which incorporate rotational as well as bending degrees of freedom. However, to date thick beam models have not been applied to textiles.

Segments of tows are also sometimes represented as simple beams supported continuously by an elastic foundation, rather than anchored at discrete points. This can be a useful method of modeling delamination (loss of the foundation) and its effect in buckling during axial compression. The foundation may also represent the constraining effects of through-thickness reinforcement, in which case it will usually be much stiffer and may be modeled as discrete rather than continuous (Fig. 5-10). However, the foundation does not have the same effect as internal shear and therefore a similar restriction of validity to long tow segments must apply. For many 3D composites, including 3D weaves and braids, this means that a simple beam model will be useful only

if the buckling deflection has a wavelength that is long compared to the spacing of the through-thickness yarns (Fig. 5-10a). If the through-thickness reinforcement is stiff enough to limit buckling to intervals between through-thickness tows (Fig. 5-10b), buckling will occur primarily via axial shear.

This leads to an interesting conjecture about what really matters in modeling the ultimate strength, including compression strength, of a 3D textile composite when the 3D reinforcement is sufficiently stiff and closely spaced to inhibit long wavelength lateral deflections, including buckling (Fig. 5-10b). In this case, the composite can be regarded as an assembly of tows whose collective strength comes from their internal stiffness. Only damage that occurs *inside* tows is significant to the composite's integrity. The most important interior damage is shear softening, kinking, and tow rupture. Damage *between* tows, i.e. matrix cracking, has minimal effect on composite strength, because the interaction of tows does not depend strongly on their connection via the resin. If the resin is cracked, friction will still lock tows together as a macroscopic structure, with very little relative movement of tows permitted by the 3D nature of the tow arrangement. This is very different to tape laminates or 2D textiles, where interply delamination can completely detach plies and lead to catastrophic failure at low loads.

### *5.1.9 Geometrical Irregularity*

Geometrical irregularity is found in all textile composites. Common types were listed in Section 2.3.3. They include inconsistency in tow spacing, tow waviness, and tow pinching.

Inconsistent tow spacing causes variance in fiber volume content. If fiber content falls, stiffness falls proportionately. In most models, the effects of variable tow separation is simply calculated by adjusting input parameters that describe the textile geometry.

Tow waviness and pinching cannot usually be dealt with in this way. Most codes are based on the assumption that the textile architecture is ideal, as laid out in the design specifications of the textile manufacturer. Fortunately, the effect of waviness and pinching on macroscopic elastic constants is almost entirely restricted to reducing the effective axial stiffness of tows. A simple and reasonably accurate estimate of this knockdown was presented in Section 3.3.

However, geometrical irregularity has one other very important implication for modeling stress distributions in the elastic regime. Because irregularity is by nature

stochastic, it always reduces the symmetry of the textile composite. In particular, the translational invariance of nominally periodic textiles will be violated; and periodic boundary conditions applied to a unit cell will no longer be strictly valid. Broken symmetry has a relatively minor effect on estimates of macroscopic elastic constants [5.22], but it can have very important implications for predicting the onset of failure, which will be taken up in Section 6.

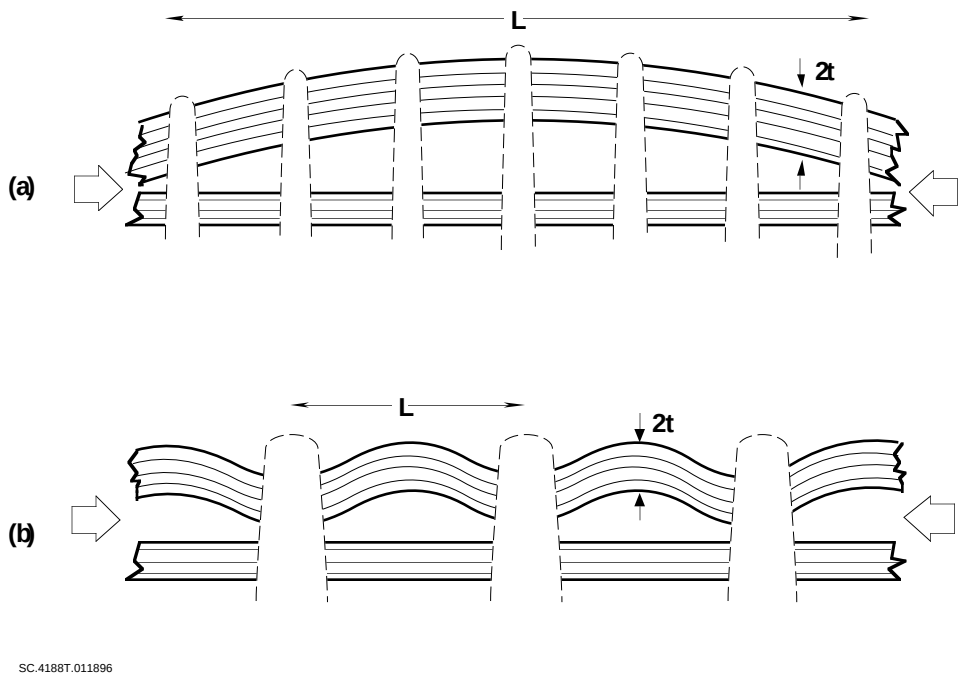


Figure 5-10. Schematics of buckling of an aligned tow under compression. (a) When relatively soft through-thickness reinforcement acts as a soft elastic foundation, allowing deflections over relatively long wavelengths. (b) When stiff through-thickness reinforcement restricts lateral deflections to the intervals between successive through-thickness tows.

## 5.2 Summary of Available Codes for Analyzing Stiffness

This handbook presents annotated documentation for various computer codes that can predict the properties of textile composites. Some of the codes were developed by the Textiles Working Group within the Advanced Composites Technology (ACT) Program sponsored by NASA Langley Research Center. Others were developed outside the ACT program. All are available for public use. The codes represent a wide range of approaches and capabilities and cover most of the classes of textile composites currently perceived to be valuable in aircraft manufacture. This section provides prospective users with a guide to selecting the best codes for analyzing the stiffness or thermal expansion of a given

textile composite. A similar guide for properties related to strength, ultimate failure, and fracture toughness appears in Section 6; and for fatigue in Section 7.

The codes covered in the handbook and their capabilities in predicting stiffness and thermal expansion are summarized in Table 5.3. The modeling approach each is based on and a comparative assessment of their accuracy, ease of use, and calibration are found in the remainder of Section 5.2. More complete details on the individual codes, including lists of the input data required, are presented in Section 8. The user's guides written by the codes' authors can be found in the appendices.

**Table 5.3 Summary of Code Capabilities**

| Code | Textile Forms | 3D Stiffness | Thermal Expansion | Plate Stiffness |
|---|---|---|---|---|
| **PW**<br>**SAT5**<br>**SAT8** | plain weave<br>5 harness satin<br>8 harness satin | | Yes | Yes |
| **CCM-TEX** | 3-D Weave<br>2-Step and 4-step braids | Yes | | |
| **μTex-10**<br>**μTex-20** | general<br>user defined | Yes | Yes | Yes |
| **SAWC** | plain weave<br>(FE code general) | Yes | | |
| **TEXCAD** | 2D weaves<br>2D braids<br>user defined | Yes | Yes | Yes |
| **WEAVE** | 3D weaves | Yes | | |
| **BINMOD** | 3D weaves | Yes | | |

### *5.2.1 Quasi-laminar and Nonlaminar Textiles*

Many of the codes recognize that the textile composites they deal with are quasi-laminar, because the fiber architecture is either a 2D structure or a 3D structure dominated by in-plane fibers arranged in layers (Section 2). The geometry will then be described in a way that bears out its quasi-laminar character; and the analysis of stresses and strains will usually include steps based on standard laminate theory. Other codes have been designed to deal expressly with nonlaminar textiles. Their descriptions of geometry and methods of predicting mechanical properties are necessarily quite different.

### *5.2.2 Geometry*

Defining the geometry of a textile composite in sufficient but not overwhelming detail is one of the most challenging tasks in its analysis. Various approaches have been implemented in the computer codes (Table 5.4).

Units Cells

Several codes use unit cells to describe textile geometry for both quasi-laminar and nonlaminar cases, since a periodic textile may be either quasi-laminar or nonlaminar. If the textile is quasi-laminar, then the unit cell may be defined to lie entirely within one ply or to span the whole thickness (Fig. 5-11). The former choice is strictly valid only if all layers are exactly equivalent, which can only be true if the textile is also 2D (Section 2). But since the volume fraction of through-thickness fibers is always relatively small in a quasi-laminar 3D textile, it is often a good approximation to regard such a structure as layers of mainly in-plane fibers that are equivalent in the elastic regime. Choosing a unit cell that spans the whole thickness will generally allow more detailed analysis. For example, the effects of stacking layers with features in and out of registry can be studied directly (Fig. 5-11b and 5-11c).

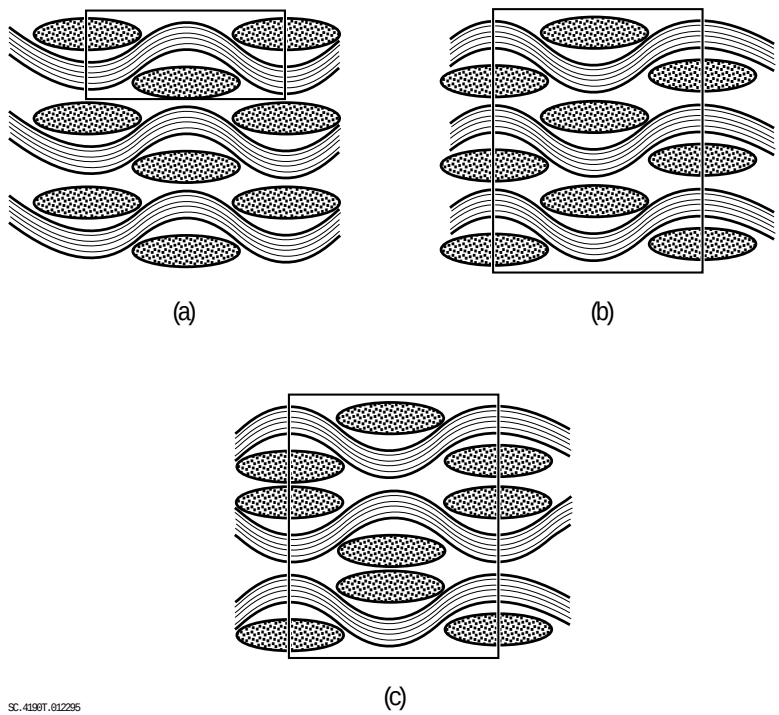


Figure 5-11. Choices of unit cell in quasi-laminar textile composites. (a) and (b): two approaches to modeling laminate properties. (c): variant of whole thickness cell in (b) for analyzing stacking effects.

The simplest unit cell approach is sometimes called the fiber inclination model [5.18]. A related concept is the diagonal brick model [5.24]. In these models, only the straight portions of the tows are represented; and the sole geometrical characteristic used for each such segment is its angle of inclination to a global frame of reference. The inclination angles may be contained in a single plane (especially for quasi-laminar textile composites) or in all three spatial dimensions. Relatively simple closed-form expressions are available for determining these angles from the weaving or braiding parameters (Section 2.3). This approach was one of the first formulated specifically for textile composites [5.18], but no codes implementing it have been included here.

In the next level of detail, tows and their cross-sections are represented as solid entities with some simple geometry defined by just a few parameters. For example, a plain weave may be modeled as a combination of straight yarn segments and cross-over regions that follow an assumed sinusoidal path (Section 2.3). **TEXCAD**, **CCM-TEX**, and **PW** are examples of codes that use this approach. **SAWC** uses a similar idealization to generate a finite-element mesh. In the more complex textile preforms, tows must twist and change cross-section with position as they pass around one another. Simple

parametric functions that represent such effects are difficult to derive. These effects are not represented in the codes.

Another level of idealization of unit cells is provided by codes that compute the preform geometry by analyzing mechanical conditions during the textile forming process. Reference [5.24] describes a code (**BRAID**; not included in the handbook) which determines yarn paths based on the tensile forces applied during the textile process, contact relations between the yarns, and the dry yarn stiffness. The yarn path and twist are predicted in terms of spline functions. **BRAID** is currently restricted to considering yarns that remain uniform in cross-section, which is not always realistic.

Finally, there are commercial solid modeling tools that may be used to create bodies with complex geometry on a grid suitable for finite element analysis. These tools use sophisticated Boolean operations and computer graphics to aid model generation. Their application to textiles has been demonstrated [5.25], but the approach is not well developed and appears too time consuming for practical use. Textile preforms involve multiple yarns touching at many cross-over points, which makes them difficult to mesh in such detail. Moreover, the agreement in the elastic regime of experimental data and models based on much simpler geometrical representations implies that the extra level of detail is unnecessary in predicting elastic constants. It may even be misleading in analyzing local stress distributions, because of the neglect of geometrical irregularity.

All of the approaches described above assume that the unit cell geometry is deterministic and repeatable.

Modified Laminates

Instead of using a unit cell, an alternative approach to modeling the geometry of quasi-laminar textiles is to represent them simply as laminates of continuous, translationally invariant plies, just like a conventional tape laminate. The geometry of the laminate is then completely described by the thicknesses, orientations, and stacking sequences of the layers.

**Table 5.4 How Codes Represent Textile Geometry**

| Code | Geometry |
|---|---|
| **μTex-10**<br>**μTex-20** | Unit cell for full thickness<br>Yarn paths defined as piecewise linear, lying in planes<br>Yarn cross-sections defined as polygons |
| **TEXCAD** | Unit cell for single layer<br>Yarn paths defined as straight and sinusoidal segments |
| **PW**<br>**SAT5**<br>**SAT8** | 2D or 3D unit cells for single layer<br>Yarn paths defined as straight and sinusoidal segments<br>Yarn cross-sections rectangular |
| **SAWC** | Unit cell for single layer of plain weave<br>Yarn paths defined as sinusoidal<br>Complex geometries formed by stacking units |
| **CCM-TEX** | Unit cell for full thickness<br>Yarn paths defined by simple analytical functions<br>Geometry computed from idealization of textile process |
| **WEAVE** | Quasi-laminar 3D interlock weaves reduced to laminates |
| **BINMOD** | Nonperiodic representative volume element<br>Piecewise linear 1D elements for axial properties of tow segments<br>Solid effective medium elements for all other properties |

Describing the layers of a textile composite as translationally invariant is, of course, an approximation. Stitching or other through-thickness reinforcement is always discrete and disrupts translational invariance. The validity of the approximation then depends on whether the contribution of the through-thickness reinforcement to macroscopic elasticity can be calculated well enough by replacing the discrete tows by a smeared out continuum. Experience suggests an affirmative answer for quasi-laminar 3D interlock weaves [5.8]. In a 2D textile composite, translational invariance is violated by the internal structure of layers, which is typically that of a plain or satin weave. The adequacy of the approximation then depends on the extent to which periodic variations of the fiber orientation within layers can be represented by a uniform, spatially averaged reduction of the effective layer stiffness. This seems to work quite well in practice for laminates of triaxially braided plies [5.26].

An example of this alternative approach to quasi-laminar textile composites is the code called **WEAVE**, which models 3D interlock weaves. Alternating layers of fillers and stuffers are modeled in **WEAVE** as continuous plies. Stuffer and filler waviness can be allowed for by including an estimate of waviness, which is then represented as a knockdown in ply stiffness by a rule similar to Eq. (3.1). The estimate of waviness might come from a theoretical model of the textile geometry, especially if waviness arises from textile architecture, as in a plain weave; or from measurements of tow loci in

photomicrographs. The estimates need not be very precise, since the knockdowns are small in most systems (see Section 3). Thus ply properties in **WEAVE** are defined without assuming periodicity. A similar code was reported in [5.26] for triaxial braids, but it is not included in this edition of the handbook.

Nonperiodic, Nonlaminar Textile Composites

When a textile composite is nonperiodic and nonlaminar, a different approach must be taken to describing its geometry. In the Binary Model (**BINMOD**), the axial properties of yarns are represented by two-noded line elements, while the transverse stiffness, shear stiffness, and Poisson's effects are represented by solid "effective medium" elements. Thus the tow architecture is represented by piece-wise straight line segments in one-to-one correspondence with the positions of tow axes in the real composite. Details of yarn cross-sectional shape and curvature over gauge lengths less than the center-to-center tow spacing are omitted: by minimizing the degrees of freedom in the model, much larger pieces of the textile composite can be simulated. Tow waviness can be introduced by offsetting nodes on the tow elements in the stress-free configuration of the model. There is in principle no restriction on the arrangements the tows may have or any requirement of symmetry or periodicity. However, the code has been developed so far to deal only with 3D interlock weaves.

Models such as the Binary Model appear to offer the best approach to modeling integral textile structures (Section 2.4), which are nearly always nonperiodic and nonlaminar. Neither are the tows in textile composites small relative to the external dimensions expected in typical integral structures. Therefore, the representation of tows as discrete entities would appear to be the minimum required level of detail.

### *5.2.3 Modeling Thermo-Elastic Properties*

The approach to evaluating macroscopic stiffness tensors and coefficients of thermal expansion once again naturally depends on whether a textile is classified as quasi-laminar or nonlaminar. It is also useful to distinguish methods of analysis according to the degrees of freedom permitted for local stress variations.

The Isostrain Approach (Orientation Averaging)

The isostrain assumption uses the lowest number of internal degrees of freedom possible in elasticity calculations without introducing symmetry elements not present on

the macroscopic scale. Under the isostrain assumption, the determination of the effective or macroscopic stiffness tensor becomes a simple volume averaging of the constituent stiffnesses, transformed from the local material coordinate system to the global coordinate system (Section 5.1.7); i.e. the method of orientation averaging. Following the formal mechanics reviewed in Section 5.1.6, this is equivalent to coupling homogeneous displacement boundary conditions (Eq. (5.4)) with an assumption of linearly varying displacements throughout the enclosed volume and finding the relation between average stress and average strain.

In most of the codes in Table 5.3, the textile is treated as being periodic and the averaging is performed over the volume, *V*, of the unit cell. In simple models that include only straight yarn segments (e.g., the diagonal brick model), orientation averaging then leads to a closed-form summation of volume weighted stiffnesses. In the more general codes, such as **TEXCAD**, numerical integration is performed to account for the curvature of tow paths.

When quasi-laminar textiles are approximated as translationally invariant in-plane, orientation averaging leads to a simple sum over layers. Indeed, standard laminate analysis applied to in-plane loads can be regarded as an instance of orientation averaging.

Orientation averaging can be applied just as well to nonperiodic textiles. This may be done by substituting a periodic approximation for nonperiodic elements of the textile architecture, defining a unit cell, and proceeding as above. Alternatively, some other representative volume element can be defined and analyzed, large enough that spatial variations associated with nonperiodic elements of the reinforcement have a small effect on the calculated macroscopic (spatially averaged) stiffness tensor.

The isostrain assumption that leads to stiffness averaging also yields simple expressions for thermal expansion coefficients. For example, the effective thermal expansion coefficients, $\overline{\alpha}_{ij}$, of the unit cell of a periodic textile follow according to [5.27]

$$\overline{\alpha}_{ij} = \overline{S}_{ijkl} \frac{1}{V} \int_V C^*_{ijkl} \alpha^*_{kl} dV \tag{5.28}$$

where an asterisk again indicates transformation of local properties to the global coordinate system and $\overline{\boldsymbol{S}}$ denotes the spatially averaged compliance (the inverse of $\overline{\boldsymbol{C}}$).

Finite Element Methods

Isostrain or isostress assumptions are unnecessary in codes based on finite element formulations, since these codes compute internal stress distributions in detail, using arbitrarily many degrees of freedom. The stiffness matrix is built up by imposing homogeneous displacement boundary conditions and either integrating the internal stresses to obtain the average stress or integrating the boundary tractions. The average stress can be related to the boundary tractions via the average stress theorem (Eq. 5.7). Building the complete stiffness matrix requires solving for six independent sets of boundary conditions. Because of the potential lack of symmetry of a general unit cell, the stiffness matrix can be fully populated (generally anisotropic). Although it can be proven that the stiffness matrix for any heterogeneous unit cell must be symmetric, finite element calculations can yield a nonsymmetric matrix due to the approximations involved. A symmetric result, $C_{\mathrm{sym}}$, is usually created by the averaging operation

$$C_{sym} = \frac{1}{2}\left(C + C^T\right) \quad , \qquad (5.29)$$

where the superscript T denotes transpose.

There is no requirement for a finite element mesh to map directly to the unit cell's internal geometry. For example, the mesh may be a regular array of cuboidal elements, independent of the yarn paths. When the element stiffness matrix is generated, the code must determine the local material stiffness at each Gaussian integration point. This gives rise to so-called heterogeneous elements, which greatly simplify the meshing problem. However, the stresses in heterogeneous elements may converge slowly with respect to mesh density.

Finite element methods are used to solve unit cell formulations in the codes **SAWC**, μ**TEX-10,** and μ**TEX-20.**

Laminate Analysis: Quasi-Laminar Textile Composites

The properties of quasi-laminar textile composites are usually and most conveniently represented by the conventional *A*, *B*, and *D* matrices of classical lamination theory. The matrix *A* defines the coupling between in-plane strains and in-plane force resultants; and *B* and *D* the coupling between in-plane strains and bending moments or bending curvatures and in-plane force resultants [5.1]:

$$\begin{bmatrix} A_{12} & A_{12} & A_{16} & B_{11} & B_{12} & B_{16} \\ A_{12} & A_{22} & A_{26} & B_{12} & B_{22} & B_{26} \\ A_{16} & A_{26} & A_{66} & B_{16} & B_{26} & B_{66} \\ B_{11} & B_{12} & B_{16} & D_{11} & D_{12} & D_{16} \\ B_{12} & B_{22} & B_{26} & D_{12} & D_{22} & D_{26} \\ B_{16} & B_{26} & B_{66} & D_{16} & D_{26} & D_{66} \end{bmatrix} \left\{ \begin{bmatrix} \varepsilon_x \\ \varepsilon_y \\ \gamma_{xy} \\ \kappa_x \\ \kappa_y \\ \kappa_{xy} \end{bmatrix} - \begin{bmatrix} \alpha_x \\ \alpha_y \\ \alpha_{xy} \\ \beta_x \\ \beta_y \\ \beta_{xy} \end{bmatrix} \Delta T \right\} = \begin{bmatrix} N_x \\ N_y \\ N_{xy} \\ M_x \\ M_y \\ M_{xy} \end{bmatrix} \tag{5.30}$$

where the axes $x$ and $y$ lie in the plane of the plate; $\varepsilon_x$, $\varepsilon_y$, and $\gamma_{xy}$ are mid-plane strains; $\kappa_x$, $\kappa_y$, and $\kappa_{xy}$ are bending curvatures; $\alpha_x$, $\alpha_y$, and $\alpha_{xy}$ are plate thermal expansion coefficients; $\beta_x$, $\beta_y$, and $\beta_{xy}$ are plate thermal bending coefficients; $N_x$, $N_y$, and $N_{xy}$ are in-plane force resultants; and $M_x$, $M_y$, and $M_{xy}$ are bending moments.

Table 5.5 summarizes the way the codes presented in this handbook deal with the application of laminate theory to quasi-laminar textile composites. There are essentially two approaches to determining the matrices $A$, $B$, and $D$:

(i) The properties of the entire plate can be computed at once, usually by defining a unit cell spanning the whole thickness; e.g. Fig. 5-11b. The response of the cell is computed under sufficient sets of boundary conditions representing in-plane loading and bending to determine all components of the stiffness matrix. This is the approach followed in the codes **μTEX**, **CCMTEX** and **SAWC.** In a nonperiodic or irregular textile, the calculation over a unit cell can be replaced by a calculation over some representative volume element of sufficient size to give consistent results for the macroscopic stiffness. This is the approach of the code **BINMOD**.

(ii) The properties of a single ply can be determined first and the plate properties then built up using laminate theory. The ply properties can be calculated by defining a unit cell within a single ply (Fig. 5-11a) or by the methods of spatial averaging described in Section 5.2 under "Modified Laminates." The code **TEXCAD** follows the unit cell approach. **PW, SAT5**, and **SAT8** also use unit cells to compute the matrices $A$, $B$, and $D$ for a single 2D layer, but leave to a subsequent application of conventional laminate analysis the determination of the plate stiffness of a stack of such layers.

**Table 5.5 How Codes Model Quasi-Laminar Plates**

| Code | Summary of Method |
|---|---|
| **μTex-10**<br>**μTex-20** | Full thickness FEM calculation<br>Traction free surfaces included in boundary conditions<br>*A*, *B*, and *D* matrices computed for full thickness |
| **TEXCAD** | 3D stiffness matrix computed for single layer<br>*A*, *B*, and *D* matrices calculated by standard laminate theory<br>Plane stress assumed |
| **PW**<br>**SAT5**<br>**SAT8** | *A*, *B*, and *D* matrices computed for a single layer<br>Stack of layers not treated (subsequent laminate analysis required) |
| **SAWC** | 3D stiffness matrix computed for single layer<br>Macro elements can be used to make stacked laminate<br>Surface boundary layer effects handled by FE solution. |
| **CCM-TEX** | 3D stiffness matrix computed for whole thickness |
| **WEAVE** | Plate treated as homogeneous, orthotropic body<br>Layer dimensions used to compute flexural rigidity only. |
| **BINMOD** | Full thickness FEM calculation<br>Boundary conditions, including traction-free surfaces, defined by user. |

If the 3D compliance tensor, $\bar{S}$, of a composite is available from one of the codes, then the *A* matrix for a plate in which plane stress conditions prevail can be computed as follows:

$$A/h = \begin{bmatrix} \bar{S}_{1111} & \bar{S}_{1122} & \bar{S}_{1112} \\ \bar{S}_{1122} & \bar{S}_{2222} & \bar{S}_{2212} \\ \bar{S}_{1112} & \bar{S}_{2212} & \bar{S}_{1212} \end{bmatrix}^{-1} \tag{5.31}$$

where *h* is the plate thickness. The codes **PW, SAT5,** and **SAT8** assume plane stress conditions to evaluate the properties of individual plies.

Thus the codes **TEXCAD**, **PW**, **SAT5**, **SAT8**, **μTEX-10**, and **μTEX-20** can all be used to predict plate properties.

Nonlaminar, Nonperiodic Textile Composites

For nonlaminar, nonperiodic composites, neither plane stress conditions nor unit cells should be part of the modeling approach. A more general method is required. To date, the only candidate is the Binary Model (implemented in code **BINMOD**), whose treatment of geometry has already been described (see above). Stiffness matrices are computed in the Binary Model by simulating some representative volume element (not a

unit cell), which typically represents a few cubic centimeters of material and contains a few thousand tow and effective medium elements. (The representative volume element needs only to be larger than the macroscopic length scales, $\lambda_i$, of Section 5.1.5. These may be defined by experiments or by exercising the Binary Model itself for simulations of different size.) The whole assembly is analyzed as a finite element calculation. The effective medium elements are implemented as eight-noded isoparametric solid elements; the tow elements as 1D springs. If geometrical irregularity has been introduced by randomly offsetting initial node positions, a single simulation becomes a Monte Carlo calculation. The effects of irregularity on macroscopic stiffness are determined by averaging over many Monte Carlo calculations.

## 5.3 Comparison of Code Predictions for a Plain Woven Textile Composite

Several of the codes in Table 5.3 can predict the stiffness of a plain woven textile composite. These codes were each run with the input parameters for a typical carbon/epoxy composite shown in Tables 5.6 and 5.7. In Table 5.6, "yarn" properties are those of a unidirectional composite having the "yarn fiber volume %" of Table 5.7. They are quoted for a coordinate system in which the *x*-axis lies along the fiber direction and the *x*-*y* plane is the plane of isotropy. The matrix properties are assigned to any volume of the textile composite not assigned to a yarn. The test case matches the parameters in Ref. [5.28], which also provides experimental data.

The codes were used to compute the properties of a single ply of plain woven composite. They yielded the predictions for the 3D stiffness matrix shown in Table 5.8 and the thermal expansion coefficients shown in Table 5.9. In these tables, $x_3$ is the through-thickness direction of the composite, and $x_1$ and $x_2$ its in-plane directions, which are equivalent in a plain weave. The stiffness predictions for the axial stiffness, $E_1$, fall within a narrow band. The largest variation is in Poisson's ratio, $\nu_{12}$. The out-of-plane stiffnesses are not available from codes such as **PW**, which are purely plate analyses. The results labeled CLT (classical laminate theory) are provided for comparison. These were obtained independently of the codes by volume averaging the stiffness matrix for a stack of flat layers corresponding to warp and weft fibers, with a resin layer added to obtain the correct overall fiber volume fraction.

**Table 5.6 Constituent property input used in code comparisons**
*(Transverse isotropy assumed in the y-z plane )*

| Component | $E_1$ (GPa) | $E_2$ (GPa) | $\nu_{12}$ | $\nu_{23}$ | $G_{12}$ (GPa) | $\alpha_1$ ($10^{-6}$ K$^{-1}$) | $\alpha_2$ ($10^{-6}$ K$^{-1}$) |
|---|---|---|---|---|---|---|---|
| Yarn | 145 | 11.7 | 0.23 | 0.30 | 5.52 | -0.32 | 14.0 |
| Matrix | 3.45 | 3.45 | 0.35 | 0.35 | 1.28 | 40.0 | 40.0 |

**Table 5.7 Geometric parameters assumed for code comparisons**

| | |
|---|---|
| Yarn Spacing (mm) | 1.41 |
| Layer Thickness (mm) | 0.26 |
| Yarn Fiber Volume (%) | 75 |
| Total Fiber Volume (%) | 64 |

The codes also give plate stiffnesses, computed assuming plane stress conditions (or using traction-free surfaces) and including bending. Plate stiffnesses are provided in the form of the *A*, *B*, and *D* matrices of classical laminate theory. Representative elements are shown in Table 5.10. There is a surprising variation in these results for both the in-plane and bending stiffnesses. For example, μ**Tex-10** and μ**Tex-20** give much lower values for the in-plane stiffness than the other codes. The authors attribute this difference to the way in which the *B* matrix terms (bending-stretching coupling) are handled. The effective in-plane modulus of an asymmetric laminate can be much less than a simple volume average would indicate, because the laminate curves under in-plane load. A single ply of a plain weave is indeed asymmetric, the upper and lower halves being orthogonal at any point. Most codes assume that the moment constraints of neighboring unit cells prevent bending, but this is not assumed in μ**Tex-10** or μ**Tex-20**. If many plies were stacked into a thicker laminate, the discrepancy between the codes would presumably diminish, since the interactions of adjacent layers would suppress the development of curvature in any one layer.

**Table 5.8 Comparison of homogenized, 3D elastic constants for a plain weave fabric, using various codes**

| Code | Notes | $E_1$ (GPa) | $E_3$ (GPa) | $\nu_{12}$ | $\nu_{13}$ | $G_{12}$ (GPa) | $G_{13}$ (GPa) |
|---|---|---|---|---|---|---|---|
| **μTex-10** | 1 | 58.1 | 11.0 | 0.097 | 0.363 | 4.83 | 4.39 |
| **μTex-20** | 2 | 63.4 | 11.1 | 0.027 | 0.402 | 4.24 | 3.79 |
| **TEXCAD** | | 64.4 | 11.5 | 0.027 | 0.395 | 4.87 | 5.63 |
| **PW** | 3 | 58.0 | ~ | 0.041 | ~ | 4.66 | ~ |
| CLT | 4 | 68.9 | 11.9 | 0.038 | 0.307 | 4.89 | 4.46 |
| FEM [5.28] | | 63.8 | 11.4 | 0.031 | 0.329 | 4.82 | 4.97 |
| Experiment [5.28] | | 61.9 | ~ | 0.110 | ~ | ~ | ~ |

**Table 5.9 Comparison of homogenized, 3D thermal expansion coefficients for a plain weave fabric, using various codes**

| Code | Notes | $\alpha_{xx}$ ($10^{-6}$ K$^{-1}$) | $\alpha_{zz}$ ($10^{-6}$ K$^{-1}$) |
|---|---|---|---|
| **μTex-10** | 1 | 1.47 | 22.7 |
| **μTex-20** | 2 | 1.36 | 21.5 |
| **TEXCAD** | | 1.33 | 20.7 |
| **PW** | 4 | 1.81 | ~ |
| CLT | | 1.55 | 21.6 |

**Table 5.10 Comparison of plate stiffnesses for a plain woven composite, using various codes**

| Code | Notes | $A_{11}$ (MN/m) | $A_{12}$ (MN/m) | $A_{66}$ (MN/m) | $D_{11}$ (N/m) | $D_{12}$ (N/m) | $D_{66}$ (N/m) |
|---|---|---|---|---|---|---|---|
| **μTex-10** | 1 | 12.7 | 3.32 | 1.24 | 0.0432 | 0.00041 | 0.00603 |
| **μTex-20** | 2 | 12.1 | 5.74 | 1.08 | 0.0423 | 0.00268 | 0.00422 |
| **TEXCAD** | | 17.0 | 0.963 | 1.25 | 0.0926 | 0.00525 | 0.00679 |
| **PW** | | 14.9 | 0.607 | 1.19 | 0.0782 | 0.00325 | 0.00616 |
| CLT | 5 | 17.3 | 0.643 | 1.25 | 0.1092 | 0.00377 | 0.00767 |
| Experiment | 6 | 16.0 | | | | | |

Notes for Tables 5.8 - 5.10:

1. 10 x 10 x 7 mesh
2. 20 x 20 x 20 mesh
3. PW is a plate (plane stress) code and cannot compute *z*-direction properties
4. Summed stiffnesses of flat layers representing warp and weft fibers, with a resin layer included to obtain the correct volume fraction. Resin layer thickness equals 0.60/0.75 x (total thickness).
5. Stacking sequence of $[0/0_r/90]_T$ assumed, where $0_r$ is the resin layer. *B* matrix ignored, which is equivalent to averaging with reversed stacking sequence.
6. Implied from the quoted experimental results: $A_{11}=E_1/(1-\nu_{12}^2)\,h$

## 5.4 Code Calibration

The macroscopic elastic constants of any continuous fiber polymer composite can be loosely divided into those that are fiber dominated and those that are matrix dominated.[2] The fiber dominated constants are those for which the associated material deformation involves axial straining, either in tension or compression, of some group of fibers. The matrix dominated constants are the rest. In a composite designed for any application requiring high stiffness, the critical elastic constants should all be fiber dominated.

### *5.4.1 Fiber Dominated Elastic Constants*

The most important geometrical consideration in predicting fiber dominated elastic constants is simply the number of fibers per unit volume that point in any given direction. For example, in estimating the in-plane stiffness of a quasi-laminar textile, getting the correct fiber count for in-plane directions is paramount. Out-of-plane components of the fiber orientations, whether they are a necessary consequence of the architecture or arise as accidental waviness, are secondary. They introduce relatively small modifications to predicted in-plane elastic constants. If the fiber count is right, then fiber dominated elastic constants will be predicted to within experimental scatter, regardless of how well the details of stress partitioning throughout the textile are computed. A simple scheme such as orientation averaging, i.e. the assumption of isostrain conditions, will suffice.

While corrections to in-plane elastic constants due to out-of-plane components of fiber orientation should not be ignored, the level of precision required in specifying the out-of-plane components is not high. Any error will cause an error in a small contribution to the overall stiffness. Therefore, there is generally not much difference between the predictions of models in which the geometry of quasi-laminar textile composites is treated by different approaches.

---

[2] The division is clearest if most fibers are straight or almost straight. Exceptions to this rule obviously arise. In a knitted composite, all fibers follow highly curved paths, which nevertheless may contain significant if short straight and roughly aligned segments. The straight segments collectively will raise the modulus in the direction of their alignment an order of magnitude above that of the matrix; yet not so high (because they are short) that the contribution of the surrounding matrix dominated material is unimportant. The modulus is neither clearly fiber nor matrix dominated. But such exceptions arise in composites whose macroscopic stiffness would not meet the requirements of airframe structures, for this very reason.

Neither is it especially critical to determine the packing density of fibers within tows. Composite elastic constants depend only slightly on the volume that is assigned to tows (the remainder being interstitial resin) *provided* the overall fiber count is correct. Recall Section 5.1.3. For carbon tows in well compacted composites with overall fiber volume fractions of 50-60%, the packing density has consistently fallen in the range 65-70%. Any value in this range will return consistent results.

### *5.4.2 Matrix Dominated Elastic Constants*

Only a few elastic constants in most textile composites could be regarded as matrix dominated. They include the through-thickness modulus in 2D and quasi-laminar 3D textiles; and the in-plane shear modulus in a weave consisting of orthogonal warp and weft yarns. Accurate prescription of fiber orientations and tow irregularities are not especially important in predicting these constants. They change relatively slowly with fiber orientation, because the stiffness of a unidirectional composite (i.e. a tow segment) is very insensitive to the orientation of the load when the load is nearly transverse (e.g., [5.2]). The only essential geometrical characteristic is the average fiber volume fraction.

### *5.4.3 Calibrating the Fiber Volume Fraction*

Thus being certain of fiber volume fraction is a critical issue in running predictive codes. Because there is no single method of describing the geometry of a textile composite and because reality so often differs from the idealizations of geometrical models, particular care must be taken. Some of the factors distinguishing real composites from popular geometrical models include the ability of tows to deform and fill space more efficiently than possible if they are constrained to have a particular cross-section; inconsistency in the spacing of tows, especially if a fabric is draped; and unpredictability in the crimp factor (ratio of arc length to projected length) of tows, especially if they are woven or braided. Generally, the best guide to fiber volume fraction is an experimental measurement. Volume fractions predicted a priori from the manufacturer's specifications for a textile preform are vulnerable to error.

It is therefore necessary to adjust the input for any analytical code to match the experimentally measured fiber volume fraction. In **TEXCAD**, fiber volume fraction is an input quantity. The unit cell geometry is adjusted internally to accommodate the specified value. **CCMTEX** attempts to calculate fiber volume fraction based on process parameters. This is a useful feature in the early design of a textile, but is not preferred once the actual material has been made and better information is available. Finite element

codes such as μ**TEX** and **SAWC** use an externally generated idealized geometry. This should be adjusted to the ensure the correct overall fiber volume fraction.

Standard measurements of fiber volume fraction, e.g. by matrix dissolution, include all fibers without distinguishing their orientation or host tow. This leaves the problem of apportioning the fibers to the various components of the architecture. Fortunately, the *proportions* of fibers in each type of tow (e.g., weaver, stuffer, warp weaver in an interlock weave; or warp and weft in a 2D weave) can be deduced from the manufacturer's setup and they may be regarded as unchanged during processing, even if the overall fiber volume fraction changes. If the predicted proportions are combined with a measurement of total fiber volume fraction, the textile is well specified for the purpose of calculating elastic constants.

### *5.4.4 Calibrating Fiber Waviness*

Fiber waviness is difficult to calibrate. Unless it is excessive, in which case changes should be made to the processing methods, it leads to knockdowns in composite stiffness that are too modest to be clearly distinguished from other sources of variance. Direct measurements of waviness require destructive inspection, which is laborious and expensive.

Nevertheless, waviness will always be present to some degree and its effects should always be monitored. A viable approach might include stiffness knockdown estimates based on simple formulae such as Eq. (3.1); combined with occasional destructive inspection of parts and control of relevant processing parameters, such as yarn tensioning.

## References

5.1 S.W. Tsai and H.T. Hahn, "Introduction to Composite Materials," *(Technomic, Lancaster, Pennsylvania*, 1980).

5.2 M.R. Piggott, "Load-Bearing Fibre Composites," (*Pergamon, Oxford*, 1980).

5.3 Z. Hashin, "Analysis of Properties of Fiber Composites with Anisotropic Constituents," *J. Appl. Mech*., 46, 543-550 (1979).

5.4 R. Hill, "Theory of Mechanical Properties of Fiber-Strengthened Materials-III. Self-Consistent Model, *J. Mech. Physics Solids*, 13, 189-198 (1965).

5.5 R.M. Christensen, "A Critical Evaluation for a Class of Micromechanics Models," *J. Mech. Phys. Solids*, 38, 379-404 (1990).

5.6 R. Naik, NASA Technical Memorandum (1992).

5.7 G.A. Van Fo Fy, *Polymer Mechanics*, 2, 593-602 (1966).

5.8 B.N. Cox and M.S. Dadkhah, "The Macroscopic Elasticity of 3D Woven Composites," *J. Comp. Mater.*, 29, 795-819 (1995).

5.9 ASTM Standard D3171.

5.10 I. Verpoest and J. Ivers, Katholieke Univ. Leuven, private communication, 1995.

5.11 C. Kittel, "Introduction to Solid State Physics," John Wiley and Sons, New York, 1967.

5.12 P. J. Minguet, M. J. Fedro, and C. K. Gunther, *Test Methods for Textiles Composites*, NASA Contractor Report 4609, Boeing Defense and Space Group, Philadelphia, 1994.

5.13 Z. Hashin, “Theory of Fiber Reinforced Materials,” NASA CR-1974, March, 1972.

5.14 Z. Hashin, “Analysis of Composite Materials - A Survey,” J. of Applied Mechanics, Vol. 105, Sept. 1983, 481-505.

5.15 Y.M. Tarnopol'skii, V.A. Polyakor, and I.G. Zhigun, "Composite Materials Reinforced with a System of Three Straight, Mutually Orthogonal Fibers, I: Calculation of Elastic Characteristics," *Polymer Mechanics*, 5, 853-860 (1973).

5.16 A.F. Kregers and Y.G. Melbardis, "Determination of the Deformability of Three-Dimensional Reinforced Composites by the Stiffness Averaging Method," *Polymer Mechanics*, 1, 3-8 (1978).

5.17 A.F. Kregers and G.A. Teters, "Determination of the Elasto-Plastic Properties of Spatially Reinforced Composites by the Averaging Method," *Mech. Comp. Mater*., 17, 25-31 (1981)

5.18 J.-M. Yang, C.-L. Ma and T.-W. Chou, "Fiber Inclination Model of Three-Dimensional Textile Structural Composites," *J. Composite Materials*, 20, 472-484 (1986).

5.19 Y.A. Gowayed and C.M. Pastore, "Analytical Techniques for Textile Structural Composites: A Comparative Study of US-USSR Research," *Fiber-Tex 90*, Clemson, SC, August 1990, *NASA Conf. Publ. 3128*, J.D. Buckley, ed., NASA (1991).

5.20 A.E.H. Love, "A Treatise on the Mathematical Theory of Elasticity," (*Dover, New York:, 1944*) Articles 12 and 49.

5.21 R.A. Naik, “Analysis of Woven and Braided Fabric Reinforced Composites,” NASA CR 194930, June 1994.

5.22 J. Xu, B.N. Cox, M.A. McGlockton, and W.C. Carter, "A Binary Model of Textile Composites - II. The Elastic Regime," *Acta Metall. Mater.* **43**[9], 3511-24 (1995).

5.23 B. N. Cox, W, C. Carter, and N. A. Fleck, "A Binary Model of Textile Composites: I Formulation," *Acta Metall. Mater.* **42**, 3463-79 (1994).

5.24 J. E. Masters, R.L. Foye, M.Pastore, and Y.A. Gowayed, “Mechanical Properties of Triaxially Braided Composites: Experimental and Analytical Results”, *J. Composites Technology & Research*, **15**[2], 112-122 (1993).

5.25 E. H. Glaessgen and O. H. Griffin, "Finite Element Based Micro-Mechanics Modeling of Textile Composites," in *Mechanics of Textile Composites Conference*, ed. C. C. Poe, Jr., and C. E. Harris, NASA Conf. Publ. 3311, 1995.

5.26 M.S. Dadkhah, J.G. Flintoff, T. Kniveton, and B.N. Cox, "Simple Models for Triaxially Braided composites," *Composites* **26**, 91-102 (1995).

5.27 B.W. Rosen, S.N. Chatterjee, and J.J. Kibler, "An Analysis Model for Spatially Oriented Fiber Composites," Composite Materials: Testing and Design (Fourth Conference), ASTM STP 617, American Society for Testing and Materials, 1977, 243-254.

5.28 R.L. Foye, “Finite Element Analysis of the Stiffness of Fabric Reinforced Composites,” NASA CR-189597, Feb. 1992.

# 6. NONLINEAR STRESS-STRAIN BEHAVIOUR AND STRENGTH

Predicting the response of a textile composite beyond the proportional limit requires knowledge of how loads are distributed among different tows. Depending on their orientation and location, tows will show markedly different degrees of plasticity[1] and will fail at different external loads. Only some of the elasticity codes described in Section 5 calculate local stresses in the required detail; and of these, only a few have been developed to deal with evolving, heterogeneous plasticity to peak load or ultimate failure. Even in these few, the nonlinear constitutive properties of tows are either assumed ad hoc or built up from barely adequate experimental measurements. There is clearly a need for further model development.

Most of the following discussion and the codes themselves are concerned with progressive failure in which damage is distributed continuously throughout the composite, at least on gauge lengths that are larger than the characteristic scale of the textile architecture, e.g. the unit cell size in a periodic structure or the macroscopic length scale, $\lambda_i$, of Section 5.1.5. Uniform damage is a reasonable assumption in predicting unnotched strength and nonlinearity up to peak load. However, stress-strain response beyond peak load and notched strength are dominated by localized damage bands or cohesive zones. For these phenomena, a different class of model is needed altogether.

## 6.1 Nonlinearity Beyond the Proportional Limit

As discussed in Section 4, nonlinearity prior to peak load in textile composites arises from matrix failure mechanisms: transverse failure of tows or transverse interply cracks; plastic straightening of wavy tows loaded in axial tension; and matrix-mediated axial shear deformation (which may include microcracking or crazing). A general model of these phenomena will take the form of a yield locus for the material in a single tow defined in a triaxial stress space together with some hardening rule. No detailed constitutive laws of this kind based on experimental data have yet been presented. Progress to date relies instead on simple assumptions. In some work, the validity of the assumptions has been checked by comparing output of the textile model with limited macroscopic property data; but whether the assumed constitutive laws are uniquely defined by those data and whether they will hold up for multi-axial loading or parts of complex geometry remain unanswered questions.

### *6.1.1 Tensile (Transverse) Matrix Cracking*

Matrix cracking among tows that are loaded in transverse tension is similar to cracking seen in tape laminates in plies oriented normal to the load axis. However, the factors determining crack spacing and crack saturation are different. In the tape laminate, crack spacing is determined by the mechanics of stress relief around each crack. Saturation is achieved when the zones of stress relief around successive cracks overlap. Further

[1] Here plasticity is used in the general sense of irreversible damage, from which a material cannot recover to its original state upon unloading. Thus plasticity is distinct from nonlinear elasticity. In a polymer composite, plasticity does not arise from the motion of dislocations, as in a metal, because the polymer is generally noncrystalline. It comes instead from microcracking, especially arrays of cracks such as those depicted in Fig. 4-1, coupled with irreversible matrix damage (crazing and tearing of polymer chains) and possibly friction.

increases in the applied load cannot then increase the average axial stress in the cracked ply. In textile composites, transverse matrix cracks form most easily *between* tows aligned normal to the load. Indeed, in many textiles, cracks may not form *within* the tows at all. In such cases, the crack spacing is simply determined by the tow diameter. Transverse cracking of this kind is seen between tows in 2D weaves and 3D interlock weaves under in-plane tension [6.1]. A credible approach to predicting the associated softening of a cracked layer of transversely oriented tows would be to embed the same mechanics used in analyzing matrix cracking in 0/90° laminates [6.2] in a quasi-laminar model of the textile. However, none of the codes available to date performs this operation.

In other textiles, transverse matrix cracks do form within tows. The effect of such internal crack systems has been modeled with some success by simply knocking down the transverse stiffness of the affected tows to some arbitrary, small value [6.3].

### *6.1.2 Shear Deformation*

Figure 4-2(a) showed shear deformation data acquired in a test of a ±45° tape laminate in uniaxial tension. Such approximately elastic/perfectly-plastic behaviour is common to most polymer composites loaded in shear, including textile composites (Fig. 4-2(b)). The ±45° laminated test specimens yield reasonable constitutive laws for tow segments in textile composites made of the same fibers and matrix and with the same fiber volume fraction. For modeling textiles, the data could be fitted with a simple elastic/perfectly plastic law with flow stress $\tau_c$ (Fig. 4-2(a));[2] or a numerical, parametric curve such as a Ramberg-Osgood strain hardening law [6.4],

$$\gamma = \tau/G_{xy}\,[1 + 3(\tau/\tau_c)^{n-1}/7] \qquad (6.1)$$

where $\tau$ is the axial shear stress, $\gamma$ the axial shear strain, $G_{xy}$ the shear modulus, and $n$ is a hardening exponent.

### *6.1.3 Plastic Tow Straightening*

Waviness in nominally straight tows allows nonlinear axial strain when the tow straightens (Section 4.3). Constitutive laws for axial plasticity due to tow straightening can be based on the constitutive law for axial shear discussed above. The resolved axial shear stress, $\tau_s$, due to the tensile stress, $\sigma_x$, in the nominal tow direction in the presence of misalignment, $\phi$, is approximately

$$\tau_s = \sigma_x\,\phi \qquad (6.2)$$

where $\phi$ is the local misalignment angle. When $\tau_s$ exceeds the flow stress, $\tau_c$, the tow segment will begin to straighten. The evolution of the straightening depends on the distribution of $\phi$. An analytic constitutive law is readily developed for the common case that $\phi$ is normally distributed. The law is completed by specification of the width, $\sigma_\phi$, of the distribution, which usually requires an experiment.

---

[2] "Shear flow" here refers to the regime of nearly perfectly-plastic shear deformation visible over large strains in Fig. 4-2. The deformation is mediated by microcracking, crazing, and frictional slip, as already noted.

Tow straightening can arise in nominally straight tows with irregularity; or in tows possessing regular oscillations, such as in plain weaves. If wavy but nominally straight tows are represented as ideally straight in a code (the most common case - see Section 5.2), tow straightening should be considered independently of axial shear due to far-field shear loading. It must be introduced as a modification of the response of the tow to axial tension, in which the tow stiffens with increasing tensile strain. Similarly, if the geometry of regular oscillations is not modeled explicitly (as in the code **WEAVE**), but introduced in the elastic regime via in-plane stiffness knockdowns, then tow straightening will again be represented as a modification of the axial properties of the tow. If, on the other hand, the paths of regularly oscillating tows are represented more or less literally in a code, the axial shear strains associated with tow straightening will usually be computed as part of the general analysis of internal stresses and strains. The constitutive laws assigned to the tows need not then be modified.

Because a tow segment stiffens when it straightens, tow straightening under tension will progressively encompass all segments of a tow. Under axial compression, in contrast, a wavy tow becomes increasingly wavy and softens. Softening will occur first in the most misaligned segments, increasing the misalignment and thus the preference for softening in the same locations. This mechanism of localization will lead to kink band formation.

## 6.2 Tessellation Models

To predict nonlinear composite behaviour and strength, the partitioning of stress amongst tow segments with different orientations must be calculated and local stresses compared with the known yield and failure characteristics of tows under general states of stress. As recounted in Section 5, macroscopic elastic properties are often approached by modeling a textile composite as a tessellation of grains within each of which the fiber orientation is approximately constant. (The grains may be finite or infinite. For example, each ply in a tape laminate or infinitely long, nominally straight stuffers in a 3D interlock weave would be described in a tessellation model as single grains.) The elastic constants of a unidirectional composite are assigned to each grain. Using the same tessellation model in predicting nonlinearity and strength, the nonlinear constitutive laws and failure criteria appropriate to each grain might also be guessed to be those of a unidirectional composite, modified to account for the higher degree of irregularity endemic to textiles. The status of our knowledge of the details of these constitutive laws and failure criteria will be summarized below.

In most of the models of nonlinearity in the codes collected here, matrix plasticity or damage is assumed to be uniform within any tow or set of equivalent tow segments, i.e., within equivalent grains. This reduces the number of degrees of freedom to a manageable level. If isostress or isostrain conditions are also assumed (more reasonably the latter when predicting nonlinearity in fiber-dominated strain components), the resulting models are straightforward generalizations of the orientation averaging models used with frequent in success in the elastic regime, with incremental stiffnesses replacing constant stiffnesses.

Assuming isostrain conditions implies displacement continuity across grain boundaries. Even when matrix cracks appear between neighbouring tows, friction inhibits sliding, especially in 3D architectures, where tow separation is opposed by their interlacing. Neglecting sliding between tows, i.e. assuming coherent tow interfaces, probably has a negligible effect on macroscopic nonlinearity, at least until high strains (typically > 0.05) bring severe damage.

## 6.3 Ultimate Strength

In many aerospace applications, loads are predominantly uniaxial and will be oriented with one set of tows in the textile. In such cases, ultimate strength will be dominated by those primary load bearing tows. The first task in predicting strength is to compute the stress partition between these tows and all other tows in the textile. But the contribution of off-axis fibers to composite stiffness is lower in proportion to the degree of anisotropy of individual tows; and the axial modulus of a tow is typically twenty or more times its transverse modulus, depending on the fiber material and the fiber volume fraction. Therefore, when loads are uniaxial and aligned, useful estimates of the stress partition can be based on very simple models of the stress distribution; and estimates of strength follow by imposing failure criteria for locally aligned loads, which are reasonably well understood.

Ultimate strength predictions under off-axis and biaxial loads are also important in design. Since tow segments of all orientations may contribute significantly under general loads, the problem of computing stress partitions must usually be solved in more detail. The failure criteria for individual tow segments must also be those for multiaxial loads. Once again, experience with unidirectional composites is probably a reasonable guide, although verification for textiles remains a topic for research. Given the state of uncertainty, computational codes that predict strength under multiaxial loads can be relied on at most for identifying trends. Absolute values of strength will have to be measured.

### *6.3.1 Ultimate Tensile Strength*

For aligned loads, consistent but high estimates of ultimate tensile strength have been found for 2D braids and 3D weaves, among other materials, by comparing the local axial stress predicted for the aligned tows with the measured strengths of either bare fiber tows or unidirectional composites [6.1,6.5-6.7]. The local stresses are calculated for given applied stresses by models equivalent to orientation averaging (Section 5). The off-axis tows may be assumed undamaged to peak load (elastic) or to be progressively damaged, e.g. elastic/perfectly plastic, with relatively little effect on the outcome, because they carry a small proportion of the total load.

Table 6.1 compares predictions of ultimate strength for some triaxial glass/urethane braids and 3D interlock carbon/epoxy weaves with measured strengths. The predictions are based on the assumption that the local axial stress in the aligned tows reaches the strength of an equivalent unidirectional composite (in the case of the AS4/1895 composites) or the strength quoted by the manufacturer for the bare fibers reduced by the fiber volume fraction (glass/urethane composites). They exceed the measured ultimate strengths for each textile composite by 20-50%. The difference is greater when the bare fiber strength is used in the predictions. This is to be expected, since the presence of a compliant matrix will generally weaken a bundle of fibers by concentrating stresses around the sites of first fiber failures.[3] Since the bare fiber bundle strength is also strongly gauge

[3] The ratio of the dry fiber bundle strength and the strength of a unidirectional composite depends strongly on the gauge length used for testing the former. However, for typical gauge lengths of a few centimeters, the stress concentrating effect of a *compliant* matrix is probably the dominant factor. It leads to stress concentrations of approx. 15% in fibers neighbouring a fiber break in a typical polymer composite [6.8,6.9]. The dry fiber bundle strength is then often greater than the strength of the unidirectional composite. In contrast, in a composite with a *stiff* matrix, such as a ceramic matrix composite, the stress concentration in fibers neighbouring a broken fiber is negligible. Furthermore, the ability of the matrix to restore the axial load in a broken fiber over a relatively short distance via interfacial friction introduces a material gauge length, much shorter than the specimen length, which becomes the relevant length for

length dependent, the more consistent estimates of textile strength will be those based on the measured strengths of equivalent unidirectional composites. From this datum, strength knockdowns of 20-30% seem typical.

Various reasons for the lower measured strengths were summarized in Section 4.3. The most important is probably damage suffered by the fibers in tows during the textile process. Irregularity in geometry, including waviness and pinching in aligned tows, has a relatively small influence on tensile strength [6.11]. Correlation between tensile strength and degree of waviness has been claimed in one report [6.12], but based on rather few, noisy data points; while it did not appear elsewhere [6.7].

**Table 6.1. Predicted and measured ultimate strengths of some triaxial glass/urethane braids and 3D carbon/epoxy interlock weaves (from [6.1,6.7]; see these references for nomenclature and detailed descriptions of composites).**

| Composite | Measured (MPa) | Predicted (MPa) | Ratio |
|---|---|---|---|
| AS4/1895 3D interlock weaves: | | | |
| *h*-L-1 | 980 | 1350 | 0.73 |
| *h*-L-2 | 935 | 1200 | 0.78 |
| *h*-T-1 | 840 | 1300 | 0.65 |
| *h*-T-2 | 895 | 1250 | 0.72 |
| *h*-O-1 | 1070 | 1360 | 0.79 |
| *h*-O-2 | 850 | 1220 | 0.70 |
| triaxial glass/urethane braids: | | | |
| 45-1-G | 200 | 350 | 0.57 |
| 45-1-A | 270 | 400 | 0.68 |
| 40-1-G | 180 | 300 | 0.54 |
| 35-2-G | 155 | 220 | 0.70 |
| 55-0.5-G | 280 | 470 | 0.60 |
| 45-0.5-G | 275 | 360 | 0.76 |
| 30-0.5-G | 290 | 400 | 0.73 |

### *6.3.2 Compressive Strength*

For aligned loads, compressive failure is either by delamination and Euler buckling of delaminated plies, especially in 2D textile composites, or, if delamination is suppressed, by kink band formation (Section 4.2). Predicting strength for delaminating composites is essentially the same problem for 2D textiles as it is for conventional tape laminates. It is therefore not an appropriate topic for this handbook. Delamination models and codes for tape laminates abound in the literature. They can be employed just as well for 2D textile composites, with the stiffness of individual plies calculated by the models described in Section 5.2 for quasi-laminar textiles.

Delamination and Euler buckling of delaminated layers can also be the mode of failure of quasilaminar 3D textiles in compression, especially following impact damage. However, if adequate yet modest volume fractions of through-thickness reinforcement are

---

analyzing the statistics of flaw distributions [6.10]. Since the strength of a material with a Weibull distribution of flaws rises as the gauge length shortens, a stiff matrix can raise the composite strength above that of the dry fiber bundle.

incorporated, laminate buckling is suppressed, regardless of the size of the delamination (Section 4). Failure then reverts to kink band formation in in-plane tows or plies, which is the desired mechanism of failure in a well designed 3D textile composite. Therefore, this section focuses on predicting failure by kinking.

According to Argon's Law, Eq. (4.1), estimates of compressive strength for aligned loads can again be based on simple calculations of the local axial stress in aligned tows for a given applied load, along with independent measurements of the critical shear stress, $\tau_c$, for axial shear flow within a tow and the distribution of the misalignment angle, $\phi$. Measuring $\tau_c$ is relatively straightforward [6.1], but measuring the distribution of $\phi$ is laborious and its prediction from models of the textile process is at present and probably always will be impossible.

Whereas misalignment angles in tape laminates are typically 3° or less, they are usually larger and subject to wider variations in textile composites. Some data for 3D interlock weaves are shown in Fig. 6-1. Two groups of composites are represented, one characterized by higher fiber volume fraction and higher degree of geometrical regularity, which reflect superior textile processing methods [6.1]. In these better processed composites, the maximum misalignment angles measured by destructive methods within typical specimen gauge sections were approximately 3-5°. In the inferior composites, they were approximately 8-11°. The measured compressive strengths were in inverse proportion to the misalignment angles. Thus the critical local axial stress for kink band formation could be predicted remarkably well by inserting the measured misalignment angles and the measured value of $\tau_c$ into Eq. (4.1). Good estimates of composite strength follow at once from the relation between the local and applied loads, which can be found accurately enough by orientation averaging (isostrain) models.

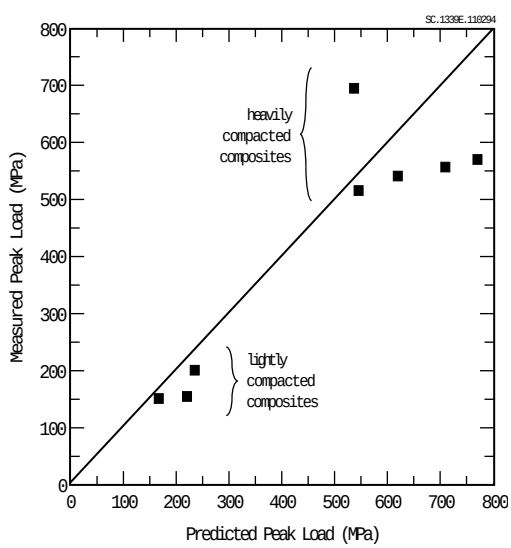


Figure 6-1. Measured compressive strengths of 3D interlock weaves compared with predictions based on measurements of misalignment angles and the critical shear flow stress (from [6.1] and [6.13]).

Knowledge of the distribution of misalignment angles and their control during processing are obviously critical to compressive strength. Unfortunately, there are at

present no certified methods of monitoring misalignments in textile composites. Design limits for compression currently depend on being able to place upper bounds on misalignment angles if certain processing conditions are met, such as control of tow tension during manufacture of a fiber preform. This is clearly an area for further work in developing manufacturing technologies.

### *6.3.3 Shear Strength*

Just as for tape laminates, the in-plane shear strength of a quasi-isotropic textile composite is dominated by the strength of tows (or plies) deforming in tension or compression. To estimate shear strength is then to estimate the critical axial stress in tows for rupture in tension or kink band formation in compression.[4]

In contrast, shear strength in composites reinforced in two orthogonal directions only is determined by the resistance of the matrix within tows or plies to axial shear. For example, a tensile test of a ±45° laminate, such as that reported in Fig. 4-2(a), creates conditions of pure deviatoric shear within plies. Figure 4-2(a) implies an ultimate shear strength of 75 MPa for the typical aerospace resin, Shell 1895. Compact shear tests have also been reported for 3D interlock weave composites containing the same resin [6.15]. The shear response of these composites is dominated by alternating layers of orthogonal stuffers and fillers. The ultimate shear strength in this test configuration was found to be 65-80 MPa for a range of different interlock architectures and filler and stuffer filament counts. The coincidence of these strengths with the shear flow stress of Fig. 4-2(a) suggests that shear failure also occurs in the interlock weaves of [6.15] when the axial shear in stuffers and fillers reaches the critical value, $\tau_C$.

Thus shear strength can be approached via the critical shear flow stress, $\tau_C$. Micromechanical arguments suggest that this strength should be influenced negligibly by the fiber stiffness, provided the fibers are much stiffer than the matrix [6.16,6.17]. It is also unlikely to vary much with the fiber volume fraction for the ranges of fiber packing expected in well consolidated composites.

### *6.3.4 Multi-Axial Loads*

Figure 6-2 shows feasible failure loci for individual tows in a textile composite under multi-axial loads. Since these are the failure criteria that would be applied to individual tow segments when the textile composite is represented as a tessellation of unidirectional grains, the failure boundaries are similar to those that might be expected in a unidirectional polymer composite.

Figure 6-2(a) shows the failure locus for combined aligned loads and axial shear. The local fiber direction is the *x*-axis. Combined axial compression and shear lead to kink band formation at a reduced critical axial stress given approximately by [6.18]

---

[4] Experimental evidence confirms that shear strength rises with the volume fraction, $V_\theta$, of off-axis fibers for small to moderate values of $V_\theta$. However, when $V_\theta$ rises above approximately 45%, the strength saturates and no longer increases [6.14]. This saturation has been attributed tentatively to easier kink band formation in the off-axis plies when they are dominant; they are conjectured to kink more easily as plies of other orientation become thinner and impose less constraint. However, most aerospace applications require material stiffness under load states that are predominantly compressive or tensile, with modest shear loads. Most fibers must then be aligned with the primary load axis and the saturation of shear strength at large $V_\theta$ will not be relevant.

$$\tau_k = (\tau_c - \tau_{xy})/\phi \tag{6.3}$$

which leads to the sloping boundaries for negative axial stress in Fig. 6-2(a). The maximum sustainable axial shear stress, $\tau_{xy}$, is $\tau_c$, which imposes the horizontal boundary in Fig. 6-2(a). Fiber rupture under aligned tension is approximately unaffected by simultaneous shear, so that the right hand boundary in Fig. 6-2(a) is vertical.

Figure 6-2(b) shows the situation for combined axial shear and transverse tension or compression. Once again, the failure locus is bounded on the shear axis by $\tau_c$, the axial shear flow stress. The right hand boundary is limited by matrix cracking under transverse tension, imposing a critical stress $\sigma_y^{(c)}$ in the absence of axial shear. Transverse compression will probably lead to transverse shear failure in tows at some stress $\sigma_{ts}$, although direct observation of the failure mechanism has not been reported. The failure locus in the space $(\sigma_y,\sigma_{xy})$ has been completed as an ellipse, following the quadratic strength rules popularized for unidirectional composites [6.19]. Fleck and Jelf defined an effective stress consisting of a quadratic combination of $\sigma_{xy}$ and $\sigma_y$ in developing a model of plasticity in polymer composites under combined transverse tension and axial shear [6.20]. They also suggested an elliptical failure locus, reasoning that failure under such biaxial loading is a plastic instability (kinking), but their experimental confirmation is sparse and indecisive.

Swanson et al. propose the simple failure criterion in 2D braids under multiaxial loads that the *axial* strain in any tow system should exceed a critical value. This leads to failure loci that are parallelograms, with encouraging but imperfect correspondence with experiments [6.21]. Their proposal, which is similar to a first ply failure condition, is reasonable as long as one set of approximately straight tows with significant volume fraction is aligned with the major stress axis. In aerospace applications, where structures must be strong and stiff, this situation will usually be the preferred design. However, their approach will be of dubious value for any textile architecture that admits failure by matrix-mediated shear.

## 6.4 Codes for Predicting Nonlinear Stress-Strain Behaviour and Ultimate Strength

The capabilities of the codes collected in the handbook for predicting nonlinear stress-strain behaviour and ultimate strength are summarized in Table 6.2.

### *6.4.1 Nonlinearity*

Different approaches have been used for modeling nonlinearity due to plastic shear and tensile microcracking. Nonlinearity due to shear plasticity is generally accompanied by material hardening (e.g. Fig. 4-2), which is modeled by replacing the shear terms of the local stiffness matrix with a strain-dependent function that approximates the experimentally measured response. Computation proceeds incrementally, following some algorithm to insure convergence to a self-consistent, equilibrium state. **TEXCAD** implements this approach. Nonlinearity due to tensile microcracking is usually handled by monitoring each

tow segment or grain for matrix failure. When it occurs, selected terms of the local stiffness matrix are reduced or set to zero. The code must then iterate to re-establish equilibrium before incrementing the load. **TEXCAD** and **SAWC** employ versions of this approach. One limitation of these codes is that the user has no control over the stiffness discount rule or the criteria for onset of nonlinearity.

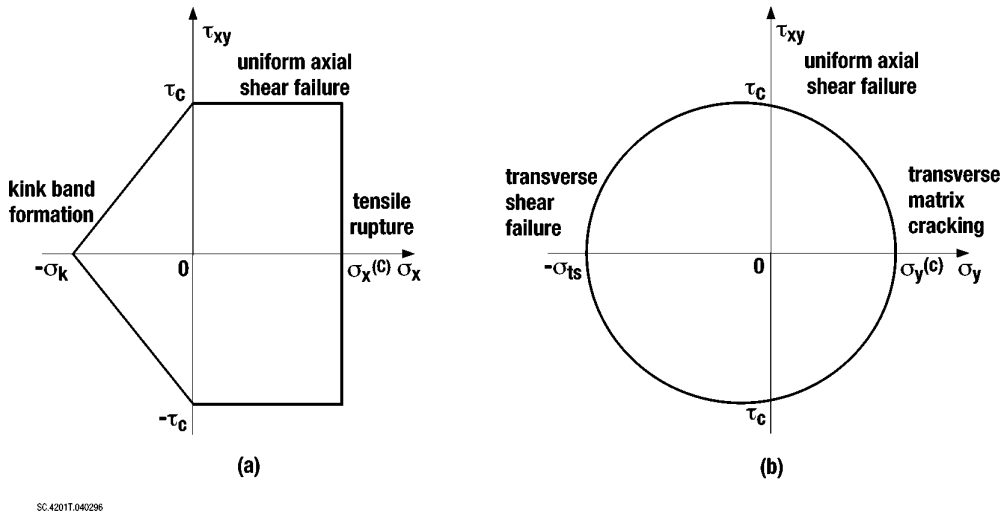


Figure 6-2. Failure loci for individual tows or plies in terms of the local stress state. (a) Combined aligned and axial shear loads. (b) Combined transverse and axial shear loads. The *x*-axis is aligned with local fiber direction. The axes are not to scale.

### *6.4.2 Ultimate strength*

In most of the codes, ultimate tensile strength is estimated by simply comparing maximum local stresses with tow or fiber strength data, using calculations in which the textile is assumed to remain wholly elastic. This is analogous to the first-ply failure method of determining the strength of laminates. In most of the codes, no provision is made for entering the tow or fiber strength data (Table 6.2); but several codes provide values for internal stresses as output. These internal stresses could be compared with empirical failure loci similar to Fig. 6-2 to predict strength. **TEXCAD** prints tables of internal stresses determined using the isostrain assumption. The finite element codes **μTex-10, μTex-20**, **SAWC**, and **BINMOD** all provide internal stresses as output, typically in the material axes (orientated with the local fiber direction).

**CCM-TEX** makes the coarsest of all estimates of composite strength, simply summing the strengths of the tows weighted by their areas. This can nevertheless be a useful estimate of tensile strength for a textile containing a dominant set of nominally straight tows under aligned uniaxial loads, e.g. the 3D interlock weaves studied in [6.1,6.5.6.6]; or the triaxial braids studied in [6.7], when loads are in the axial tow direction. It is not useful for compressive strength, since the strength of the tow is undefined without reference to misalignment angle distributions.

**Table 6.2. Code capabilities for predicting nonlinear behaviour and strength.**

| Code | Textile Forms | Local Stress | Nonlinearity | Strength |
|---|---|---|---|---|
| **PW**<br>**SAT5**<br>**SAT8** | plain weaves<br>5 harness satin<br>8 harness satin | | | |
| **CCM-TEX** | 3-D Weave<br>2-step braids<br>4-step braids | | | yes |
| **μTex-10**<br>**μTex-20** | general<br>user provides | yes | | |
| **SAWC** | plain weave<br>(FE code general) | yes | stiffness discount | yes |
| **TEXCAD** | 2D weaves<br>2D braids<br>user defined | yes | shear hardening, stiffness discount | yes |
| **WEAVE** | 3D interlock weaves | | | |
| **BINMOD** | 3D interlock weaves | | yes | not directly |

## 6.5 Notched Strength

Notch sensitivity in textile composites is limited by two mechanisms: splitting parallel to the load axis, which isolates the notched material from adjacent material; and the formation of blunting damage bands (Section 4). Models for splitting have been developed extensively to deal with a similar effect in continuous fiber ceramic matrix composites and layered systems, including tape laminates [6.22]. Nonlinear damage bands can be modeled as cohesive zones or bridged cracks, much like craze zones in polymers or damage zones in concrete [6.23-6.27]. Unfortunately, very few models have been formulated for dealing with either splitting or cohesive zones in textile composites, where they are generally far more important than in any other class of material. In fact, their unusual characteristics in textile composites are the source of the extraordinary notch insensitivity these materials possess (Section 4).

The crucial material property in a cohesive zone is the relation, $p(u)$, between the tractions, $p$, acting across the damage band and the effective opening displacement, $2u$. One would expect that the characteristics of $p(u)$ that are essential to notch sensitivity should be contained in no more than two parameters, for example, the critical stress, $p_c$, for the onset of damage and either the work of fracture, $W_f = 2\int p\,du$, or the critical opening displacement, $u_c$, beyond which $p$ vanishes. The length of the cohesive zone is then characterized approximately by the length scale, $l_{ch}$, of Equation (3.2). Notch sensitivity is generally restricted to holes or notches that are larger than $l_{ch}$. The parameters ($p_c$, $W_f$) or ($p_c$, $u_c$) should be evaluated by a set of standard tests, for example of notched strength. Strength in parts of general shape should then be predicted by application of the calibrated cohesive zone model. In the absence of developed codes, notched strength in textile composites can receive no further treatment in this edition of the handbook. This problem requires further work.

**References**


6.1 B. N. Cox, M. S. Dadkhah, and W. L. Morris, “Failure Mechanisms of 3D Woven Composites in Tension, Compression, and Bending,” **42**[12], 3967-84 (1994).

6.2 L. N. McCartney, “Theory of Stress Transfer in a 0°/90°/0° Cross-Ply Laminate Containing a Parallel Array of Transverse Cracks,” *J. Mech. Phys. Solids* **40**, 27-68 (1992).

6.3 D.M. Blackketter, D.E. Walrath, and A.C. Hansen, "Modeling Damage in a Plain Weave Fabric-Reinforced Composite Material," *J. of Composites Technology & Research* **15**[2], 136-142 (1993).

6.4 B. Budiansky and N. A. Fleck, “Compressive Failure of Fiber Composites,” *J. Mech. Phys. Solids* **41**[1], 183-211 (1993).

6.5 K. Pochiraju, T-W. Chou, and B. M. Shah, "Modeling Stiffness and Strength of 3-D Textile Structural Composites," to appear in the *Proceedings of 37th joint AIAA/ASME/ASCE/AHS/ASC Structures, Structural Dynamics, and Materials Conference*, Salt Lake City, 1996.

6.6 K. Pochiraju, T-W. Chou, and B.M. Shah, "Experimental Characterization of 3-D textile structural Composites," to appear in the *Proceedings of the 37th Joint AIAA/ASME/ASCE/AMS/ASC Structures, Structural Dynamics, and Materials Conference*, Salt Lake City, 1996.

6.7 M. S. Dadkhah, W. L. Morris, T. Kniveton, and B. N. Cox, "Simple Models for Triaxially Braided Composites," *Composites* **26**, 91-102 (1995).

6.8 J. M. Hedgepeth and P. Van Dyke, “Local Stress Concentrations in Imperfect Filamentary Composite Materials,” *J. Comp. Mater.* **1**, 294-309 (1967).

6.9 M. A. McGlockton, R. M. McMeeking, and B. N. Cox, “The Strength of Ceramic Matrix Composites,” to be submitted to *Acta Metall. Mater.*

6.10 W. A. Curtin, “The ‘Tough’ to Brittle Transition in Brittle Matrix Composites,” *J. Mech. Phys. Solids* **41**, 217-245 (1993).

6.11 J. Xu, B. N. Cox, M. A. McGlockton, and W. C. Carter, "A Binary Model of Textile Composites - II. The Elastic Regime," *Acta Metall. Mater.* **43**[9], 3511-24 (1995).

6.12 A. K. Roy, “In Situ Damage Observation and Failure in Model Laminates Containing Planar Yarn Crimping of Woven Composites,” *Mechanics of Composite Materials and Structures*, in press.

6.13 B. N. Cox, M. S. Dadkhah, W. L. Morris, and J. Zupon, “Mechanisms of Compressive Failure in 3D Woven Composites,” *Acta Metall. Mater.* **40**[12], 3285-98 (1992).

6.14 G. Flanagan, unpublished work; see also J.M. Whitney, D.L. Stanbarger, and H.B. Howell, "Analysis of the Rail Shear Test - Applications and Limitations," *J. Composite Materials* **5**[1], 24-34 (1971).

6.15 P. J. Minguet, M. J. Fedro, and C. F. Gunther, *Test Methods for Textile Composites*, NASA Contractor Report 4609, Boeing Defense and Space Group, Philadelphia, 1994.

6.16 N. A. Fleck, "Brittle Fracture due to an Array of Microcracks," *Proc. R. Soc. London* **A432**, 55-76 (1991).

6.17 Z. C. Xia and J. W. Hutchinson, "Mode II Fracture Toughness of a Brittle Adhesive Layer," *Int. J. Solids Structures* **31**, 1133-1148 (1994).

6.18 W. S. Slaughter, N. A. Fleck, and B. Budiansky, "Compressive Failure of Fiber Composites: The Roles of Multiaxial Loading and Creep," *J. Engng Mater. Tech.* **115**, 308-13 (1993).

6.19 N. A. Fleck and P. M. Jelf, "Deformation and Failure of a Carbon Fibre Composite under Combined Shear and Transverse Loading," *Acta Metall. Mater.* 43[8], 3001-7 (1995).

6.20 S. W. Tsai and H. T. Hahn, *Introduction to Composite Materials*, Technomic Publishing Company, Westport, Connecticut, 1980. Chapter 7.

6.21 S. R. Swanson and L. V. Smith, "Multiaxial Stiffness and Strength Characterization of 2-D Braid Carbon/Epoxy Fiber Composites," in *Mechanics of Textile Composites Conference*, Hampton, Virginia, December, 6-8, 1994, ed. C. C. Poe, Jr., NASA Conference Publication 3311 (NASA, 1995).

6.22 K. S. Chan, M. Y. He, and J. W. Hutchinson, "Cracking and Stress Redistribution in Ceramic Layered Composites," *Mater. Sci. Engng* **A167**, 57-64 (1993).

6.23 A. Hillerborg, "Analysis of One Single Crack," *Fracture Mechanics of Concrete*, ed. F. H. Wittman (Elsevier Science Publishers, Amsterdam, 1983) pp. 223-49.

6.24 R. M. L. Foote, Y.-W. Mai, and B. Cotterell, "Crack-Growth Resistance Curves in Strain softening Materials," *J. Mech. Phys. Solids* **34**, 593-607 (1986).

6.25 Z. P. Bazant, ed., *Fracture Mechanics of Concrete Structures* (Elsevier Applied Science, London, 1992).

6.26 B. N. Cox and D. B. Marshall, "Concepts for Bridged Cracks in Fracture and Fatigue," *Acta Metall. Mater.* **42**[2], 341-63 (1994).

6.27 T. H. Walker, L. B. Ilcewicz, D. R. Polland, and C. C. Poe, Jr., "Tension Fracture of Laminates for Transport Fuselage - Part II: Large Notches," *Third NASA Advanced Composite Technology Conference*, NASA CP-3178 (NASA, 1992). pp. 727-758.

# 7. FATIGUE LIFE

None of the codes reported in this handbook provides fatigue life predictions. Nevertheless, some of the principles by which such a prediction could be made have been discussed in the literature; and the output of codes that calculate the distribution of stresses in different tows could be combined with test data to make predictions at least for the flat panel composites that are the focus of this first edition.

## 7.1 Kink Formation in Compression-Compression Fatigue

As discussed in Section 4, in a well-designed 3D composite delamination and Euler buckling are suppressed in compression and failure under aligned loads occurs by kink band formation. This is true for both monotonic and cyclic loads. The kink bands form at locations where tows (or plies) are most severely misaligned because the topology of the textile architecture necessitates misalignment or some irregularity has been introduced during manufacture. Damage apparently accumulates through nonlinear processes inside the tow in proportion to the magnitude of the axial shear stress in the misaligned segment. It appears to be weakly correlated with features of the reinforcement architecture other than the local misalignment angle.

Two mechanisms have been proposed by which damage may accumulate [7.1,7.2]. Cyclic axial shear may exhibit ratchetting, causing the tow to rotate to greater misalignment angles; or accumulating plastic damage in the resin within tows may lower the effective flow stress, $\tau_c$. In 3D interlock weaves, the absence of observed rotations before kinking supports the latter mechanism, but this remains a topic of research. In either case, the elapsed cycles to kink band formation can be modeled by steps analogous to those commonly used for low cycle fatigue. For example, a law for the rate of accumulation of damage consisting of changes in $\tau_c$ in some misaligned tow segment can be written [7.2]

$$\frac{d\tau_c}{dN} = -A\left(\Delta\sigma_s\phi\right)^m \tag{7.1}$$

for some material constants $A$ and $m$, with $\sigma_s$ the local axial stress. For a fixed local cyclic stress amplitude, $\Delta\sigma_s$, this leads to an expression for the total cycles, $N_k$, to kink band formation:

$$N_k = \frac{\tau_c - \Delta\sigma_s\phi}{A\left(\Delta\sigma_s\phi\right)^m} + 1 \quad . \tag{7.2}$$

Load Control

In applications where the applied load rather than the applied strain is constrained, fatigue failure follows the formation of just a few kink bands. Test specimens of 3D interlock weaves containing 200-300 $mm^3$ of material fail when two or three kink bands have formed in separate aligned tows [7.2]. In stitched laminates, the first kink band to form is usually catastrophic. The fatigue life of load controlled textile structures that fail by kinking can accordingly be estimated by substituting a value for the misalignment angle, $\phi$, in Eq. (7.2) that is representative of the extremes of the distribution of misalignment angles.

Equation (7.2) leads to fatigue load-life curves that are not far from straight on log-log plots, with slope $\approx m$. Typical values of $m$ for carbon/epoxy systems are 30 [7.2]; for glass/urethane systems, 15 [7.3]. Comparison of predicted and measured load-life curves in carbon/epoxy 3D interlock weaves and glass/urethane triaxial braids supports the adequacy of the power law of Eq. (7.1) and the low cycle fatigue approach.

If the material constants $A$, $\phi$, and $m$ are known, fatigue life thus follows from prediction of the local axial stress, $\sigma_s$. As long as the applied loads are sufficiently small that widespread plasticity is not induced, which will be a design condition in an airframe, the required prediction of local stresses can be made by one of the computer codes presented in Section 5.

In practice, neither the constants $A$ and $m$ nor the distribution of misalignment angles will be known a priori. They will be evaluated for a particular material by calibrating tests. The life prediction method outlined above would then be used to assess the effects of variations in load or structural geometry, provided the latter are confined to operations such as cutting out holes that would not affect the distribution of misalignments.

Strain Control

In applications where strain rather than load is constrained, structural failure in 3D textile composites such as interlock weaves may not follow the formation of the first few kink bands. Under strain control, these materials exhibit exceptional damage tolerance in cyclic as well as monotonic loading. Life predictions based on substituting values of the distribution of misalignment angles into Eq. (7.2) would then be unduly conservative. Ultimate failure could be the combined effect of many separate kink bands. Better predictions should account for the gradual evolution of the population of kink bands in

individual tows, calculating the effects of load redistribution following each new kink event. The code **BINMOD** is currently being enhanced to perform such calculations.

## 7.2 Tension-Tension Fatigue and Load Ratio Effects

Computational models relating fatigue life to textile architecture have not yet been developed other than for compression-compression loading. Limited data suggest that damage rates during a tensile cycle are much lower than during compression cycles (e.g., [7.4]). The most dangerous mode of damage is presumably shear plasticity leading to kinking, which is a compression failure. Tensile failure requires fiber rupture, which is brought about relatively slowly by fatigue.

Load ratio effects on the fatigue life of textiles remain a subject for research.

## 7.3 Delamination Crack Growth in Quasilaminar Textile Composites

The initiation of delamination fatigue cracks in a 3D quasilaminar composite, such as a stitched laminate, will be similar to initiation in a conventional tape laminate. Initiation sites will include delaminations caused by impact and points of stress singularity where anisotropic plies meet a free edge. However, propagation following initiation will be very different, with through-thickness reinforcement playing a strong and crucial role.

Delamination cracks may then propagate with various mode mixtures, from pure Mode I under out-of-plane loads in certain symmetric specimens or parts to pure Mode II under bending loads. Through-thickness reinforcement will supply bridging tractions across the delamination crack, shielding the crack tip from the applied load. The mechanics of bridged delamination cracks in polymer composites have been extensively studied in recent years, especially in reference to stitched laminates [7.5-7.8]. If the bridging reinforcement (stitching) remains intact, a steady state configuration will be reached when the crack is sufficiently long in which the net crack tip stress intensity factor is independent of the crack length (e.g., [7.9,7.10]). For cyclic loading, application of the J integral yields an analytical relationship between the applied stress range, $\Delta\sigma_a$, and the range of the net tip crack intensity factor, $\Delta K_{tip}$. For example, for a delamination crack growing in the curved stitched laminate shown in Fig. 4-8, where the bridging tractions follow a linear law, one has [7.7]

$$\Delta K_{tip} = [E' h / F_s E_s]^{1/2} \, \Delta\sigma_r, \qquad . \qquad (7.3)$$

where $\Delta\sigma_r = \eta\Delta\sigma_a$ is the cyclic amplitude of the through-thickness stress corresponding to $\Delta\sigma_a$ and $f_s$ and $E_s$ are the spatially averaged volume fraction and axial modulus of the stitching fibers. Since $\Delta K_{tip}$ is independent of crack length, the delamination crack growth rate should take a constant value, $v_{ss}$, in this limit. Furthermore, provided there is no delamination notch or region of failed stitches, $v_{ss}$ will be an upper bound to the growth rate for all crack lengths. Thus Eq. (7.3) provides the basis for simple, rigorous bounding estimates to fatigue life. Similar relations can be demonstrated for Mode II and mixed mode fatigue crack growth.

A fatigue life strategy based on Eq. (7.3) is currently being developed.

**References**


7.1. N. A. Fleck and W. S. Slaughter, "Compressive Fatigue of Fibre Composites," *J. Mech. Phys. Solids* **41**[8], 1265-84 (1993).

7.2. M. S. Dadkhah, W. L. Morris, and B. N. Cox, "Compression-Compression Fatigue in 3D Woven Composites", *Acta Metall. Mater.* **43**[12], 4235-45 (1995).

7.3. B. N. Cox, M. S. Dadkhah, J. Flintoff, R. V. Inman, M. R. Mitchell, and W. L. Morris, *Design and Reliability Guide for Triaxially Braided Composites*," Rockwell Science Center, Final Report to Plastic Products Division, December, 1993.

7.4 B. N. Cox, M. S. Dadkhah, and W. L. Morris, *Failure Models for Textile Composites*, NASA CR-4686 (NASA, 1995).

7.5 L. K. Jain and Y.-W. Mai, "On the Effect of Stitching on Mode I Delamination Toughness of Laminated Composites," *Composites Sci. Tech.* **51**, 331-45 (1994).

7.6 T.-J. Lu and J. W. Hutchinson, "Role of Fiber Stitching in Eliminating Transverse Fracture in Cross-Ply Ceramic Composites," *J. Amer. Ceram. Soc.* **78**[1], 251-3 (1995).

7.7 B. N. Cox, R. Massabò, and K. Kedward, "Suppression of Delamination in Curved Parts by Stitching," *Composites*, in press.

7.8 R. Massabò and B. N. Cox, "Concepts for Bridged Mode II Delamination Cracks," submitted to *Mech. Materials.*

7.9 R. M. McMeeking and A. G. Evans, "Matrix Fatigue Cracking in Fiber composites," *Mech. Materials* **9**, 217-27 (1990).

7.10 B. N. Cox and D. B. Marshall, "Concepts for Bridged Cracks in Fracture and Fatigue," Overview No. 111, *Acta Metall. Mater.*, **42** (1994) 341-63.

# 8. SUMMARY OF AVAILABLE CODES

Many codes are available for computing the properties of textile composites, especially their macroscopic stiffness, their strength, and occasionally aspects of their damage tolerance. The following brief descriptions summarize the capabilities of the codes that are documented in this handbook. The information given here is intended to introduce the reader quickly to each code's capabilities, the types of textiles it analyzes, the method of analysis, and the range of output produced. More complete details will be found in the user's guide in one of the handbook's appendices or in the cited references.

Even where a user's guide has been provided, it will often be found not to explain all theoretical aspects of the analysis. It is highly recommended that the listed references also be read before using any code. In some instances, the required input will not be clear unless the reference material is used.

Not all references to relevant papers by the authors are listed in this section. They may be found either in the user's guide or in the papers that have been cited.

## 8.1 μTex-10

Authors: Ramesh V. Marrey and Bhavani V. Sankar

References:

B.V. Sankar and R.V. Marrey, "A Unit-Cell Model of Textile Composite Beams for Predicting Stiffness Properties," *Composites Science and Technology*, 1993, **49**, pp. 61-69.

B.V. Sankar and R.V. Marrey, "Micromechanical Models for Textile Structural Composites," *Proceedings of 13th Army Symposium on Solid Mechanics*, 1993, pp. 189-200.

R.V. Marrey and B.V. Sankar, "Evaluation of Finite Element Micromechanical Analysis Methods for Textile Composites," *Proceedings of the 1994 ASME Winter Annual Meeting*, 94-WA/AERO-1, Nov. 6-11, 1994.

User Manual:

*User Manual for* ***μTex-10*** *and* ***μTex-20***. Includes well documented description of input and output; instructions for compiling on different computers; limited discussion of theory.

Format:

FORTRAN code which can be recompiled for the target machine. A parameter file is provided for changing the maximum problem size.

Geometric Model:

The user must provide a series of points describing the locus of the centre of each yarn. An additional set of points must be provided to give the cross-section of each yarn in terms of an *n*-sided polygon. The yarn path is assumed to lie in a single plane, which can be rotated to an arbitrary orientation. Multiple yarn paths can be defined to generate various textile forms. Fiber volume fraction is computed from the given geometry.

Stiffness Model:

Finite element analysis is used to determine a general displacement field. Periodic or cyclic-symmetry boundary conditions are applied to the edges of the unit cell. The finite element code is integral to the program. The user can select the degree of mesh refinement (number of elements on an edge). Heterogeneous elements are used, in which the material (yarn or matrix) may be different at each integration point. The user may select a 3D solution or a plate solution. In the plate solution, *A*, *B*, and *D* matrices are computed using traction free surfaces to represent the plane-stress condition. Average stiffness is computed using both volume averaged stresses and the summation of edge forces.

Strength Model:

No strength prediction is given, but stress and strain distributions from the linear analysis are available. Stresses are computed for unit applied strains (6 components).

Data Required:

Yarn and matrix linear elastic stiffness. Different yarns may have different properties. Points describing yarn paths and cross-sections must be generated external to the program.

Output:

6x6 average stiffness matrix, *A*, *B*, and *D* matrices (plate option), thermal expansion coefficients, and yarn volume fractions. Point stresses available for unit strains. Finite-element nodal coordinates and connectivity arrays are also given.

Experimental Validation:

None offered.

Comments:

- Since the problem is solved by finite elements, no assumptions are made regarding the internal displacement field. Point stresses are available. Unlike isostrain models, the strains corresponding to these stresses may vary within a constituent.

- Convergence of stresses is slow as the number of elements is increased when heterogeneous elements are used.

- Some inconvenience results from the code needing point-by-point yarn path and cross-section data as input. As a practical matter, this is preferably obtained from another code or solid modeler.

- The assumptions that cross-sections are constant and yarn paths lie in a single plane prevent the code from being used for some textile forms, such as 3D braids.

- The code is computationally intensive. If computational speed was important, the code would at least be useful for generating reference solutions for comparison to faster, simpler approaches.

## 8.2 $\mu$Tex-20

Authors: Ramesh V. Marrey and Bhavani V. Sankar

References:

B.V. Sankarand R.V. Marrey, "Micromechanical Models for Textile Composites," to be published in *the Proceedings of the Mechanics of Textile Composites Conference*, Dec. 6-8, 1994, Hampton Va.

User Manual:

*User Manual for $\mu$Tex-10 and $\mu$Tex-20*. Includes well documented description of input and output; instructions for compiling on different computers; limited discussion of theory.

Format:

FORTRAN code which can be recompiled for various target machines. A parameter file is provided for changing the maximum problem size.

Geometric Model:

User must provide a series of points describing the locus of the center of each yarn. An additional set of points must be provided to define the cross-section of each yarn in terms of an *n*-sided polygon. The yarn path is assumed to lie in a single plane, which can be rotated to an arbitrary orientation. Multiple yarn paths can be defined to generate various textile forms. Fiber volume fraction is computed from the given geometry.

Stiffness Model:

Implements a procedure called the Selective Averaging Method. The unit cell is discretized into slices normal to the load direction or parallel to the plane of shear. Slices are further divided into elements that are somewhat smaller than the yarn diameter. A combination of isostrain and isostress assumptions is used to determine an average stiffness of the slices and thence of the unit cell. Periodicity is not enforced.

Strength Model:

None.

Data Required:

Yarn and matrix elastic constants. Different yarns may have different properties. Points describing yarn paths and cross-sections must be generated external to the program.

Output:

6x6 average stiffness matrix, *A*, *B*, and *D* matrices (plate option), thermal expansion coefficients, and yarn volume fractions. Finite-element nodal coordinates and connectivity arrays are also given.

Experimental Validation:

None offered.

Comments:

- Combining isostrain and isostress can be physically justified in a composite. However, the user should be aware that there is no way to tell if an upper or lower bound is being obtained.

- Like μ**Tex-10**, this code computationally intensive. A solution for μ**Tex-20** using a 20x20x20 mesh required about an hour on an HP 7000 workstation. The authors report a quarter of this time using a different computer.

- Stress output is not available.

- Given that the effort to set up data files is identical for μ**Tex-10** and μ**Tex -20**, the advantages of μ**Tex-20** are not obvious. It may be preferable to obtain an upper bound solution from μ**Tex-10**, which is known to converge with increasing mesh density, rather than to introduce the uncertainty of the selective averaging method.

## 8.3 TEXCAD

Author: Rajiv A. Naik

References:

R.A. Naik, "Analysis of Woven and Braided Fabric Reinforced Composites," NASA CR 194930, June 1994

R.A. Naik, "Failure Analysis of Woven and Braided Fabric Reinforced Composites," NASA CR 194981, Sept. 1994.

User Manual:

*TEXCAD - Textile Composite Analysis for Design, Version 1.0 User's Manual*, NASA CR 4639, Dec. 1994. Includes extensive documentation; example problems for each of the predefined textile forms; and on-line graphics files to aid in understanding the geometric relations and input parameters.

Format:

Executables are available for Apple Macintosh and Microsoft Windows.

Geometric Model:

**TEXCAD** uses a series of predefined geometric models for plain weaves, 5-harness satin weaves, 8-harness satin weaves, 2x2 2D triaxial braids, 1x1 2D triaxial braids (with two different axial patterns), and 3D, multi-interlock, 5-layer braids. These models require input of a limited number of parameters, including yarn spacing, yarn count, filament diameter, and braid angle. From these, the code generates an idealization using straight and sinusoidal segments that matches the specified yarn volume fraction. A method is provided for entering customized unit cells. In addition, conventional laminates and *n*-directional 3D reinforced materials may be analyzed (the orthogonal weaves of Section 2).

Stiffness Model:

Macroscopic stiffness is computed by orientation averaging (isostrain conditions). Each yarn is discretized into slices. Volume averaging is effected by numerical integration along yarn paths, using the local material properties and spatial orientation. The code also gives laminated plate stiffness matrices (*A*, *B*, and *D*) and can stack multiple layers using lamination theory. Nesting patterns are not accounted for when layers are stacked.

Strength Model:

**TEXCAD** has several nonlinear features that aid in estimating failure.

- The nonlinear shear response of the impregnated yarns and resin is represented by a power-law relation.

- Bending of undulating yarns is modeled as the response of curved beams on elastic foundations. Yarn splitting is also accounted for in this model.

- There is a stiffness reduction algorithm that is applied when local damage is detected.

- First order effects of geometric nonlinearity due to yarn straightening or wrinkling are included.

- Failure is based on the constituent stress obtained from an isostrain model. Failure may also occur if the bending stresses in the models of beams on elastic foundations reach a critical value.

Data Required:

Stiffness and strength for yarns and matrix. Geometric parameters depend on the textile analyzed. They generally include yarn spacing, fiber volume fraction in yarn, yarn filament count, filament diameter, overall fiber volume fraction, and braid angle.

Output:

Three-dimensional stiffness matrix, plate stiffness elements, thermal expansion coefficients, nonlinear stress-strain response (tabulated), failure sequence.

Experimental Validation:

Comparisons to measured elastic properties, nonlinear response, and strength data are tabulated in the documentation. Parametric trends for strength with respect to braid angle, crimp angle, yarn spacing, and volume fraction are presented with available data.

Comments:

**TEXCAD** is well documented and easy to use. It is a thorough implementation of the isostrain approach. It performs failure analysis as well as can be expected in the context of an isostrain model. The parametric input for geometry is logical, using data that are typically available when designing with textiles.

## 8.4 PW, SAT5, SAT8

Author: Ivatury S. Raju

References:

I.S. Raju and John T. Wang, "Classical Lamination Theory Models for Woven Fabric Composites," *J. of Composites Technology and Research*, **16**[4], 1994, pp. 289-303.

User Manual:

None. Example data files provided with code.

Format:

FORTRAN code which may be compiled for the target machine.

Geometric Model:

2-dimensional unit cells are defined for plain weaves, 5-harness satin weaves, and 8-harness satin weaves. Non-rectangular, minimal unit cells are used for the satin weaves. Within the unit cells, regions are defined in which the yarns are either straight or undulate sinusoidally. Yarn cross-sections are effectively rectangular. The length of the undulating cross-over points is computed to match the specified fiber volume fraction.

Stiffness Model:

Isostrain assumptions are used to derive plate stiffness matrices (*A*, *B*, and *D*). Thermal expansion coefficients are computed.

Strength Model:

None.

Data Required:

Yarn and matrix stiffness properties. Yarn spacing, tow thickness, ply thickness, yarn volume fraction, yarn packing fraction.

Output:

Plate stiffness matrices, thermal expansion coefficients. Various intermediate results.

Experimental Validation:

Comparisons to measured fabric elastic properties are given in the cited reference.

Comments:

- These codes implement an analysis similar to the classical fabric models, such as the fiber undulation and bridging models, without some of the simplifying assumptions used in previous presentations. In principle, the more general **TEXCAD** should supersede these earlier isostrain codes. However, the actual results for plate stiffness are significantly different for the two codes. (See Tables of results in Section 5.) There appears to be some difference in the way in which plane stress assumptions are implemented.

- The 2D materials analyzed by these codes would usually be stacked to form a structure. The stiffness for the stacked laminated must be computed elsewhere.

## 8.5 SAWC (Stress Analysis of Woven Composites)

Author:

John Whitcomb

References:

J. Whitcomb, K. Woo, and S. Gundapaneni, "Macro Finite Element Analysis of Textile Composites," *J. of Composite Materials*, **28**[7], 607-618, 1994.

J. Whitcomb, G. Kondagunta, and K. Woo, "Boundary Effects in Woven Composites," *J. of Composite Materials*, **29**[ 4] , 507-524, 1995.

J. Whitcomb, K. Srirengan, and C. Chapman, "Evaluation of Homogenization for Global/Local Stress Analysis of Textile Composites," presented at *AIAA/ASME/ASCE/AHS/ASC 35th Structures, Structural Dynamics, and Materials Conference*, Hilton Head, SC, April 18-20, 1994.

User Manual:

"Stress Analysis of Woven Composites." The manual lists the input required for each of the three programs included in this package. The input required for the mesh generation code, **PWMeshGen**, is straight-forward, although some terms are not defined. The finite element code **Flex94** involves some complex, nonstandard input. For the plain weave geometry, the input file for **Flex94** is automatically generated by **PWMeshGen**. Many of the concepts and terms are not defined in the manual. The user must be familiar with the reference material to grasp the analysis the code is performing.

Format:

FORTRAN, C, and C++ code. Graphics utilities require the use of the openGL graphics library, and the MOTIF user interface.

Geometric Model:

The mesh generator **PWMeshGen** is limited to a plain weave fabric in which the tow path is assumed to be sinusoidal. This basic unit cell can be converted into a macroelement which may then be stacked and assembled to form more complex assemblies of the underlying plain weave units. The finite element code, **Flex94**, is general. However, for any geometry other than a plain weave, the user must provide nodal coordinates, connectivity arrays, and material orientations.

Stiffness Model:

**Flex94** can be used to generate a conventional average stiffness matrix for the unit cell using the finite element method and periodic boundary conditions. However, the strength of this approach is the ability to generate macroelements which include the internal microstructure, but may be used like conventional elements.

Strength Model:

The finite element code can be used to perform a progressive failure analysis by reducing material stiffness at integration points when the local stress exceeds a given strength value. There is no control over which stiffness components are affected or the degree of reduction.

Data Required:

Mesh generation for a plain weave requires the layer thickness, waviness ratio, number of elements, and number of resin elements above and below tows. Loads, boundary conditions, and material properties are needed for the finite element analysis. Utilities are provided for conveniently setting up boundary conditions, including periodic displacements.

Output:

Point-wise stresses are generated. These stresses may be viewed using the graphics routine **Plot94**. Contour maps of failure locations may also be generated.

Experimental Validation:

None offered.

Comments:

Orientation averaging (stiffness averaging) approaches are valid when strains do not vary significantly over the scale of the unit cell. The macroelement approach will be more accurate when stress gradients, such as bending effects, are important. This code demonstrates a powerful methodology that may be used to generate structural models when textile preforms cannot be accurately homogenized. However, the code has limited applications in its present form.

## 8.6 CCM-TEX

Author:

Kishore Pochiraju

References:

User Manual:

None provided. Data input is interactive with prompts.

Format:

FORTRAN code which may be compiled for target machine.

Geometric Model:

The code treats 3-dimensional weaves and braids. Geometric idealizations are used to compute yarn angles and fiber volume fraction.

Stiffness Model:

Orientation averaging of stiffness (isostrain model).

Strength Model:

Prints a predicted strength in the warp and weft directions. Strength calculation is based on local stress in isostrain model and the specified tow strength.

Data Required:

Yarn and matrix elastic constants and tow strength. Geometric input for 3D weave includes weave pitch, width of unit cell, thickness of plate, number of axial yarns per unit width and thickness, number of wefts per unit length and thickness, and number of *z* weavers per unit width and thickness. Code distinguishes between layer-to-layer and through-the-thickness angle interlock. For 2-step and 4-step braiding, the code requires the braiding angle, tow size ratio (axial/braider), and either the column and row numbers of axial yarns (2-step) or number of axial and braider yarns (4-step).

Output:

Three-dimensional stiffness matrix. Strength estimates for tension in warp and weft directions.

Experimental Validation:

None offered in code documentation.

Comments:

The strength of **CCM-TEX** is in converting parameters used to specify braids and 3D weaves into a geometric representation, including a prediction of the fiber volumes in each yarn. Lack of documentation is a problem. Although the code is usable in the interactive mode, most users will need to know the internal mechanics of the program before applying to real problems. The strength estimates are based on isostrain calculations of internal stress distributions.

## 8.7 WEAVE

Author:

Brian Cox

References:

B.N. Cox and M.S. Dadkhah, "The Macroscopic Elasticity of 3D Woven Composites," *J. Composite Materials*, **29**[6], 785-819, 1995.

B.N. Cox, "Failure Models for Textile Composites," NASA CR 4686, August, 1995.

M. S. Dadkhah, J. G. Flintoff, T. Kniveton, and B. N. Cox, "Simple Models for Triaxially Braided Composites," *Composites* **26**[8], 561-77 (1995).

User Manual:

Brief description of required input provided as electronic file with program.

Format:

FORTRAN code which may be compiled for target machine.

Geometric Model:

The volume fraction assigned to stuffers, fillers, and warp weavers is required. The code covers orthogonal interlock, layer-to-layer angle interlock, and through-the-thickness angle interlock. Waviness of stuffers and fillers is accounted for by allowing the user to input statistical data for angle variation. Warp weaver orientation is assumed to be either normal to plane (orthogonal interlock), or at 45° for the angle interlocks (controlled by an internal data statement).

Stiffness Model:

Orientation averaging, with tow stiffness knockdowns based on statistics of waviness. Tow stiffness is computed from constituent data (fibers and matrix) using one of five standard micromechanical models.

Strength Model:

None.

Data Required:

Fraction of all fibers lying in stuffers, fillers, and weavers. Total fiber volume fraction. Second moment of normal distribution of misalignment angles, yields of stuffers and fillers, number of ends and picks, thickness of plate.

Output:

Tow elastic constants computed by micromechanical model. Three-dimensional stiffness matrix for homogenized plate. Plate bending stiffness.

Experimental Validation:

Large data base of measured elastic constants for several weaves is given in the references.

Comments:

**WEAVE** offers several novel features.

- **WEAVE** incorporates micromechanical models for tows. The elastic constants of an impregnated tow are not generally available from experiments. The user must predict values to use any of the codes. It is convenient to have the prediction tool built-in.

- **WEAVE** (and **MLM** for braids - see third listed reference) incorporates a simple rule (Eq. (3.1) of this handbook) for reducing the stiffness of tows to account for stochastic waviness integration of the yarn stiffness over the specified distribution of angles. The distribution may be obtained by analyzing micrographs or assigned typical values in a sensitivity study.

## 8.8 BINMOD

Author:

B. N. Cox, W. C. Carter, N. A. Fleck, J. Xu, M. A. McGlockton, and R. M. McMeeking

References:

B. N. Cox, "Failure Models for Textile Composites," NASA CR 4686, August, 1995.

B.N. Cox, W.C. Carter, and N.A. Fleck, "A Binary Model of Textile Composites. I Formulation," *Acta Metall. Mater*. **42**[10], 3463-79 (1994).

J. Xu, B.N. Cox, M.A. McGlockton, W.C. Carter, "A Binary Model of Textile Composites: II The Elastic Regime," *Acta Metall. Mater*. **43**[9], 3511-24 (1995).

User Manual:

NASA CR 4686 includes operating instructions. Comments are also included in electronic form.

Format:

FORTRAN, which may be compiled for target machine.

Geometric Model:

The binary model consists of line elements to represent the tow axial properties, and three-dimensional "effective medium" elements to represent the transverse and shear properties. General configurations of tows can be modeled, but only 3D interlock weaves are handled automatically.

Stiffness Model:

The code uses the finite element method. By applying forces or displacements to various planes, all macroscopic elastic constants can be found. Cyclic symmetry is not automatically imposed. In addition to the line and 3D elements, there are springs

to account for transverse stiffness at yarn crossing points. Waviness can be accounted for by randomly offsetting nodes in the model according to a specified normal distribution.

Strength Model:

The binary model prints the stresses and strains for the effective medium elements and tow elements. The code is designed to handle nonlinear behavior. With these capabilities, it should be ideal for studying progressive failure. Indeed, it is the only code available that should be able to model events at large strains, where mechanical lockup between yarns starts to occur. However, use of the code for progressive failure is not currently documented.

Data Required:

- Mesh data for effective medium elements (element size and mesh density), grid data for line elements. Automatic meshing assigns line elements to nodes based on a regular pattern defined by first position, last position, and increment.

- Axial stiffness of yarns and stiffness of effective medium elements (documentation describes how to assign latter). Standard deviation in *z* axis location of nodes for stuffers and fillers can be entered, which the code uses to assign random *z* offsets. Loading conditions are prescribed strains or forces applied to specific planes.

Output:

Iteration summary, total forces acting on loaded plane, stress and strain at each element quadrature point.

Experimental Validation:

Large database of elastic properties for several weaves provided in references. Failure data and observed failure progression are also documented.

Comments:

Given the difficulties of making 3D finite element models of plain weaves, the binary model makes a reasonable compromise between geometric fidelity and practicality. The simplification of the geometry allows representation of complex

weaving patterns, while retaining many important aspects of the physics. The authors have used the code to simulate a variety of complex failure phenomena. However, the progressive failure capability is unavailable in the version of the code provided here.

# 9. SELECTIVE ANNOTATED BIBLIOGRAPHY

This bibliography samples recent papers on the mechanics of textile composites, especially those dealing with modeling issues. In this rapidly evolving field of study, any bibliography will soon be incomplete. Significant new results are already being presented at conferences or in preprint form. However, as a partial assurance of quality, papers in conference proceedings or still awaiting publication in refereed journals are not listed here, except for some that have been cited in the handbook.

Comments are provided to indicate the kind of information to be found in each paper. The comments are not intended to be criticisms, but merely to point readers to appropriate sources.

The table has been sorted by the “key” entry, which classifies the type of textile, and then by author. If the table is available electronically, Microsoft Word will allow sorting by other criteria.